QUEEN MARY UNIVERSITY OF LONDON

School of Engineering and Materials Science

CENTRO DE INVESTIGACIÓN EN MATERIALES AVANZADOS (CIMAV)

Departamento de Física de Materiales

Master Thesis

PRESENTED BY: Emilio Gómez Sánchez

THESIS:

"Multifunctional PLA composites reinforced with exfoliated, expanded, and turbostratic graphite for a sustainable future."

Thesis Supervisors: Dr. Dimitrios Papageorgiou and Dr. Ivanovich Estrada Guel

Chihuahua, Mexico. June 22nd, 2024

Index

1.-Introduction

Polymers have been manipulated throughout history, and materials have been the cornerstone of human progress, elevating our production capabilities and living standards. From the earliest tools to the most complex structures, our ability to manipulate materials such as metals, ceramics, and polymers has demonstrated our understanding and ability to reshape nature. In the current era of rapid scientific and technological advancement, the role of materials in driving development and innovation is nothing short of pivotal. These materials can be classified as either structural, focusing on mechanical properties like strength and deformation, or functional, emphasizing their behavior in light, sound, electricity, heat, and magnetic fields.

Composite materials, which are formed by combination of different materials, have the goal to increase the number of applications and to change the nowadays materials with high-performance composite materials. The field of materials research is not just evolving; it's innovating. It's moving away from traditional empirical methods and towards a more purposeful approach to materials design. A prime example of this paradigm shift is the emergence of composite materials, a blend of materials that preserve their original properties and acquire new ones. This exciting transition is driven by the desire to expand the scope of applications and to revolutionize today's materials, replacing them with high-performance composites with enhanced properties [1].

2.- Theoretical framework

2.1 Composite materials

Composite materials result from a harmonious union between two primary components. Usually is possible to achieve unusual combinations of properties, which can include increased designed to unlock enhanced properties not inherent in the individual materials. As a result, a composite material embodies a significant portion of the properties of both component phases, leading to a superior amalgamation of properties. This unique design approach often paves the way for extraordinary combinations of properties, such as heightened stiffness, mechanical strength, density, high-temperature performance, corrosion resistance, hardness, abrasion and impact resistance, and thermal and electrical conductivity.

These materials comprise two immiscible elements: the matrix (continuous phase) and the reinforcement (discontinuous phase). Fig. 1 shows an image of a composite material with its different components.

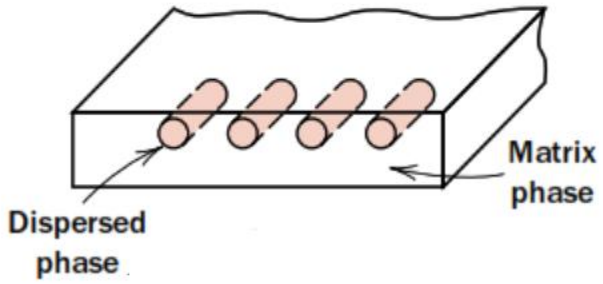

Figure 1. Illustration of a composite material and its constituents [2].

The matrix's functions are to isolate the reinforcement from the environment, provide a good bond with it, fix it in its position, and distribute and transfer the stress to it. It is also important that the matrix possesses the desired corrosion and high-temperature resistance.

On the other hand, the reinforcement's functions are to resist the exerted tension, increase the matrix mechanical strength, decrease the failure due to high temperatures, and stop the cracks propagation.

Some properties of composite materials such as electrical, chemical, and high-temperature properties depend on the matrix [2, 3, 4].

2.2 Composite materials classification

Depending on the matrix type, which can be metallic, polymeric or ceramic-based, there will be different characteristics and applications. And, therefore, the bulk properties of the composite material.

2.2.1 Metal matrix composite

Metals commonly used are aluminum, titanium, or magnesium. Aluminum is the most widely used due to its cost-effectiveness, low density, effortless-ease manipulation, and resistance to degradation. Copper is also frequently used as a matrix owing to its good thermal and electrical conductivity. These kinds of composites are reinforced with ceramic particles and fibers. The final properties of these materials are linked to the characteristics of the individual components of the composite and the phase transitions occurring during the cooling and solidification processes.

Metal matrix composites are designed especially for structural applications in the automotive, aerospace, military, electric, and electronic industry due to the demands for material with high stiffness, mechanical strength, and specific module. In the electric and electronic sectors, designing thermomechanical and thermophysical properties like good heat transfer and low thermic distortion is crucial for these materials to be adequate suitable candidates [5].

2.2.2 Polymer matrix composite

Thermoplastics and thermosets can be found reinforced with glass fibers. The processes for fabricating this kind of composite include hand layup method, autoclave method, filament winding method, reaction molding method, and pultrusion. For high-temperature applications, thermoset aromatic polyamides are often preferred.

These types of composite materials are characterized by their low-cost production, malleability, and corrosion resistance. They are used in airplane fuselages, wings, automotive parts, panels, insulations, pressure vessels, fishing rods, and golf clubs [4].

The most used thermosets are epoxy, polyester, and polyimide resins. Unsaturated polyester is a vital resin for the manufacture of composites molded at atmospheric temperature, this is why these materials are reinforced with glass fiber. It can cure at room temperature, be molded at atmospheric temperature, and be machined easily. Its crucial disadvantages are the curing volumetric shrinking and the poor heat resistance, which is why it is rarely used as a matrix of carbon fiber composite materials.

Adding agents to the matrix, which include curing agents, diluents, toughening agents, plasticizers, thixotropic agents, fillers, and pigments, can enhance the performance of the resins, cure process, and reduce costs.

Thermoset resins are highly cross-linked, which provides them with a high modulus, creep resistance, and strength. However, it also causes high brittleness, which means fast crack propagation. Standard thermoplastic resins include polypropylene, nylon, thermoplastic polyesters, and polycarbonate. Moreover, emerging thermoplastics like polyamide-imide, polyphenylene sulfides, and polyether ether ketone. Among these, the ketone is the most attractive one to be used in polymeric matrix composites owing to its toughness and impact properties as a result of its high crystalline percentage and morphology [1, 6].

2.2.3 Ceramic composite materials

Composite materials often possess brittle material such as ceramic materials, as the matrix. These composites are distinguished by their excellent high-temperature properties and are lighter than their metallic counterparts, performing the same function.

The qualities of these composites are high-temperature resistance, hardness, low thermal expansion coefficient, compression strength, and corrosion resistance. Short metallic fibers are often used as reinforcement, this combination resists thermal shock. Also, carbon fibers are frequently selected to increase mechanical strength along with other ceramic fibers [4, 5].

2.3 Classification based on the reinforcement

The composite materials can be classified into three categories: reinforced with particles, fibers, and sheets. Some examples are concrete, glass fiber, and plywood. These materials can be isotropic or anisotropic depending on the sort of external stimulus: the behavior of composite material reinforced with particles used to be isotropic. In contrast, the behavior of the composite material reinforced with sheets is anisotropic [4]. A scheme of composites classification based on the reinforcement is shown in Fig. 2.

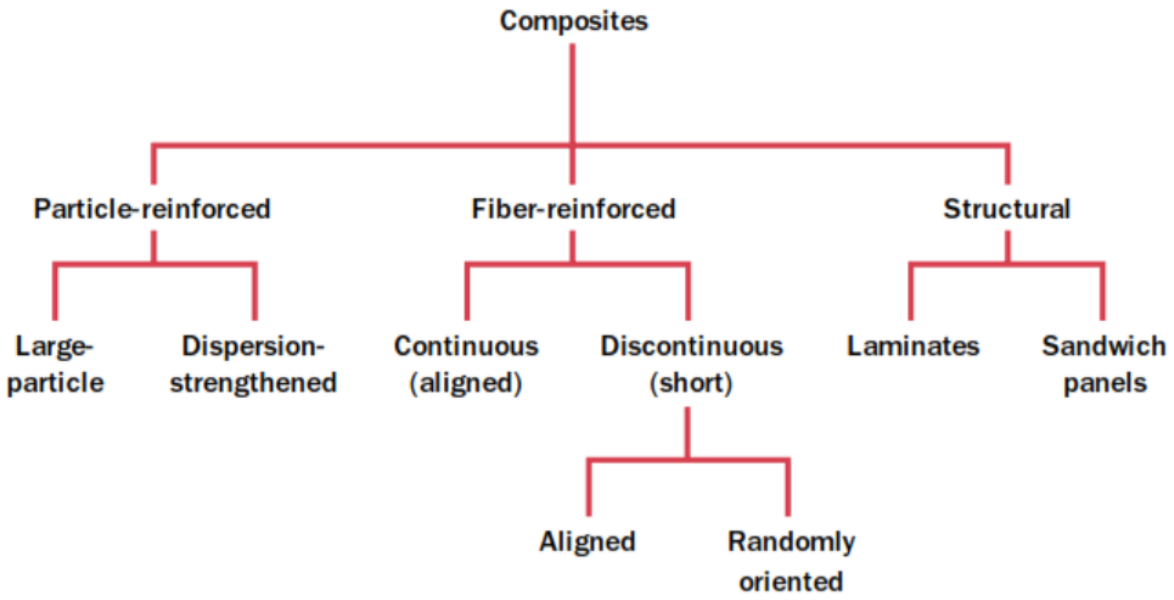

Figure 2. Scheme of composite materials based on the reinforcement [2].

2.3.1 Composite material reinforced with particles

This composite material is reinforced with a dispersed phase in the form of particles whose diameter ranges is between 10 and 250 nm [4, 5]. The difference between large-particles and dispersion-strengthened composites is based on the reinforcement or strengthening mechanism. The term “large” indicates that the interaction scale between particles and matrix is beyond the atomic or molecular level. In most cases, the particles are harder and stiffer than the matrix, impeding the movement of the matrix near to each of the particles. The improvement of the mechanical behavior depends on how strong the bonding at the matrix-particle interface is.

For dispersion-strengthened composites, particles are smaller, whose diameter is ranged from 0.01 to 0.1 μm. The interaction between the matrix and reinforcement occurs at the atomic or molecular level. A similar strengthening mechanism is seen in the precipitation hardening. This results in restricted plastic deformation, increasing the yield, tensile strength, and hardness.

Carbon black is commonly employed as reinforcement in polymeric matrix composite. It is small particles of carbon pigments formed in the gas phase by the

thermal decomposition of hydrocarbons, a crucial process in producing composite materials. Among the various reinforcements used, carbon black stands out for its significant role in enhancing the mechanical properties and durability of the final product.

Notably, ferrites, ceramic compounds primarily composed of iron oxide and certain other metallic elements, are also utilized as reinforcements. These materials are chosen for their exceptional magnetic and dielectric properties, which enable them to effectively absorb electromagnetic radiation [7]. Fig. 3 provides a visual representation of a composite material reinforced with particles.

Figure 3. Illustration of a composite material reinforced with particles [3].

2.3.2 Composite materials reinforced with fibers

The critical features producing these materials are the length, diameter, orientation, amount, and properties of the fiber composite materials reinforced with fibers, which offer a range of advantages. These materials demonstrate superior resistance to fatigue, stiffness, and strength-weight ratio, thanks to stiff fibers within a ductile matrix. This unique structure allows for an effective distribution and transmission of stress from the matrix to the fibers, thereby supporting any stress applied, even at high temperatures.

The concentration and distribution of the fibers play an essential role in the strength and other properties of the composite material. In addition, the orientation can vary from a parallel alignment of the longitudinal axis of the fibers in only one direction or an utterly random alignment. The first configuration generates a highly anisotropic material, whose properties depend on the direction in which they are measured. A scheme of different types and orientations of fibers inside a composite material is shown in Fig. 4.

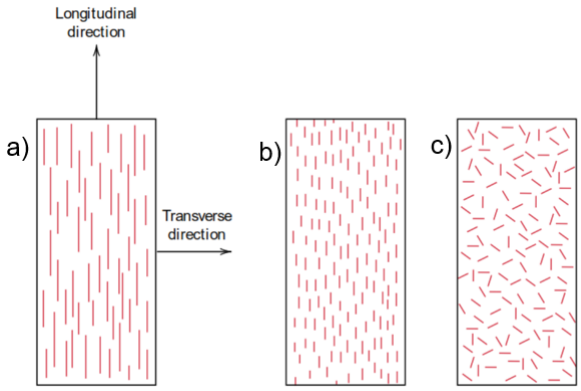

Figure 4. Illustration of different types and orientations of the fibers in a composite material: a) continuous and aligned, b) discontinuous and aligned, and c) discontinuous and randomly oriented [2].

The main types of fibers used to produce composite materials are continuous and discontinuous. The properties obtained with composite reinforced with discontinuous fibers, whose diameter ranges a from 3 to 5 µm, tend to be inferior to those with continuous fibers. On the other hand, discontinuous fibers make the production of the material cheaper. There is another discontinuous fiber called whiskers with a diameter of a micron and 100 µm of length, is another discontinuous fiber not commonly used since they are harmful to health and very expensive. Whiskers are fragile single crystals; their size gives them high strength owing to their high crystallinity degree. These fibers can include graphite, silicon carbide, silicon nitride, and aluminum oxide [2, 4, 5]. A scheme of composite materials reinforced with continuous and discontinuous fibers is shown in Fig. 5.

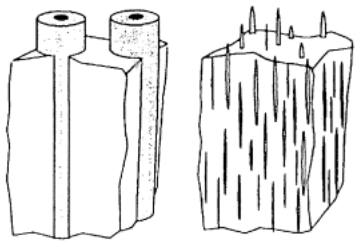

Figure 5. Illustration of composite materials reinforced with continuous and discontinuous fibers [3].

Most polymeric composite material intended for structural applications are reinforced with fibers, especially long fibers. These materials' elastic modulus and resistance

strength are several times higher than homogeneous materials. Some widely used fibers are glass, carbon, alumina, silicon carbide, and some other inorganic fibers.

The glass fiber has the same composition based mainly on SiO_2 and amorphous supercooled liquid structure as the bulk glass. These fibers possess high tensile strength and a low elasticity modulus. Its tensile strength decreases at high temperatures, the longer the time at high temperatures, the more the strength decreases. For glass fibers, the thermal conductivity and thermal expansion coefficient are low. However, except for hydrofluoric acid, it has corrosion resistance to almost all the acids, salts, alkalis, and organic solvents. Despite its excellent corrosion resistance due to the increased surface area of the glass fibers, the corrosion resistance is lower than that of bulk glass.

Carbon fibers are obtained from the pyrolysis of organic fibers in an inert atmosphere (for chemical protection), resulting in a percentage of carbon between 90% and 99%. Its structure is graphic, which is a three-dimensional hexangular crystal lattice. The carbon atoms within the layer have a sp^2 hybridization bond, allowing them to get covalent bonds with the other three carbon atoms. Van der Waals forces link the bond between layers. An increase in the carbonization temperature increases the modulus of carbon fibers because this increases the crystal growth. The regions of hexatomic rings enlarge, and the degree of crystal orientation rises. However, after 1,700°C the strength is reduced due to the increased fibers defects.

The elastic modulus of carbon fibers is higher than that of glass fibers. Therefore, the strain is lower than it is in glass fibers. These carbon fibers are brittle, they have lousy impact resistance. The fiber's resistance to high temperature reaches t0 2,000°C under an inert atmosphere. Carbon fibers possess good thermal conductivity along the fiber axial direction and the thermal expansion coefficient along the fiber axial direction has a negative temperature effect, which means that the increase in the temperature drives a preferential contraction. General acids and alkalis have little impact on carbon fibers. However, strong oxidants such as concentrated nitric acids, hypochlorite, and dichromate can affect the fibers [1, 6].

2.3.3 Structural composites

This group includes thin coating, coarse protector surfaces, metal coating, bimetallic, and laminated. Laminated composites comprise two-dimensional sheets or panels with a preferred high-strength direction. The layers are stacked and cemented together, so that the orientation of the high-strength changes with each layer. Thus, a laminar composite has relatively high strength in more than one direction in the

two-dimensional plane. Several laminated composites are designed to obtain higher corrosion resistance while being low-cost, high mechanical strength, and low density. Other essential features are higher wear resistance and unusual thermic expansion. A scheme of the stacking of successive layers for a laminar composite is shown in Fig. 6.

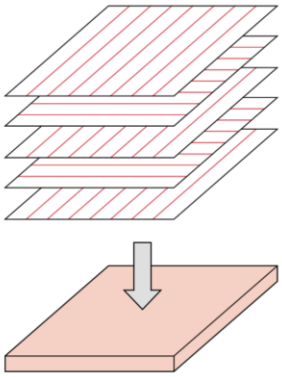

Figure 6. Illustration of the stacking of successive layers for a laminar composite [2].

Sandwich panels are considered structural composite and consist of two outer sheets or faces separated by a less dense material or core layer, which is less stiff and has lower strength. The core has two functions: it separates the faces, resists perpendicular deformation to the face plane, and provides some degree of shear rigidity along planes perpendicular to the faces. Materials like polymers, synthetic rubbers, cement, and wood are commonly used to fabricate this composite type. Sandwich panels configuration is used in roofs, floors, and walls of buildings, in aircraft for wings, fuselage, and tailplanes skins [2, 4]. A schematic diagram of the construction of a sandwich panel is shown in Fig. 7.

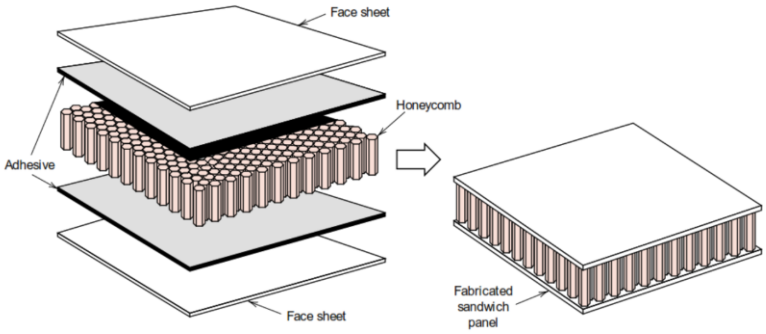

Figure 7. Diagram of the construction of a sandwich panel [2].

2.4 Matrix-reinforcement interface

This is a variable chemical composition region in which the bond between the matrix and reinforcement takes place; owing to the interface, the tension transfer from the matrix to the reinforcement is possible. Therefore, the interface's state can condition the composite material's properties. If the bond between the matrix and reinforcement is not good, the matrix will withstand most of the tensions.

The matrix and the reinforcement are independent and interdependent due to the interface. The interface's structure, properties, and adhesion strength are directly related to the composite performance. The parameters to obtain an ideal interface are the following:

- The wettability between the matrix and the reinforcement must be adequate, depending on the surface energy of the components and their thermodynamic nature. The tension transfer will be efficient if the interface is in a satisfactory thermodynamic equilibrium.
- The bond must last over time and within the application's required temperature range.
- The reaction between the matrix and reinforcement must be minimized, so that the reinforcement is not affected.
- The thermal expansion coefficient of the matrix and the reinforcement must be similar to minimize the internal tension resulting from the temperature increase.

2.4.1 Bonds in composite materials

It can be classified based on the type of reaction carried out between the matrix and reinforcement:

- The matrix and the reinforcement do not react and are not miscible into each other.
- The matrix and the reinforcement do not react, but they are miscible into each other.
- The matrix and the reinforcement react, giving place to a third component in the interface.

The bonds made by a mechanical nature can also be considered when chemical reaction is not carried out. Reinforcements with high roughness more propense to generate a mechanical bond. Any contraction of the matrix results in the reinforcement being gripped by the matrix, when the matrix in the composite shrinks more than the reinforcement when cooling from a high temperature. Mechanical bonding is efficient in load transfer. The matrix fills the hills and valleys on the surface of the reinforcement. On the other hand, if the matrix cannot fill the hills and valleys, then the matrix will solidify and leave interfacial voids. An illustration of a good mechanical bond and a lack of wettability leading to the generation of interfacial voids is shown in Fig. 8.

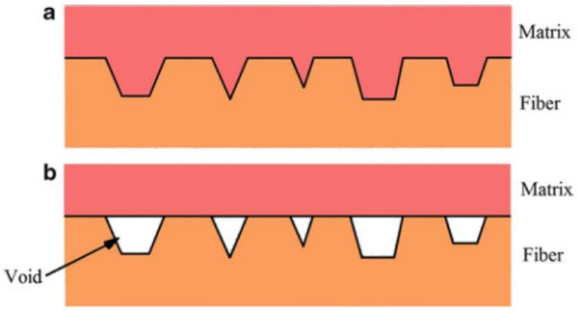

Figure 8. Scheme of mechanical bond: a) good mechanical bond, and b) lack of wettability leading to the generation of mechanical interfacial bonds [6].

In a bond without a chemical reaction, a mechanical bond can contribute to the composite's mechanical properties. However, the fact that a chemical reaction is not carried out decreases the material's mechanical properties since the mechanical bond is weaker. Electronic interactions at atomic distances can occur in a bond without chemical reaction but with solubility between the components

When a chemical reaction is formed in the interface, it can be simple, involving atomic transfer, molecular transfer, or a diffusional process from one or both components, or it can be a more complex reaction involving a chemical reaction sequence. Whatever the case, it results in a third component with a certain thickness.

Other factors that can affect the interface stability are instability by dissolution, in which due to the Kirkendall effect, it is possible to lose a part of the reinforcement, instability due to interfacial reactions, or instability for decomposition of the interface [3, 5, 6].

2.4.2 Interface in a polymer matrix composite

For polymeric composites, two stages form the interface. The first is contracting and infiltrating between reinforcement and matrix. The reinforcement possesses a different absorption capacity; it only absorbs what makes it reduce its surface energy, preferably the one that reduces its surface energy. The second stage is the curing stage of the polymer, which is cured by physical or chemical changes to form a fixed interface layer. The first stage influences the curing stage because it determines the structure of the interface layer.

Something important that must be considered is the wettability between the matrix and the reinforcement. Wettability tells us about the ability of a liquid to spread on a solid surface. When you drop a droplet of any substance on the surface of a solid, sometimes the droplet immediately spreads on the surface of the solid, this process is called infiltration. On the other hand, sometimes the droplet stays spherical, when this happens, there is no wettability or poor infiltration. The wetting angle or contact angle θ is helpful to express the wettability of a liquid on a solid. If the value of this angle is less than 90°, it is called partial wettability, if it is more significant than 90°, there is no wettability, but if the angle is 0° or 180° the wettability is complete [1, 6]. An illustration of the complete wettability, no wettability and partial wettability is shown in Fig. 9.

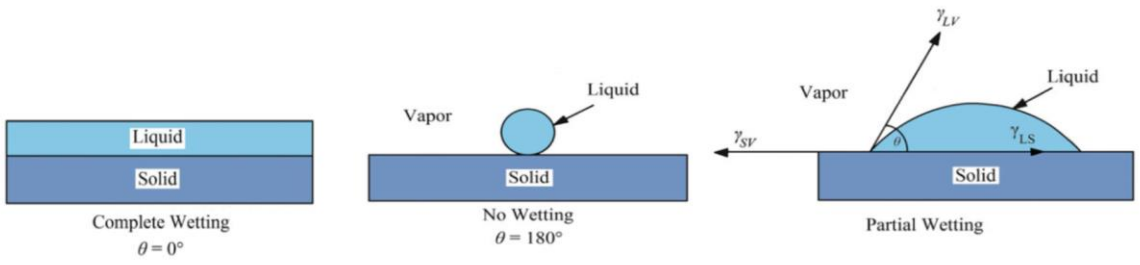

Figure 9. Scheme of complete wettability, no wettability and partial wettability [6].

Wettability between matrix and reinforcement will depend on essential variables: time and temperature contact, interfacial reactions, stoichiometry, surface roughness and geometry, heat of formation, and electronic configuration.

The mechanism of the cure at the interface is still unclear. However, some theories try to explain it.

- **Infiltration absorption:** According to this theory, there are two stages. In the first stage, polymer molecules move from the solution to the surface of the adhesive by macro-Brownian motion. Then, the macromolecular chain approaches the surface polar group of adherents by micro-Brownian motion. If there is no solvent, the macromolecular chain can only partially approach the surface employing pressure, and heat can make it move closer. The second stage is absorption, in which the intermolecular distance is less than 0.5 nm, and the Van der Waals forces form a dipole-dipole bond, dipole-induced dipole bond, hydrogen bond, and so on. The adhesive strength is based on an adhesive material that can stick to various materials, and the general adhesive has a large inert with adherent, so it is hard for a chemical reaction to occur.
- **Chemical bond:** This theory argues that the molecule of a coupling agent should contain at least two kinds of functional groups. The first one can react with the reinforcement material, and the second should be able to participate in the resin's curing reaction, forming chemical bonds with the resin molecular chain. This molecular coupling agent is a bridge that links the reinforcement with the matrix using covalent bonds. The above-mentioned loses some power in complex systems cases without a coupling agent or without forming a chemical bond even with a coupling agent.
- **Diffusion:** This theory argues that the bonding between two polymers is the same as the diffusion between the same molecules. It is also caused by the diffusion-by-diffusion of different macromolecule chains or chain segments, obtaining a strong adhesive force. All the above is based on the macromolecular chain structure flexibility, one of the main characteristics of polymers.
- **Electron electrostatic:** This theory considers that the adherent and the adhesive are two capacitor plates. When both get in contact, the capacitor charges to form a double electric layer. This double electric layer can be formed by absorbing the polar group of one phase to another; this can be carried out by electrons in the polymer functional group going through the interface. This theory, like the others, has its limitations. For example, this theory says non-polar polymers cannot generate a bond, but they do.
- **The mechanical link:** This theory states that bonding is purely based on mechanical action. The liquid infiltrates the reinforcement gaps and solidifies or cures under certain conditions. The geometrical factors of the material determine this mechanical bonding. However, no bonding system is only formed mechanically.
- **Deformation layer:** According to this theory, there is a coupling agent coating layer on the surface that is flexible and provides the chemical bond with self-

healing capabilities, which is the dynamic balance state of continuous formation and fracture under outer loads. The dynamic balance not only avoids water and other low-weight molecular compounds but also relaxes the partial stress of the interface for the existence of the low-weight molecular compounds. The treatment agent between the matrix and the reinforcement is the one that provides the chemical bond with self-healing capabilities. The treating agent can slide to a new location along the surface of the reinforcement under external stress, and the broken bonds can reform new bonds, maintaining the adhesive strength between the matrix and reinforcement. At the same time, stress is relaxed in the process.

- **Priority absorption:** This theory states that the reinforcement surface first absorbs the matrix. Thus, the distribution of the interfacial layer in the matrix is gradient, which will affect the properties and structure of the interface layer, which also has a gradient change. This can eliminate stress and improve the mechanical properties of composites.

Several factors influence the bonding strength of the interface:

- **Size and specific surface of the reinforcement**: The larger the specific surface area is, the larger the physical interface is, and the higher the adhesive strength is. However, it also depends on the pores, distribution, size of the pores, surface reaction groups, and concentration.
- **Soakage:** As the soakage increases, the bond strength increases, and decreases with the porosity because the decrease in the interface area increases the stress concentration.
- **Interfacial reaction:** The interfacial adhesive strength increases with the increase of interfacial reaction. This is why it is crucial to introduce as many reactive groups as possible to generate more chemical bonds in the interface when preparing a composite.
- **The effect of the residual stress on the bonding strength of the interface:** The interfacial residual stress is caused by the volume shrinkage of the resin in the curing process. This is because of the difference in thermal expansion coefficient between the matrix and the reinforcement. When the temperature is decreased, the resin transits to the glass state with significant volume shrinking, but the shrinkage of the reinforcement is low, and the interface bonds try to avoid this shrinkage. At the end, the resin is subjected to tensile stress, the reinforcement to compressive stress and the interface to shear stress.

2.5 Applications of polymer matrix composites

2.5.1 Automotive applications

Using composites in transportation applications saves weight, reduces fuel consumption and increases payload. Since the initial budget for composite manufacturing is still lower than for metals, composites are competitive for vehicles manufactured in short series. There are several examples of the use of composites in automotive applications. The most common examples can be the exterior body panels and several components under the hood, in the integrated front ends, battery trends, and protective shields. All these parts have something in common: none of them carry a relevant structural load. On the other hand, there are some parts where composite materials are needed. For example, leaf springs, drive shafts, pressure vessels, etc. However, its use in the primary structure is minimal nowadays.

2.5.2 Marine applications

For many years, most leisure crafts, from the smallest yachts to competition power boats and sailing yachts, have been manufactured from composites. This is because the manufacturing of boats from composites is relatively inexpensive. The initial budget is generally low since few specialized tools and facilities are needed.

These composites are used in the hall of a small boat, and almost always, single-skin composite laminate, deck, and floorboards are sandwich structures to achieve the required stiffness. In a larger boat, the sandwich structure tends to be used all along the hull: deck and floorboard. Recently, composites have become adequate materials for masts, booms, and rangers. Composites have also been considered in shipbuilding since they are deficient and nonmagnetic.

2.5.3 Aerospace applications

Saving weight in a flying craft directly translates into increased capacity to transport more load, enhance the craft's performance, or can the difference between life and death in a fighter aircraft. In aerospace applications, composites may lower the manufacturing cost due to the integration of some parts.

Between the standard aircraft composites, we can find rudders, flaps, wing skins and substructures, leading edges, complete vertical and horizontal stabilizers, fairings, engine nacelles, thrust reversers, propellers, landing gear doors, access doors, large parts of the cabin, and cargo compartments. Sandwich-type composites are widely used in aircraft although modern helicopters make even greater use of composites

than aircraft. Rotor blades have been composites for years, and many helicopters are made of composites to reduce manufacturing costs and save weight.

In the case of spacecraft, weight savings are even more critical than in aircraft and helicopters for both payload and launch vehicles, and this results in the use of composites and offers to design a new structure like satellite antennae, practically no thermal expansion in an extensive range of temperatures.

2.5.4 Construction applications

Composites rehabilitate damaged concrete in bridge columns caused by earthquakes by supporting them with composite jackets. Something similar is used to upgrade the capacity of carrying loads of engineering structures, including bridges.

2.5.5 Electrical and electronic applications

In these fields, insulating properties are more critical than structural capabilities. The applications include equipment housing, transformer spacers, cable trays, etc. A ground makes the composite attractive for these applications to eliminate the direct electrical contact between electricians and potentially hot wires.

2.5.6 Other applications

Some well-known composites applications include golf clubs, racquets, and skis in sporting goods. Still, the list of applications in this field is endless, and there are several reasons for this: the main ones are fashion, improved performance, lower weight, durability, and sometimes, lower cost [8].

2.6 Fabrication processes of polymer composite materials

Several methods for manufacturing polymeric matrix composites. The process is selected based on the materials type and required application.

2.6.1 Hand layup method

In this method, the mold is prepared as one side open with the required shape, the reinforcement fibers are put on the surface and the matrix material is printed over the fibers as a gel. Still, spraying both matrix and reinforcement together onto the mold surface is also possible. The printing process keeps on until the desired thickness is obtained. This process is the most economical since it involves less equipment. Due to this process being done by hand, it gets better control of the fiber's orientation. However, this method has low productivity and lousy working conditions. It is labor-intensive, so it is hard to control product quality, which leads to poor performance and low strength compared with other methods. The mold is commonly made of wood, sheet metal, plaster, and FRP composites. Most aerospace composites are fabricated by this method [6, 9]. An illustration of the hand layup method by and by spray is shown in Fig. 10.

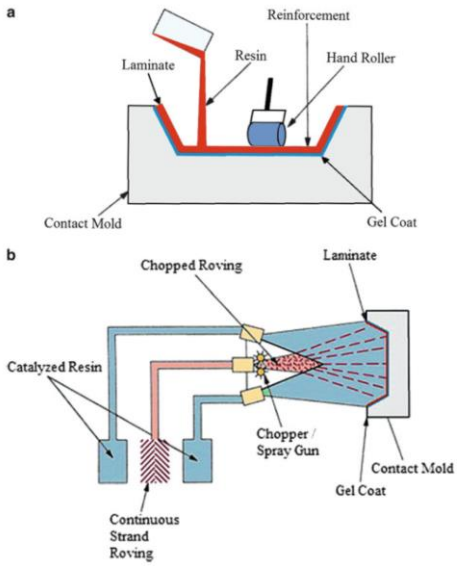

Figure 10. Schemes of the hand layup method: a) fibers are laid onto a mold by hand and resin sprayed or brushed on, and b) fibers and resin are sprayed together onto the mold surface [6].

2.6.2 Autoclave method

This is a part molding process by one of the open molding methods in which the part is cured by subsequent application of vacuum, heat, and inert gas pressure. The mold part is placed into a plastic bag where a vacuum pump extracts the air. These

bags consist of a flexible thin membrane made of rubber that separates the layup from the gas, which generates compression. This allows the removal of air inclusions and volatile products from the molded part. Pressure and heat are applied to the autoclave promoting curing and densification of the material. This enables the fabrication of consistent homogenous materials. This method is relatively expensive and is used to manufacture high-quality aerospace products.

The autoclave is a closed vessel in which processes are carried out under pressure and heat are applied simultaneously. The pressure allows for superior parts because the voids are reduced. This method is used to make the wings of the Boeing 787 plane [6]. Fig. 11 shows a scheme of autoclave method.

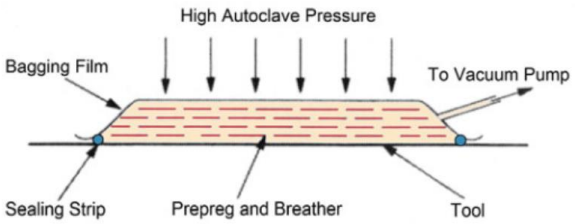

Figure 11. Illustration of the autoclave method [6].

2.6.3 Filament winding method

This method involves continuous filaments of reinforcement materials wound around the mandrel in layers and used to make cylindrical parts. The constant filament or roving consists of thousands of individual filaments that pass through a resin impregnation bath and are wound over a rotating or stationary mandrel; successive layers are laid on at a constant or varying angle until the desired thickness is obtained. Finally, the curing of the resin is done at high temperatures and the mandrel is removed. This process can be automated, provides a high production rate, and allows different sizes of products to be made. However, complex geometrics cannot be obtained. This method produces pressure vessels, storage tank pipes, rocket motors, launch tubes, and drive shafts. A disadvantage is the limitation of the design of the components due to the need to remove the mandrel on which the product is formed. However, inflatable, sectional, and demountable mandrels overcome the problem [2, 6, 9]. A scheme of filament winding method is shown in Fig. 12.

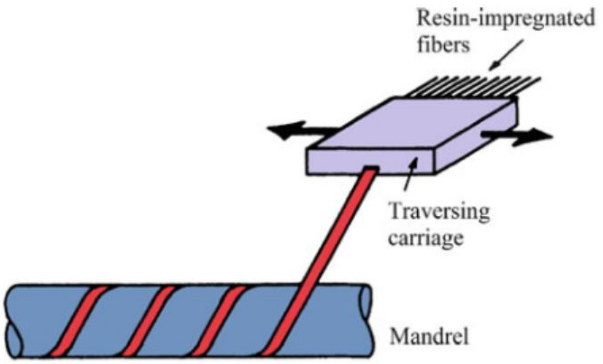

Figure 12. Illustration of filament winding method [6].

2.6.4 Reaction injecting method

The reactive ingredients are pumped at high pressure and speed into a mixing container and injected into a mold cavity where solidification and curing occur because of a chemical reaction and high pressure. The laminated stacks consist of fibers impregnated with enough thermoplastic matrix and polymer films of complementary weight to obtain the required fiber volume fraction at the end. This process is characterized by high productivity and low energy consumption [1, 9]. A scheme of the process is shown in Fig. 13.

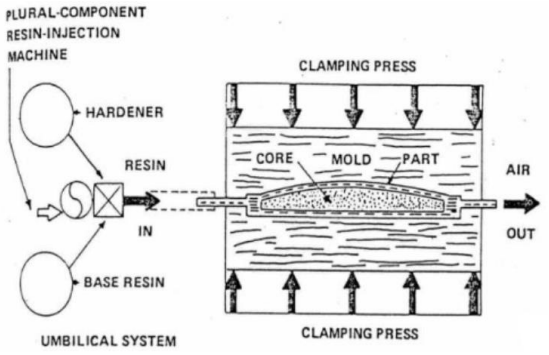

Figure 13. Illustration of the reaction injecting method [9].

2.6.5 Pultrusion

This is a process in which layers of fibers are bathed with resin and pulled through a heated die creating a desired cross-sectional shape with no limitation on length. This method fabricates a wide range of solid and hollow components with constant or almost constant cross-sections. The continuous fibers are pulled through a resin bath and then through a heated die which completes the impregnation of the fibers, controls the resin content, and cures the resin into its final shape. This method is easily automated, the production rate is high, and several shapes are possible [1, 2, 9]. A scheme of the pultrusion method is shown in Fig. 14.

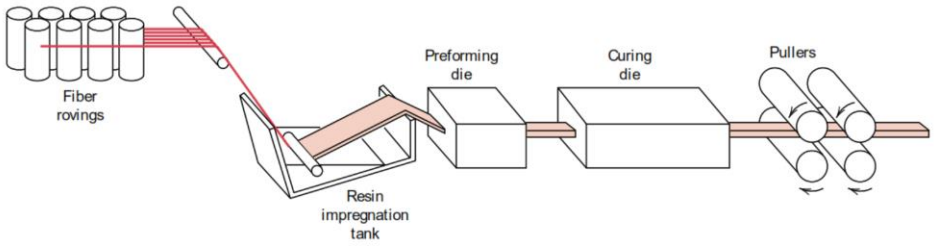

Figure 14. Illustration of the Pultrusion method [2].

2.6.6 Resin transfer molding

This is a closed-mold and a low-pressure method. The preform made of the desired fibers is placed inside a mold and liquid resin is injected into mold. The preform of reinforcement keeps its shape during the injection. Finally, the resin cures, giving rise to the polymer matrix composite. This method is found to be cost-effective and has a high production rate. Since the liquid monomer is exothermic, when the polymerization reaction occurs, heat from an external source is no longer necessary. Therefore, energy consumption is reduced [1, 6].

2.6.7 Thermoforming

It involves producing a heated and stamped sheet followed by vacuum or pressure forming. This method takes advantage of the thermoplastic's softening upon heating; therefore, this melt flow method can be used [6].

2.6.8 Pressing and folding method (P & F)

This method can create nanocomposites with well nanofillers dispersion levels without losing dispersion efficiency even at ultra-high reinforcement loads. The method is based on the process of preparation of puffy pastry to make croissants.

The process starts by adding nanoparticles between two polymer films and applying P & F cycles several times. Fig. 15 shows the nanofiller dispersion process. Image a) shows the P & F cycles draw inspiration from the puffy-pastry preparation technique to make croissants, where the dough is the polymer and the butter is the reinforcement, together with its stretching and folding effect that can be idealized as a Baker's transformation, in the image b) is shown a scheme of the P & F method, such method is composed of the folding step in which an approximately circular layer is folded twice to generate a quadrant slice and a pressing step at temperatures slightly higher than the melting point of the polymer, this step produces a strong flow that breaks down the agglomerates, align the dispersed particles and increases the contact area between the matrix and reinforcement, all of this, after several cycles. This process implements the Baker's transformation at very high applied viscous stress, in image c) are shown several top-view photos a simple of linear-low density polyethylene (LLDPE) containing 4.8% of reinforcement after different numbers of P & F cycles, where is possible to see agglomerations at small number of cycles, but as this number of cycles increases the aggregations decreases, so that, after 20 cycles the agglomerations are no longer detectable to the naked eye.

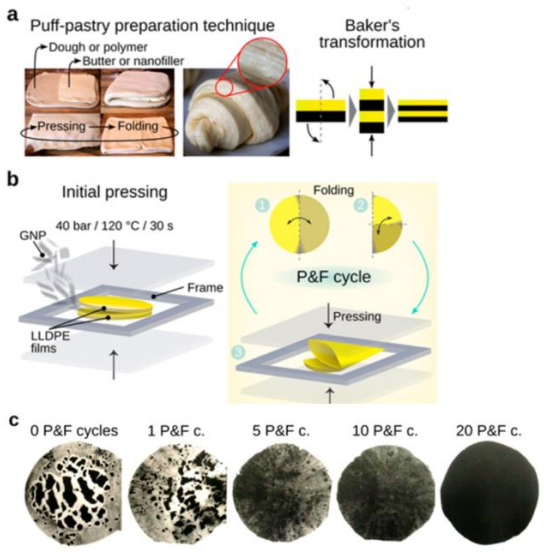

Figure 15. Image of nanofillers dispersion process: a) the P & F cycles draw inspiration from the puffy-pastry preparation technique to make croissants, b) scheme of the P & F method and c) several top-view photos of a simple linear-low density polyethylene (LLDPE) containing 4.8% of reinforcement after different numbers of P & F cycles [10].

It is not possible to obtain the level of dispersion and orientation obtained by this process with other conventional methods like twin-screw-melt-compounding or multilayer co-extrusion since they use temperatures much higher than the polymer melting point and, therefore, do not achieve such high shear rates to distribute the reinforcement and orient it [10].

2.6.9 Solvent casting

This is a simple and cost-effective process in which a polymer is dissolved in water or any volatile solvent. Once the polymer is dissolved, the fillers are added to the mixture. Afterward, it is vigorously stirred, cast into a recipient, and dried to eliminate the solvent.

The solvent casting process can be used for applications like bone tissue engineering, whose bones can support osteoblastic cell growth and mineral deposition, fabrication of food and drug containers made from polymers like polycaprolactone which exhibits excellent biocompatibility and mechanical strength. Scaffolds with high porosity can be produced which is essential for porous channels for cell migration and surfaces for cells attachment. This process is also commonly used to blend polymers and fabricate composite materials.

Some advantages of this process include better homogeneity in thickness and clarity than in methods like extrusion, the wafer being free of defects, and having more flexibility and physical properties.

On the other hand, some disadvantages of this process include that the polymer must be soluble in water or the volatile solvent, the solution should be stable, with minimum solid content and viscosity, and multiple casting methods can be selected depending on the fluid rheology, desired applied mass, and dosage uniformity [11, 12, 13].

2.7.1 Polylactic acid (PLA)

This is a thermoplastic biopolymer in which the precursor molecule is lactic acid. Due to its biodegradability, barrier properties, and biocompatibility, this biopolymer has found industrial and medical applications since it presents a wide range of

unusual properties, from the amorphous to the crystalline state. Due to the asymmetric carbon atom in its molecule, lactic acid (LA) exists in two forms, L-LA and D-LA. These two forms are mirror images of each other. Their pure forms have identical physical and chemical properties [14]. An illustration of both forms of LA is shown in Fig. 16.

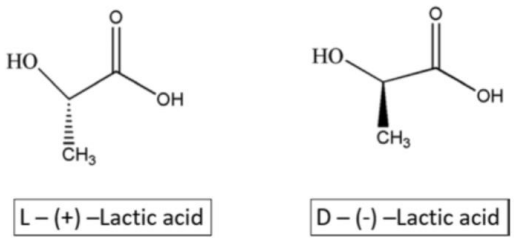

Figure 16. Image of both forms of LA [14].

Thermal and mechanical properties depend on the radio, and L-LA and D-LA distribution in the polymer chain. Because of the -CH_3 group in the polymer, PLA is a hydrophobic material, so it is more resistant to hydrolysis than PGA.

In the PLA structure, L-lactide produces semicrystalline polymers. On the other hand, DL-lactide is an amorphous polymer. Since the PLA is mainly made of L-LA (PLLA), the polymer tends to be semicrystalline, so its structural regularity is high. The glass transition temperature for crystalline and amorphous phases is 50 to 70°C. The degradation half-life depends on the stereochemistry and molecular weight.

In the case of poly (L-lactic acid), it is transparent and rigid. Its elongation at break is less than 10%, tensile strength between 45 and 70 MPa, Young's modulus of 3GPa, failure strength at 100 MPa, the melting point is from 170 to 180°C, and its glass transition temperature is 53°C. However, the poly D-Lactide (PDLA) blending, the melting and heat deflection temperature can be increased by 40 to 50°C and 60 to 190°C, respectively. Besides, polymer PDLA has no melting point but has a glass transition temperature of 55°C, which decreases its tensile strength. Therefore, the tensile strength properties of PLA will change with the content of D.

Another critical feature is the crystallinity, in the case of the PLLA the recrystallization from high to low temperatures during the cooling is spontaneous, but crystallization will decrease with increased in D-LA content. Production of commercial PLA usually uses contents of 98 to 99% of L-LA and less than 1 to 2% of D-LA.

There are 3 methods to synthesize PLA: formation of the lactic acid through microbial fermentation, purification of lactic acid and preparation of its cycle dimer, and ring-opening polymerization (ROP) of lactides or lactides polycondensation of the PLA monomer.

The microbial fermentation of lactic acid uses renewable sources like sago and cassava starch. Then comes purification, which can be used in several methods like nanofiltration and electrodialysis, ion exchange resin, hybrid short path evaporation, and reactive distillation. Finally, lactic acid is converted into PLA using the ROP process, the most widely used method to polymerize lactic acid. In this process the end of the terminal chain acts as a reactive center. Thus, a longer polymer chain can be formed when the further cycle monomers open their ring system. Initially, lactic acid is dehydrated at high temperatures under vacuum conditions and poly-condensed into its oligomers. Afterward, by internal transesterification, it is catalytically depolymerized by lactide. PLA is obtained when the ring of lactide is open.

PLA can be derived from renewable resources like rice, wheat, corn, potato, and sugar. It is also biodegradable, recyclable, and compostable, which means almost no environmental impact occurred during its disposal. Since it is biocompatible, PLA is suitable for biomedical applications since it breaks into H_2O and CO_2, not interfering with tissue healing. Between its applications, we can not only find in biomedical like substitution and repairment of synthetic bones, drug delivery systems, and tissue engineering, but also in food packaging, agriculture, automotive industry, electrical industry, construction, and textile industry [14, 15, 16].

Despite all its advantages, PLA's mechanical and biological features require improvement. The mechanical properties are still deficient for some applications, and the biodegradation is too low for most medical applications. Several methods have been employed to address this challenge, one of the most promising being the incorporation of fillers into a PLA matrix [14].

Zerankeshi and coworkers fabricated a composite material using PLA as the matrix with 1 wt.% of graphite particles as reinforcement employing a novel modified mixing technique. The glass transition temperature increased from 59.8 to 62.4°C, and the ultimate compressive strength and the ultimate tensile strength increased from 26.71 to 38.6 MPa and 32.6 to 46.24 MPa, respectively [17].

Chieng and coworkers used PLA as composite material matrix reinforced with graphene nanoplatelets in loads from 0.1 to 1 wt.% utilizing a melt blending process. Besides, epoxidized palm oil was added to increase the elongation of the final composite. The elongation and tensile strength at a load of 0.3 wt.% were increased

by 60.6 and 26.5 wt.%, respectively. The composite also showed higher thermal stability. The highest initial and final degradation temperature increase was 23 and 68°C, respectively [18].

Zhou and coworkers fabricated a composite material using PLA modified with poly (butylene adipate-co-terephthalate) (PBAT) and carbon nanotubes with a carboxyl group (CNTs-COOH) by employing the melt blending technique. The tensile strength increased with contents from 0 to 0.5 wt.% and decreased slightly. Similar behavior was noticed in impact strength. Moreover, the initial decomposition temperature, and the glass transition temperature increased with reinforcement content to 0.5 wt.%. On the other hand, the melting temperature was decreased with the reinforcement content [19].

Kim and Jeong used PLA as the matrix of a composite material reinforced with exfoliated graphite in amounts of 0.1, 0.5, 1, 2, 3, 5, and 7 wt.% by using a hot extruder to melt and disperse the reinforcement inside the polymer. The initial degradation temperature was increased in the composite with content up to 3 wt.% from 350 to 364°C. The tensile strength increased from 62 to 70 MPa at 2 wt.% and remained constant up to 5 wt.%, and above this amount, the tensile strength decreased slightly. On the other hand, the strain at break for the composite was somewhat lower than that for neat polymer. Moreover, electrical conductivity decreased between 3 and 5 wt.% of reinforcement content. In addition, the initial degradation temperature increased by 14°C at a load of 3 wt.% of reinforcement [20].

Ivanov and coworkers fabricated different composite materials using PLA as the matrix reinforced with multi-walled carbon nanotubes and graphene nanoplates in contents from 0 to 6 wt.% employing the melt extrusion method. At the maximum reinforcement content, electrical conductivity increased almost 7-8 orders of magnitude for the two components system, with graphene nanoplates and multi-walled carbon nanotubes, reaching values of 8.4 x 10-3 (S/m) and 2.1 x 10-2 (S/m), respectively [21].

Batakliev and coworkers used PLA to fabricate a composite material reinforced with graphene nanoplatelets and multiwall carbon nanotubes, varying the reinforcement content from 0 to 12 wt.% using the melt extrusion method. The reinforcement had a beneficial effect on hardness and Young's modulus since both properties were increased, and the composites with a reinforcement content of 6% had the highest values in these properties [22].

Przekop and coworkers fabricated composite materials using PLA as the matrix reinforced with graphite in amounts of 1, 2.5, 5, 7.5, and 10 wt.% by twin-screw

extrusion. The samples for the different tests were made by 3D printing. The mechanical properties changed significantly. The composite reinforced with 10 wt.% showed 11% lower tensile strength and 21% higher Young's modulus. Moreover, the highest increase was achieved at 5 wt.% of reinforcement with a rise of 14 °C [23].

Gao and coworkers used PLA to fabricate composite materials reinforced with two types of graphite nanoplatelets varying in lateral size, small and large, and in amounts of 5, 7 and 10 wt.% by melt-compounding. The addition of graphite nanoplatelets improved Young's modulus of the composites by 10 and 24% for small and large nanoplatelets, respectively. The reported maximum reinforcement of 24% for PLA composites incorporating 5 wt.% is among the highest reported for PLA/graphite nanoplatelets systems. PLA/Graphene sheets systems showed improved electrical conductivity and a significantly increased percolation threshold from 3 to 6 wt.% [24].

Wang and coworkers fabricated composite materials using PLA as the matrix reinforced with flake-shaped nano graphite whose amount was 5 wt.% by regular solid injection molding, regular foam injection molding, and mold-opening foam injection molding. Compared with the solid and pure PLA, the specific tensile strength, the modulus, and the toughness of the microcellular PLA/graphite nanocomposite foam were increased by 35%, 50% and 250%, respectively. The PLA/graphite composite showed much higher electrical conductivities than the neat sample, because the injection process had increased the nanographite's connectivity by reorienting the nano graphite flakes. The improved electrical conductivity gave the composite foams a superior EMI shielding performance [25].

Using the solution-blending method, Li and coworkers used PLA to fabricate composite materials reinforced with graphene sheets in amounts of 0.01, 0.1, 0.2, 0.5, 1, and 2 wt.%. Adding graphene sheets to the PLA matrix improved the tensile strength from 36.64 to 51.14 MPa with a content of 1 wt.%. The thermal stability was also increased at 2 wt.% of graphene sheets by 150 and 20 °C in the initial and final degradation temperatures, respectively [26].

Piñon-Vázquez and coworkers fabricated composite materials using porous PLA as the matrix reinforced with exfoliated graphite in amounts of 0.5, 1, 2, and 3 wt.% by solvent casting. Compared directly with the blank, the tensile strength properties and elongation percentage improve significantly in the material reinforced with 0.5 wt.%, which means that adding exfoliated graphite to the matrix had a positive effect on its tensile properties, which can be related to better reinforcement distribution [27].

By a two-step melt-compounding process, Sullivan and coworkers used PLA to fabricate composite materials reinforced with exfoliated graphite nanoplatelets in 1,

5, 10, and 15 wt.%. The in-plane electrical conductivity increases around 3 orders of magnitude. Moreover, mechanical performance was improved. The modulus increased with increasing exfoliated graphite nanoplatelets content, indicating good matrix/reinforcement interaction [28].

2.7.2 Modified graphite

Graphite is an allotropic form of carbon. It is a soft, black material chemically stable, odorless, heat resistant and has good thermal and electrical conductivity. It is a refractory material whose melting point is 3827°C, resistant to thermal shock, and with a low thermic expansion coefficient of $8x10^{-6}$ K^{-1}.

In graphite, the carbon atoms are joined by covalent bonds in groups of six, giving place to a hexagon, being this hexagon very firm, not happening in that way between one hexagon and another. The graphitic structure comprises layers of these hexagons, one above the other. Still, unlike the firm bond inside the hexagons, the bond between the layers of hexagons is not that strong since the forces that bond them together are Van Der Waals forces; this is what allows the layers to displace between each other, being this effect what generate the lubrication properties of the graphite, but at the same time creates anisotropy. As a result of this structure, thermal and electrical conductivity along the parallel direction of the hexagon layers is good. However, they are poor perpendicular to the layers [29, 30, 31]. An image of the hexagons in the structure of the graphite is shown in Fig. 17.

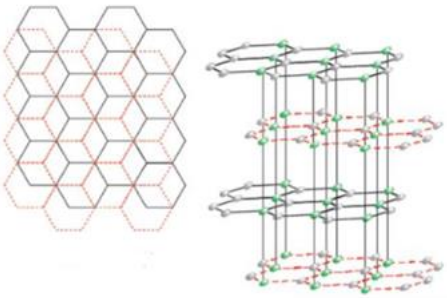

Figure 17. Structure of graphite [29].

The graphites used as row materials for this project are similar to the one described above but have significant differences that give them special characteristics.

2.7.2.1 Exfoliated graphite

This graphite results from an eco-friendly method based on a dry mechanochemical process. This method can avoid problems related to the use, dispose, manipulation, and elimination of corrosive and dangerous reagents. The method starts with a mixture of graphite flakes and calcium carbonate in equimolar proportions, which is milled for 12 hours in a high-energy milling, followed by a leaching process with an aqueous solution of acetic acid (8%) with magnetic stirring. Afterward, the powders are filtered and cleaned with deionized water. Finally, the powders are dried in an oven.

As a result of all these steps, the graphite particle size is reduced with a high level of exfoliation, which increases the surface area, providing adsorbing capabilities. This feature is a valid alternative for use as a multi-compositional filler, thermal isolation component, adsorbent for oil spilled in water, and material for organic dye removal [32].

2.7.2.2 Expanded graphite

This type of graphite is obtained by a green chemistry-based method, using a mixture of intercalation chemicals (sulfuric acid and hydrogen peroxide). These chemicals eliminate transition metal salts like permanganate or dichromate, generating a cleaner and simpler process. It not only avoids the use of higher amounts of those chemicals and water but also reduces energy costs.

The method starts with the mechanical milling of graphite flakes with sulfuric acid; a paste is obtained due to the milling process. Afterward, the paste is put in a cool bath with temperatures below 0°C. Once the paste is solidified, the hydrogen peroxide is added, and the reaction is carried out for at least 10 hours. Then, the graphite is filtered and dried in an oven, and finally, the dry powders are put in a domestic microwave for 15 seconds to expand the graphite particles. As a result of the process, graphite shows a high specific volume that provides high oil-water selectivity and adsorption rate [33].

The graphite before the expansion is in the form of flakes, which have the graphite c-axis perpendicular to the plane of the flake. Due to the significant expansion, the expanded flake becomes long in the c-axis direction of the flake. Consequently, the expanded graphite made from a graphite flake looks like a worm and is known

similarly. It is because of this structure that the expanded graphite exhibits properties (mechanical, thermal, electrical, dielectric, and other properties) that differ from those of conventional graphite and has numerous applications, including gaskets, electromagnetic interference (EMI) shielding, electrochemical electrodes, vibration damping, adsorption, thermal interfacing, etc.

The high surface area of expanded graphite is particularly valuable in applications such as adsorption (e.g., oil removal and phase change material incorporation), electrochemical uses (e.g., electrodes, supercapacitors, batteries, and gas sensors), and EMI shielding. The latter is desirable due to the skin effect. Expanded graphite is also a raw material for flexible graphite sheets, which find wide applications in sealing due to their properties like compressibility, resilience, thermal stability, and corrosion resistance [34, 35, 36].

2.7.2.3 Turbostratic graphite

This graphite comprises of carbon layer structures that are not ordered as in the case of the ordinary graphite. In contrast, turbostratic carbon layers are not fully aligned parallel. Therefore, its structure can correspond to graphene and exfoliated graphite. Its applications include sensors, composite strengthening, hydrogen storage, and lithium-ion batteries, among others. The synthesis method consists of a reaction between magnesium and carbon dioxide, as the following reaction shows.

$$2Mg_{(s)} + CO_{2(g)} \longrightarrow 2MgO_{(s)} + C_{(s)}$$

The next step is graphite purification since it ends up mixed with magnesium oxide and magnesium remanent. Before the leaching process, the powders of material must pass through mechanical milling to expose the magnesium oxide and magnesium to eliminate them during the next step. Aqua regia, whose composition is HNO_3:HCl 3:1 (in vol.), is the reactive used to make the leaching process. Afterward, the powders are filtered, cleaned, and dried. As a result of the process mentioned above, the surface area is also increased [37].

Work justification

Over the last decades, the broad commercial penetration of multiple petroleum-based polymers has led to severe environmental problems. Some of them include the accumulation of microplastics, excessive greenhouse gas emissions, the difficulty of recycling, and their persistence in marine and terrestrial environments. Bio-derived and/or biodegradable polymers could be considered a solution to the excessive use of most petroleum-based polymers if not for their weak inherent properties.

This project aims to study the introduction of exfoliated, expanded, and turbostratic graphite nanoparticles and their reinforced effect in the PLA matrix to produce a bio-friendly alternative to reduce the use of petroleum-based plastics.

General objective

To fabricate composite materials by Press and Fold, and solvent casting method using PLA as the matrix and exfoliated, expanded, and turbostratic graphite as the reinforcement phase, and evaluate their mechanical, electrical, and thermal properties with contents from 0.02 to 0.1 wt.% (in the case of Press and Fold process) and 1, 2, and 3 wt.% (in the case of solvent casting method).

Specific objectives

- Green fabrication and primary characterization (via Raman spectroscopy and microscopy techniques) of the exfoliated, expanded, and turbostratic graphite reinforcement.
- Nanocomposite synthesis through the distribution of the fillers via the press and fold method and solvent casting method.
- Mechanical, electrical, thermal, and morphological characterization of the produced nanocomposites.

Hypothesis

The incorporation of the exfoliated, expanded and turbostratic graphite in the PLA matrix using the Press and Fold method and solvent casting method will have a positive reinforcing effect on the properties of the final composites (an anticipated increase of about 15% in their mechanical properties). Due to the high surface area, electrical conductivity, and thermal stability, incorporating these reinforcements is

expected to increase the PLA's Young's modulus, tensile strength, electrical conductivity, and thermal stability, which are valuable properties for many industrial applications.

3.- Experimental methodology

3.1 Raw materials

PLA pellets and three modified graphites in powder form are available. Naturework LLC supplies PLA, and modified graphites were synthesized in Centro de Investigación en Materiales Avanzados (CIMAV). Graphite flakes, +10 - 325 meshes, and 99.8% purity (metal basis) supplied by Alfa Aesar were also used as material reference.

3.2 Fabrication processes

3.2.1 Press & Fold method (P&F)

The P&F cycles method was used to fabricate the biopolymer matrix composite; the number of cycles depends on how fast and easily the reinforcement can be homogeneously distributed in the matrix. A hot press will be used at temperatures just above the polymer's melting point (180°C). The pressure will be 100 bars.

First, the polymer pellets are put on a special paper sheet to avoid direct contact between the plates of the press and the pellets; the sheet placed between the two plates, and both plates get close without making contact for two minutes. Thus, the polymer's temperature is increased, facilitating the pressing step. Afterward, the pressing is sustained for 5 minutes. Once this time is over, the plates are separated and the sheets with the polymer are removed and put over an aluminum plate to reduce the polymer temperature. Then, the reinforcement is manually spread over the polymer sheet spread over the sheet with a spoon. After this, a second sheet of polymer prepared just like the first is put over the other polymer sheet, making a sandwich in which the element in the middle is the reinforcement; this sandwich is pressed with the same temperature and pressure parameters. After that, the polymer is folded twice to generate the quarter slide and put back inside the press to repeat the above-mentioned process. The number of cycles will depend on the distribution of the reinforcement in the polymeric matrix.

The equipment for this process is a Hot Press Collin P300E, which has a cooling water system and a controller to set up the pressure and temperature conditions, from 40 to 200 bar and from room temperature to 300 °C, respectively.

3.2.2 Solvent Casting method

To begin with this method, the PLA pellets are put inside a baker with 150 mL of chloroform (used as solvent), and magnetic stirrer is used until the PLA pellets are dissolved. Afterward, the corresponding amount of reinforcement is sonicated in an ultrasonic bath with 20 mL of chloroform for 30 minutes in another baker. Once the dissolved PLA and the sonicated reinforcement are ready, they are mixed, and the stirring lasts for 2 hours. Then, the mixture is sonicated now in a tap sonicate whose parameters are the following: 40% amplitude, room temperature, 20 KHz, 6 times for 15 seconds. Finally, the mixture is cast into a metallic container and is left to dry at room temperature overnight, followed by an additional drying process at 80°C overnight [38, 39]. It is worth mentioning that PLA was also dissolved without any amount of reinforcement to be used as the reference.

3.3 Characterization

3.3.1 FTIR

This technique will be used to characterize the biopolymer, so it is possible to identify its functional groups. It is based on the vibration of the atoms inside a molecule. An infrared spectrum is obtained when infrared radiation passes through a sample, thus, determining what fraction of the incident radiation is absorbed in a specific energy. That energy, in which a peak of absorption shows up, corresponds to a vibration frequency of a part of the molecule. To show absorption, the molecule must present an electric dipole moment; such dipole must be able to change during the vibration. Besides, the molecule must be heteronuclear. The more significant change in the dipole moment is, the higher the absorption is as the link expands and contracts [40].

The equipment to be used is FTIR-Bruker TENSOR27 with selectable sample dimensions between 1/8 and 1/2”. They fixed an 80-degree angle of incidence and used liquid nitrogen to cool the instrument detector. The spectrum range is from 7500 to 370 cm^{-1}, the resolution is better than 1 cm^{-1}, and the scan speed is 3 velocities: 2.2 - 20 kHz.

3.3.2 SEM

This technique will be used to observe the reinforcements' morphology and size, and the composites' microstructure. SEM is used for observing very small objects in stereographic and amplified images. One important feature of this equipment is that it can cover a wide range of amplifications from 10 to 1´000,000X. The equipment is a Hitachi SU3500 and an FEI Inspector Scanning Electron Microscope. This technique provides information about the sample's morphology, particle size, and distribution at different amplifications. Thanks to an electron beam, which provides better resolution due to its short wavelength instead of visible light in an optical microscope, chemical mappings can also be made to observe the distribution and concentration of the particles or elements in the sample.

There are several ways to obtain this electron beam, but the most used is thermionic emission. This phenomenon occurs when the heated tungsten filament gives place to the expulsion of the electrons from the solid. Then, these electrons are accelerated by a potential difference and directed by electromagnetic glasses until the sample is reached. As a result of the interaction between the electron beam and the sample some signals are generated that can provide information about the sample having suitable detectors. We can find secondary electrons, backscattered, absorbed, characteristic X-ray and auger electrons, and transmitted and diffracted electrons [41].

3.3.3 Raman spectroscopy

This technique will be used to obtain structural information on the reinforcements. The equipment is a Raman microscope INVIVA model Qontor. This high-resolution photonic technique provides chemical and structural information on organic/inorganic materials, allowing its identification. The analysis is based on the scattered light from a material when a monochromatic light beam hits its surface. A small portion of the light is scattered inelastically undergoing slight changes in frequency; such changes are characteristic of the material and independent of the frequency of the incident light. This analysis does not make any change in the surface of the material.

Ions and atoms chemically bond to form molecules and crystal lattices to form molecules and crystal lattices are subjected to constant vibrational and rotational movements at well-determined frequencies. Any of these vibrational and rotational movements corresponds to a determined value of molecular energy [42].

3.3.4 Tension test

This test is used to obtain the stress-strain curves, Young's modulus, and tensile strength of the composites and the polymer without reinforcement. The dimensions of the sample are specified in the standard ASTM D638 (type V). The equipment for this test is an Instron Frame 5967, which has a video extensometer, crosshead, load cell, and manual controller.

This destructive test process provides information about material's tensile strength, yield strength, and ductility of materials. It measures the force required to break a specimen and the extent to which the specimen stretches or elongates to that breaking point. These produce a stress-strain curve to determine Young's modulus [43].

3.3.5 Four points test

This technique is used to obtain the conductivity and resistivity of the composites and neat polymer. The equipment is an Agilent 6614c with system power (0-100V/0.0.5A), a pico ammeter (Keithely 6485, 2nA–20mA), and a personal computer.

A four-point probe measurer is commonly used to measure resistivity and conductivity. This measure relies on four probes: two for electric current and the other for voltage when applied to the sample. The resistivity value needs to be measured for a certain area and thickness to determine and review the characteristics of the material. It is called four-point probe because four points touch the sample surface. Those four points (probes) are lined in a straight line with the distance between probes arranged so that each of the probes has the same distance. A constant electric current is streamed along the sample through two outermost probes. If the sample has resistance, there will be a voltage drop when the current flows along the sample. The voltage change is measured through two inner probes. The electrical quantity that shows the quality of material conductivity, such as output voltage and output current, can be determined meticulously using the four-point probe method [44].

3.3.6 DSC

This technique will be used to determine the melting enthalpy of the samples. The equipment is a DSC 25 from TA Instruments. This dynamic technique provides information about the amount of heat the sample absorbs or releases through the enthalpic difference between the analyzed material and reference material. This method can determine specific heat, crystallinity, compound purity, reaction enthalpies, glass transition temperature, melting point, polymerization reactions, and the curing process. Any reaction followed by an enthalpic change can be detected by this technique [45].

3.3.7 TGA

This technique will be used to determine the thermal stability of the materials. The equipment is a TGA 5500 from TA Instruments. In this instrument, the mass of the sample is registered continuously inside a controlled atmosphere as a function of either the temperature or the time. The representation of mass as a function of the time thermogram or degradation curve. This method is used to study polymers since these thermograms provide information about degradation mechanisms. Moreover, in some cases, this method can identify polymers since each polymer's degradation models are characteristic. This technique also allows us to determine the amount of inorganic load, moisture, and composition [45].

3.3.8 XPS

This technique will be used to determine the chemical information about the reinforcements. The equipment is an XPS Thermo Scientific Nexsa. This technique is based on the photoelectric effect in which the electrons are emitted from surfaces when irradiated with light. XPS (X-ray photoelectron spectroscopy) is a surface analytic technique in which X-rays are irradiated on a material's surface, and the emitted electron's kinetic energy is measured. Two advantages of this technique are its surface sensitivity and its ability to reveal chemical environment information from the elements in the sample, all elements except hydrogen and helium. XPS can be used in almost any kind of material: plastics, textile, soils, semiconductors, and so on. Any electron with a binding energy lower than the X-ray source should be emitted from the sample and observed using this technique. The binding energy is a material property independent of the x-ray source [46].

4.- Experimental

4.1 Raw materials

- PLA polymer pellets supplied by Naturework LLC (98% purity).
- Graphitic reinforcement in the form of powder.
- Chloroform supplied by Sigma-Aldrich (99.5% of purity).
- Graphite flakes, +10 - 325 mesh (99.8% purity) supplied by Alfa Aesar.

4.2 Used equipment

- Hot press Collin P300E
- FTIR-Bruker TENSOR27
- Instron Test Frame 5967
- Agilent 6614c
- Ultrasonic probe
- DSC 25
- TGA 5500
- Raman microscope INVIVA
- Scanning Electron Microscope Hitachi SU3500
- XPS Thermo Scientific Nexsa

5.- Results

5.1 Characterization of raw materials

5.1.1 PLA

The spectrum obtained by FTIR analysis of PLA shows characteristic peaks of C=O, asymmetric -CH_3, symmetric -CH_3, and C-O around 1746, 2995, 2946, and 1080 cm^{-1}, respectively. Some peaks can also be identified around 1120 and 1180 cm^{-1} due to the presence of ester groups [47, 48, 49]. In addition, C-H bending around 1450 cm^{-1} are shown. The spectrum obtained from the FTIR analysis is shown in Fig. 18.

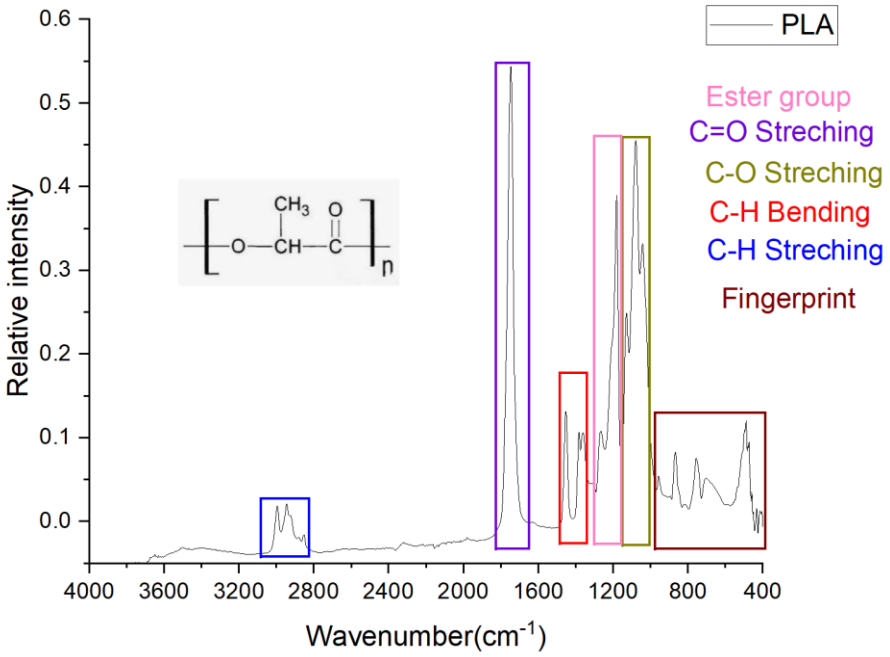

Figure 18. FTIR spectrum of PLA.

5.1.2 Exfoliated graphite

In the images of exfoliated graphite taken by SEM, the reinforcement particles tend to agglomerate in bigger particle sizes, mostly around 2 µm in diameter. As a result of the milling process, the graphite suffers an exfoliation in which the compressive and shear forces dominate over the Van de Waals forces and reduce the particle size by breaking the graphite sheets [32]. Fig. 19 and 20 show the images of the exfoliated graphite and the corresponding frequency histogram with the size distribution of it, respectively.

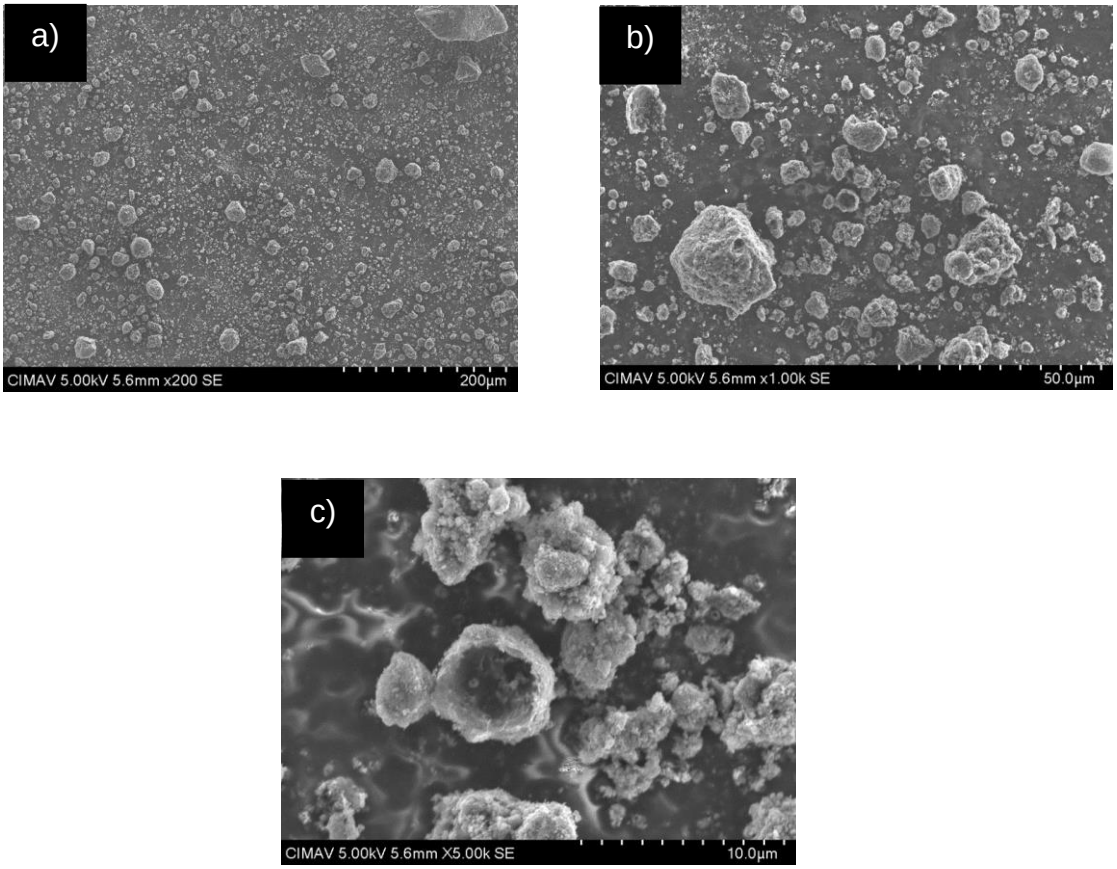

Figure 19. SEM-SE images of exfoliated graphite.

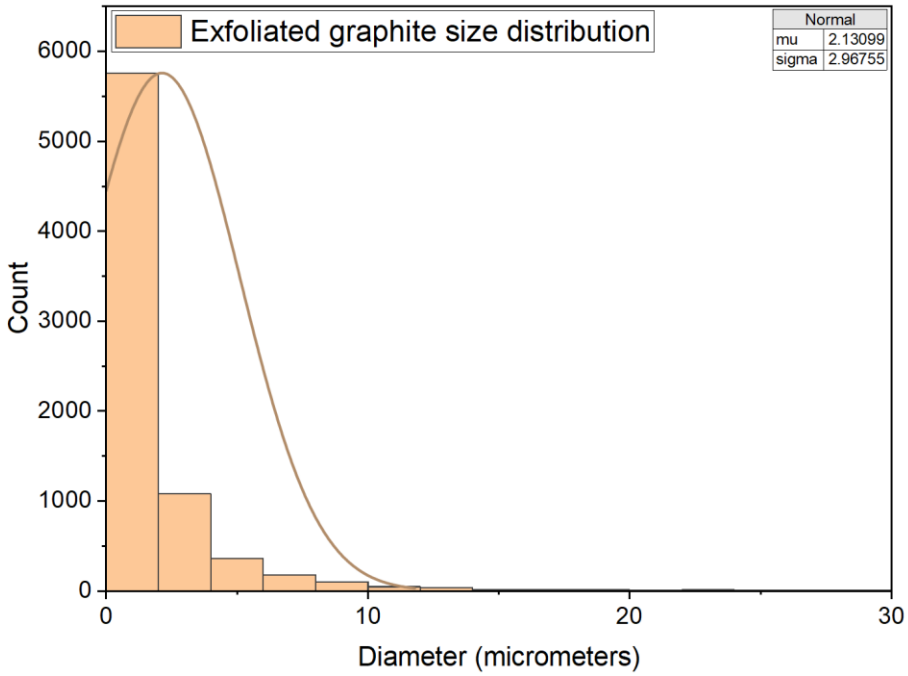

Figure 20. Frequency histogram with the size distribution.

In contrast, the original graphite shows a clear form of flakes with sizes between 74 and 7 µm, most of them being between 10 and 30 µm with a surface flatter than the one of the exfoliated graphite. In addition, these flakes also show a trend to agglomerate. In Fig. 21, images of the original graphite are shown.

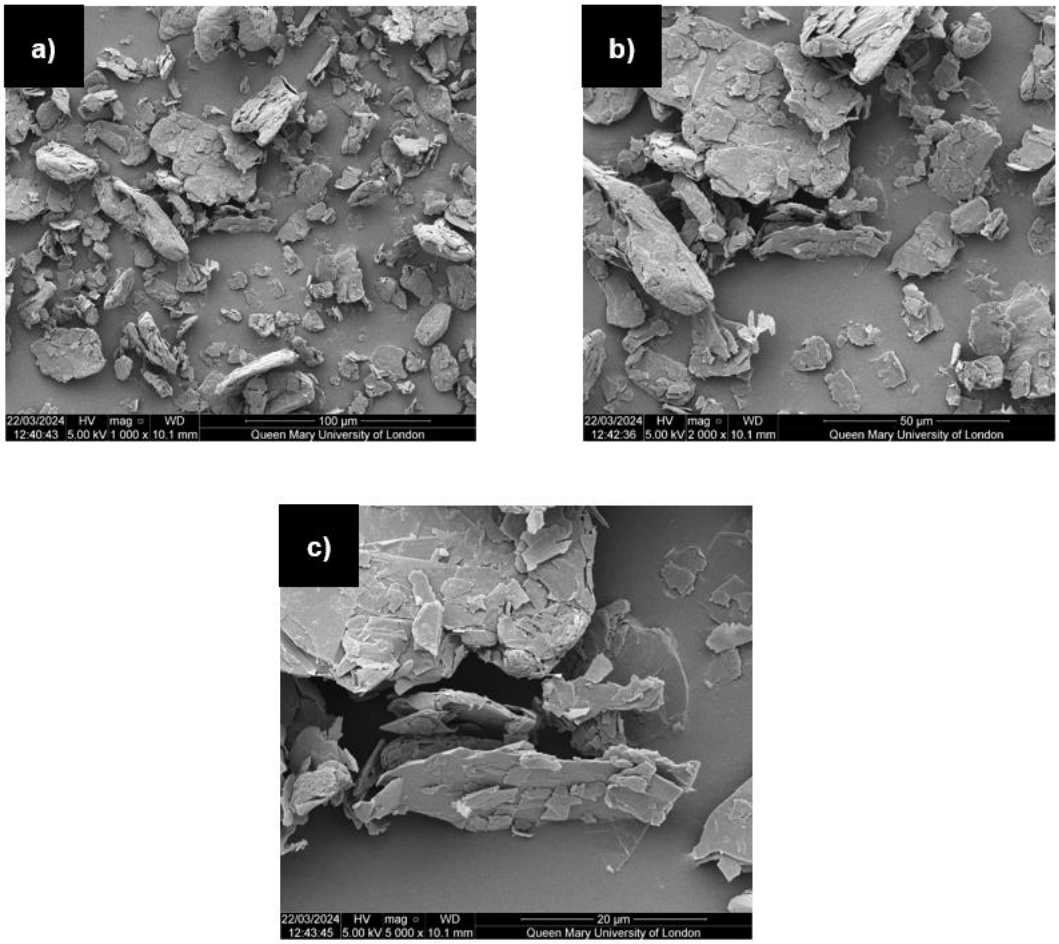

Figure 21. SEM-SE images of original graphite.

The spectrum obtained by Raman spectroscopy shows the representative signals of graphitic structures commonly known as D, G, and 2D, which are usually seen in case of original graphite at 1350, 1580, and 2700 [32, 40, 51]. However, in the case of the original graphite used as reference the D, G, and 2D bands can be seen at 1373, 1578, and 2756 cm^{-1}, respectively. In Fig. 22 the Raman spectrum of the original graphite is also shown.

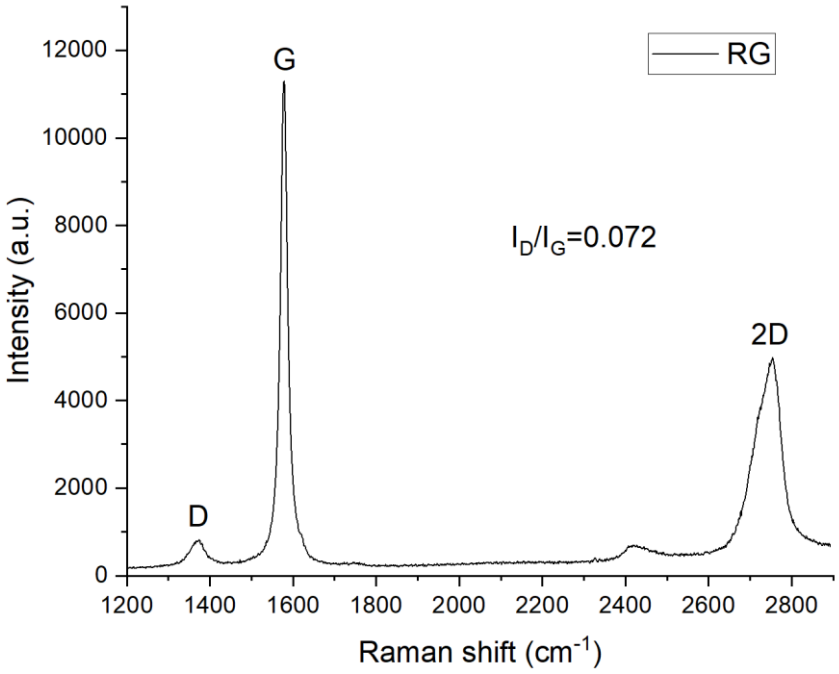

Figure 22. Raman spectrum of original graphite.

The exfoliated graphite D, G, and 2D bands are around 1348, 1582, and 2685 cm^{-1}, respectively. The D band is associated with the disorder-induced scattering due to imperfections or loss of disordered graphite's hexagonal symmetry, including vacancies or inclusions generating tetrahedral sp^3 carbon. On the other hand, the G band is related to the vibration of sp^2-bonded carbon atoms in a two-dimensional hexagonal lattice. The 2D band is an indicator of the exfoliation of the graphite. The shape and position of this band provides information on the number of graphene layers per flake. As the material moves from original graphite to a specific number of graphene layers, the 2D band moves from higher to lower wavenumbers. Since it is proportional to the number of graphene layers whereby with more layers, higher energies are required to generate an in-plane vibration. Ma and coworkers generated an exfoliation process to obtain a graphene layer from pristine graphite using an ammonia solution together with an ultrasonic bath [52]. They noticed the changes mentioned above in the 2D band, which is proof of the exfoliation of graphite. [51, 53, 54, 55, 56]. Therefore, the 2D band is at 2685 in the Raman spectra, indicating the exfoliation received by mechanical milling process.

Another important parameter is the intensities ratio of D and G bands (I_D/I_G) which is generally used as a measure of disorder or graphitization. This value, 0.19, indicates fewer defects [58]. This also explains the lower value of this ratio in original graphite

compared with exfoliated graphite, which is 0.072. In Fig. 23, the Raman spectrum of exfoliated graphite is shown.

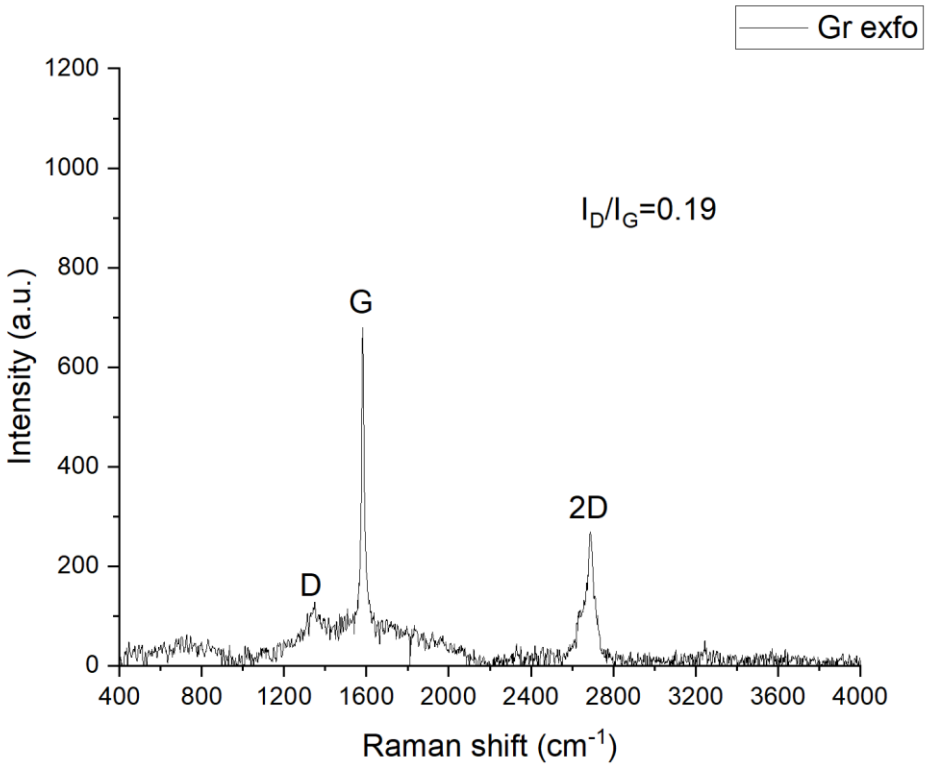

Figure 23. Raman spectrum of exfoliated graphite.

The XPS analysis shows the chemical composition of this reinforcement; the spectrum and the composition are shown in Fig. 24 and Table 1, respectively. Some characteristic peaks of carbon and oxygen can be seen around 285 and 233 eV, respectively. Both characteristic peaks come from the 1s orbital of each of the atoms. In addition, some auger peaks can also be seen from both elements in the same spectrum. Since there is no calcium detected in the analysis, the presence of oxygen in the reinforcement is due to the formation of functional groups as a result of the milling process.

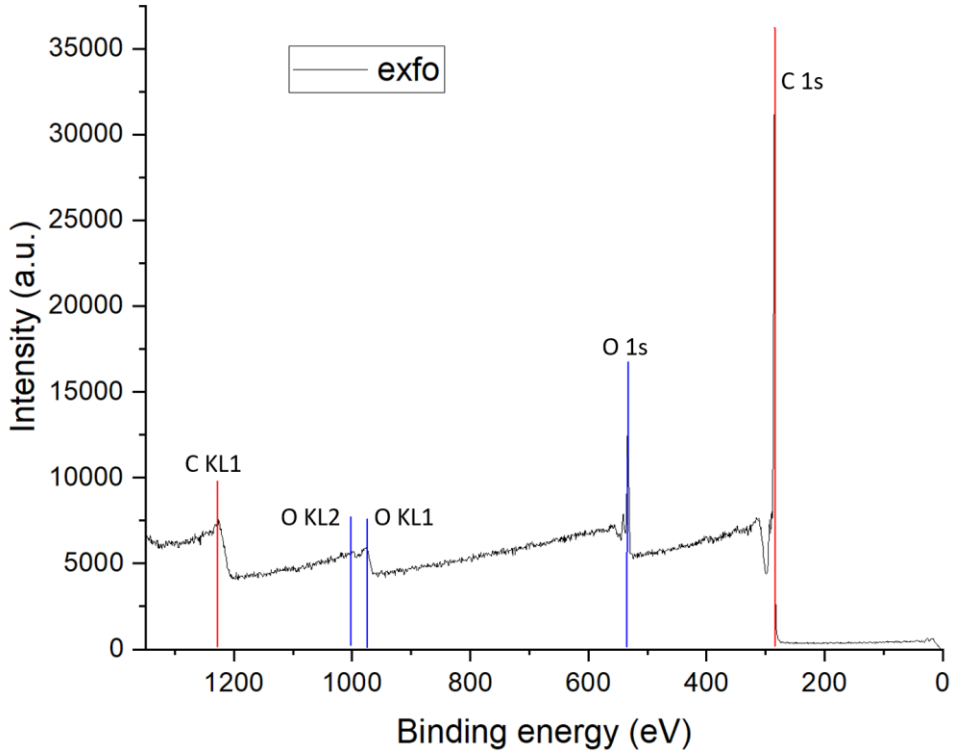

Figure 24. XPS spectrum of the exfoliated graphite.

Table 1. Chemical composition of the exfoliated graphite

Element	Atomic %
C	87.77
O	12.23

A high-resolution scan of the C 1s peak can be seen in Fig. 25, in which the different bonds that perform carbon are shown. The most prominent peak is the C=C bond related to the graphitic carbon in a sp^2 hybridization. In addition, the second most prominent is the C-C bond related to the disorder carbon structure sp^3 hybridization. The fact that the C=C bond percent is higher than the one of the C-C agrees with the analysis made by Raman spectroscopy in which is clear that the disorder degree is relatively low despite the large mechanical milling process. The third peak is related to the C-O bond representing hydroxyl and ether functional groups located on the graphene basal plain. The next peak represents the C=O bond due to the presence of carbonyl group located at the edges of the graphene sheets [59, 60, 61, 62, 63, 64, 65, 66]. The last peak seen in the spectrum is a characteristic shake-up

satellite due to the aromatic ring structure [67, 68, 69, 70, 71, 72]. In table 2 the bonds percentage in exfoliated graphite are shown.

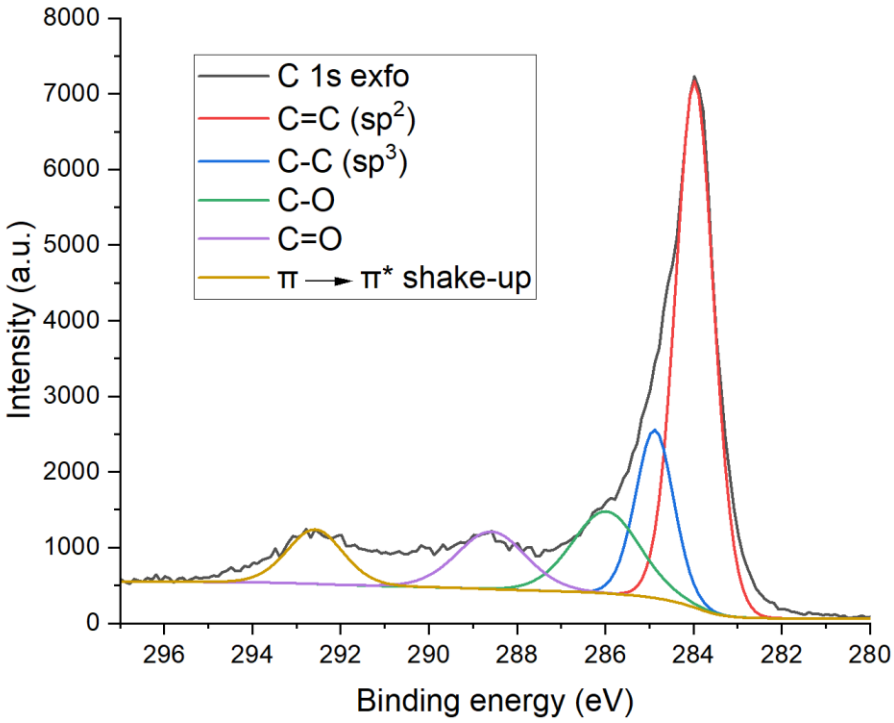

Figure 25. High-resolution scan of C 1s peak of exfoliated graphite.

Table 2. Bonds percentage of exfoliated graphite.

C 1s	Bond %
C=C (sp^2)	55.66
C-C (sp^3)	17.87
C-O	15.48
C=O	10.99

5.1.3 Expanded graphite

In the images of expanded graphite taken by SEM, the characteristic worm form can be seen as a result of the expansion process [34, 36]. The length of these worms can be up to around 500 µm and width of around 200 µm. The expansion along the c-axis perpendicular to the plane flake in the particles is clear. In addition, it is

possible to see the openings between the layers of around 20 µm generating a huge increase in the surface area of the material. In Fig. 26 are shown SEM images of expanded graphite.

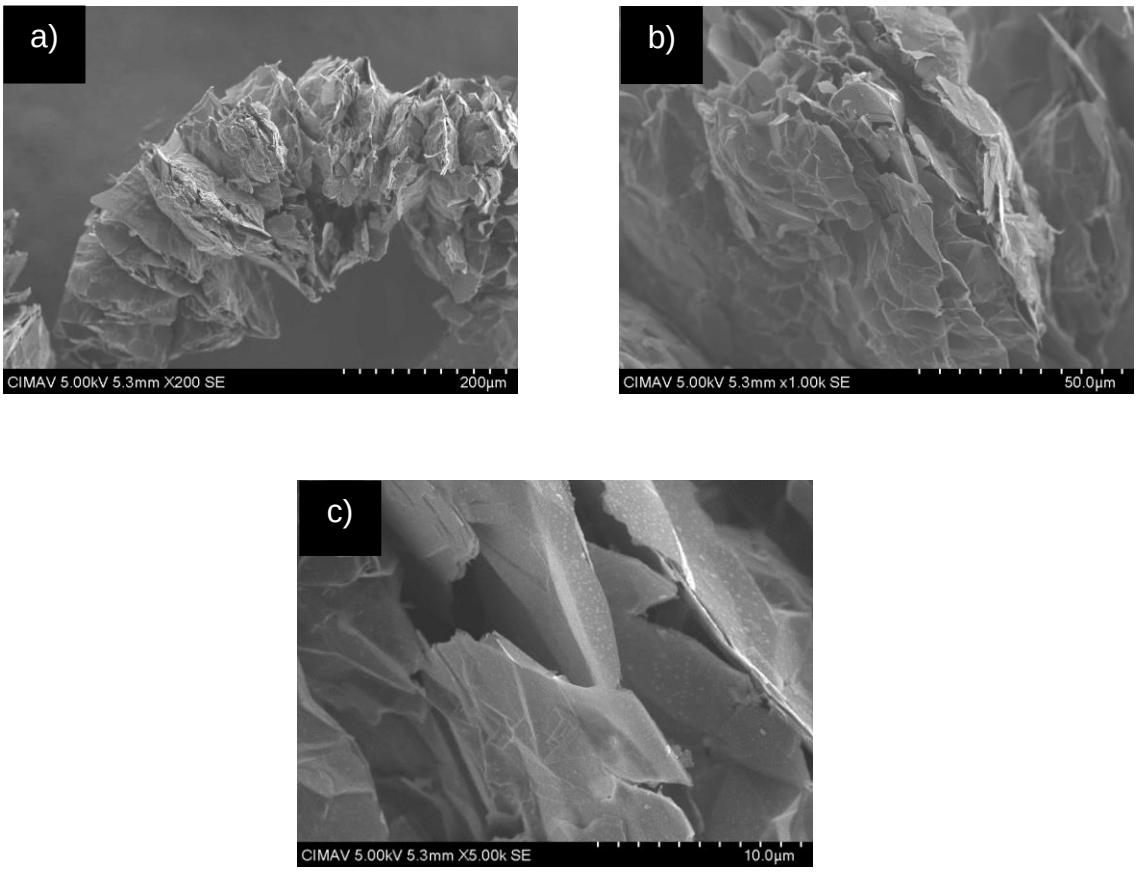

Figure 26. SEM-SE images of expanded graphite.

The Raman spectroscopy analysis yielded a spectrum exhibiting characteristic bands, identical to those observed in exfoliated graphite, at the D, G, and 2D positions of 1372, 1578, and 2756 cm^{-1}, respectively. The presence of the 2D band at 2756 cm^{-1} suggests that a higher vibrational energy is required, which might be attributed either to the separation between layers following the expansion process or to the fact that some layers within the worm-like structure remained compact and closely aligned, driving the wavenumber up. Notably, the G band appears more prominently than in the exfoliated graphite, likely because the expansion process, which lacks extensive mechanical milling, introduces fewer defects. This is corroborated by the lower I_D/I_G intensity ratio of 0.049. Figure 27 shows the Raman spectrum of the expanded graphite.

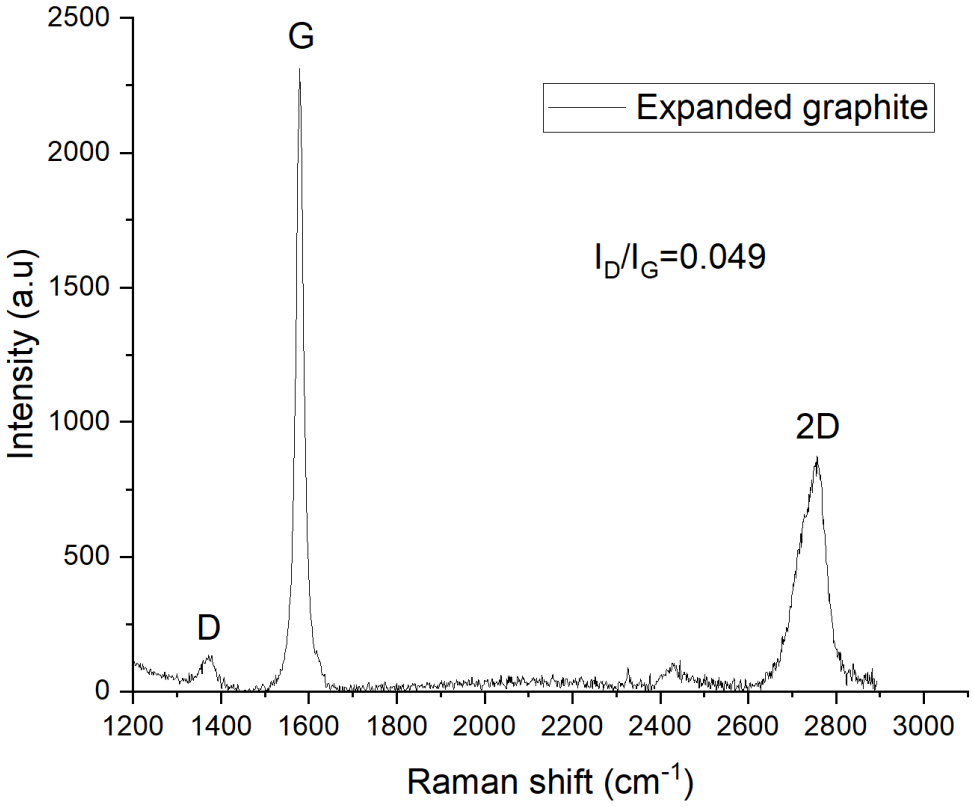

Figure 27. Raman spectrum of the expanded graphite.

The chemical analysis made by the XPS technique shows the presence not only of carbon and oxygen, but also of nitrogen and sulfur, two more elements than in the case of exfoliate graphite. The sulfur found in the XPS spectrum can be due to the interaction of the sulfuric acid with the graphite in the synthesis process. In addition, the presence of oxygen is for the same reason. However, nitrogen must be due to some contamination which would explain the low amounts of this element in the analysis. Characteristic carbon, nitrogen, sulfur, and oxygen peaks can be seen as a result of electrons ejected from the 1s, 2s and 2p bands, along with some auger peaks only for carbon and oxygen. In Fig. 28 and Table 3 the XPS spectrum and the chemical composition of expanded graphite are shown, respectively.

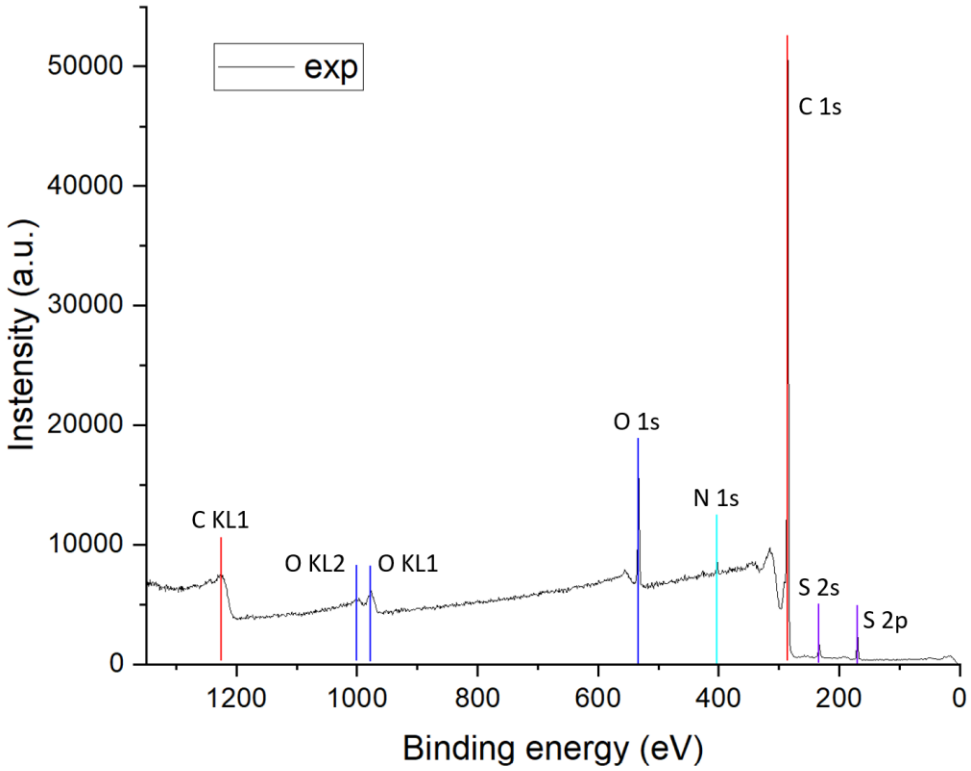

Figure 28. XPS spectrum of expanded graphite.

Table 3. Chemical composition of expanded graphite

Element	Atomic %
C	87.28
O	9
S	2.25
N	1.47

The high-resolution scan of the C 1s peak shows the same peaks seen in the exfoliated graphite scan with the addition of C-S and C-N bonds. The peak that is related to the C-O bond possesses a binding energy similar to the C-S bond, which is related to the other functional group. Therefore, both bonds contribute to the size of this peak [70]. Remarkably, the difference between the percentage between C=C and C-C bond is higher, which also confirms the lower disorder degree in the expanded graphite compared with the exfoliated graphite. Moreover, the percentage of the C-O and C=O bonds is lower than in the exfoliated graphite, even when the oxygen percent in the filler is only 3% lower than in exfoliated graphite. A possible explanation is that since the sample contains nitrogen and sulfur, the oxygen has

generated some bonds with these elements, decreasing the percentage of carbonyl, hydroxyl and/or ether groups in the sample. Lastly, the presence of C-N bond is detected around 286 eV related to the amine functional group [73]. Fig. 29 and Table 4 show the high-resolution scan of the C 1s peak and the bond percentage of the expanded graphite, respectively.

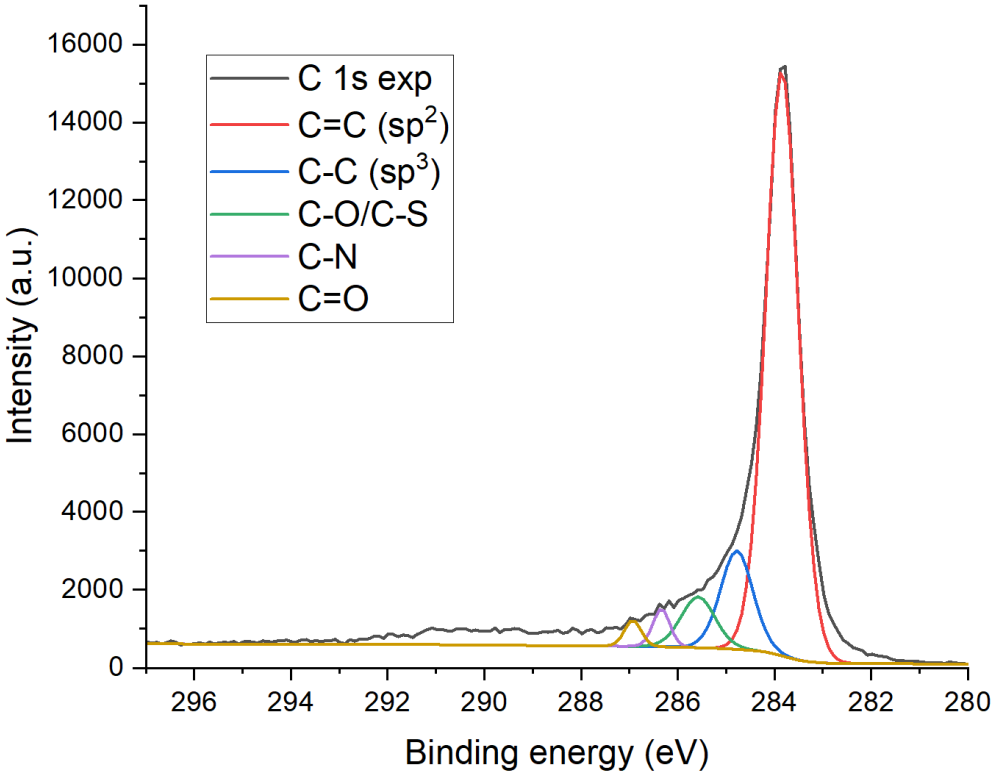

Figure 29. High-resolution scan of the C 1s peak of expanded graphite.

Table 4. Bond percentage of expanded graphite.

C 1s	Bond %
C=C (sp^2)	76.03
C-C (sp^3)	12.75
C-O/C-S	6.9
C-N	2.58
C=O	1.73

5.1.4 Turbostratic graphite

In SEM images the particles tend to agglomerate into bigger particles, mostly around 2.7 µm. These particles show very well-defined sharp corners, edges, and rough surfaces. Likewise, it is possible to identify some particles in flake form. In Figs. 30 and 31, SEM images of turbostratic graphite and a frequency histogram with the size distribution of the turbostratic graphite particles are shown, respectively.

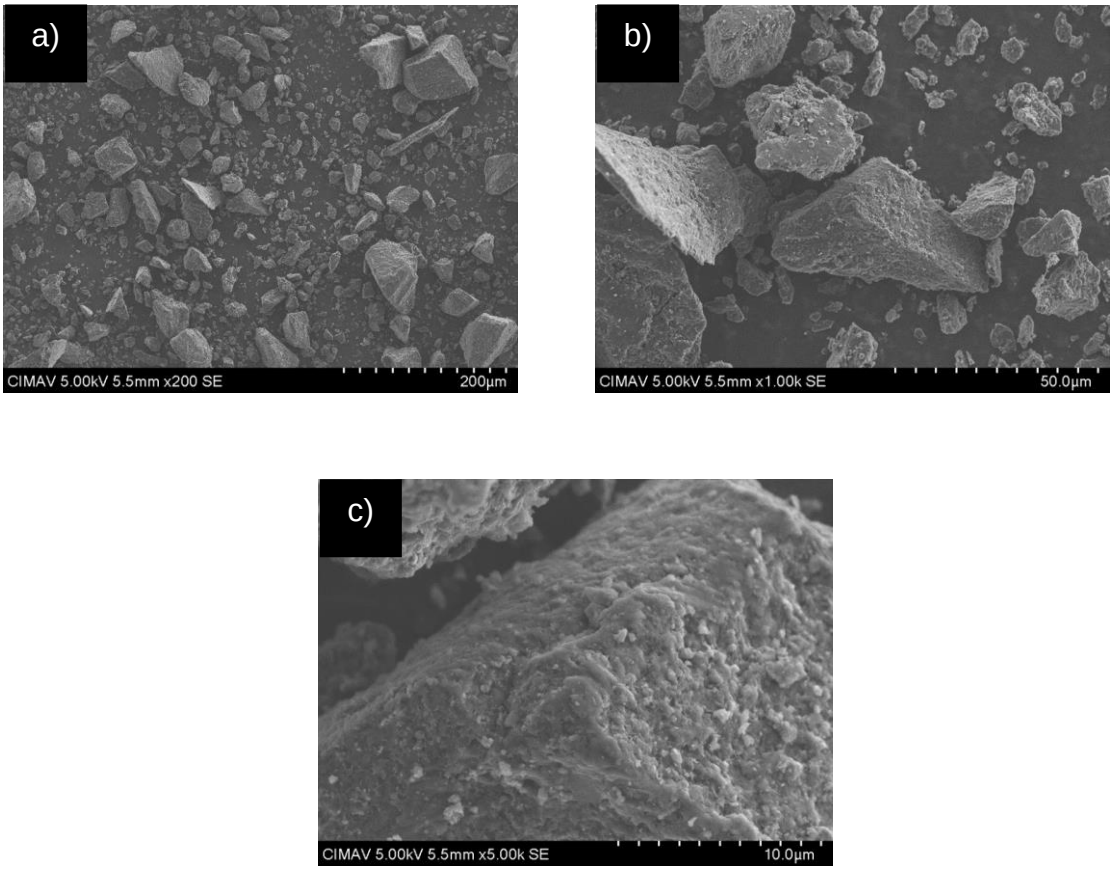

Figure 30. SEM-SE images of turbostratic graphite.

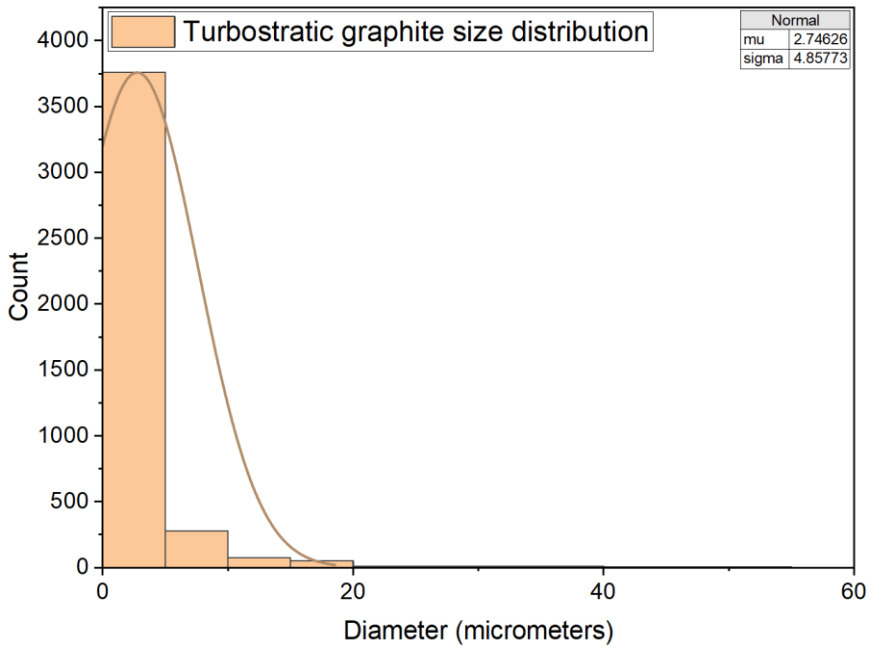

Figure 31. Frequency histogram with the size distribution.

The spectrum obtained by Raman spectroscopy shows the same signals viewed in the expanded and exfoliated graphite. The D, G, and 2D signals can be seen at 1332, 1600, and 2660 cm^{-1}. The first thing to note is that D band increased considerably compared to the other graphites, even higher than the G band, which gives a value of the intensity ratio (I_D/I_G) of 1.37. This can be explained due to the disorder in the structure of turbostratic graphite. Since the structure is characterized by an irregular stacking of parallel graphite monolayer with no periodicity existing along the c-axis. In this structure the layers are shifted and rotated randomly, and the space between layers varies from plane to plane. Moreover, the shape of the 2D band is different, while in the other 2 graphites, the 2D band shows a shoulder, giving it an asymmetric shape; in turbostratic graphite, this shape is symmetric, just like the 2D band of the graphene Raman spectrum. With an increase in the number of graphene layers, the shape of the 2D band tends to be more like the 3D original, exfoliated, and expanded graphite, an asymmetric shape. This asymmetry in the 2D band is the result of 3D graphitic ordering (AB stacking) of the lattices. Therefore, the lack of stacking order among the graphene planes weakens interplanar interaction and allows turbostratic graphite to be considered a 2D structure. In addition, the 2D band is now at 2660 cm^{-1}, which denotes that less energy is necessary to generate a vibration in the in-plane structure. Another feature to remark on is a peak around 2913 cm^{-1}. This peak is assigned to a combination of 2D overtone, and G and D modes (G+D) characteristic of disordered graphitic

structures. Radhika and coworkers studied the tribological behavior of turbostratic graphite using different ceramic balls for the wear tests; they found the 2D peak with the characteristics mentioned above and the 2D overtone. In addition, in work carried out by Binder and coworkers, the same features were found in the spectrum obtained from graphite nodules produced by powder injection molding and sintering of SiC particles dispersed in the matrix to obtain an iron-based self-lubricating composite. Likewise, Kumar and coworkers developed high-temperature treatments over turbostratic graphite, and the same peaks and features were found [74, 75, 76]. Fig. 32 shows the Raman spectrum of turbostratic graphite.

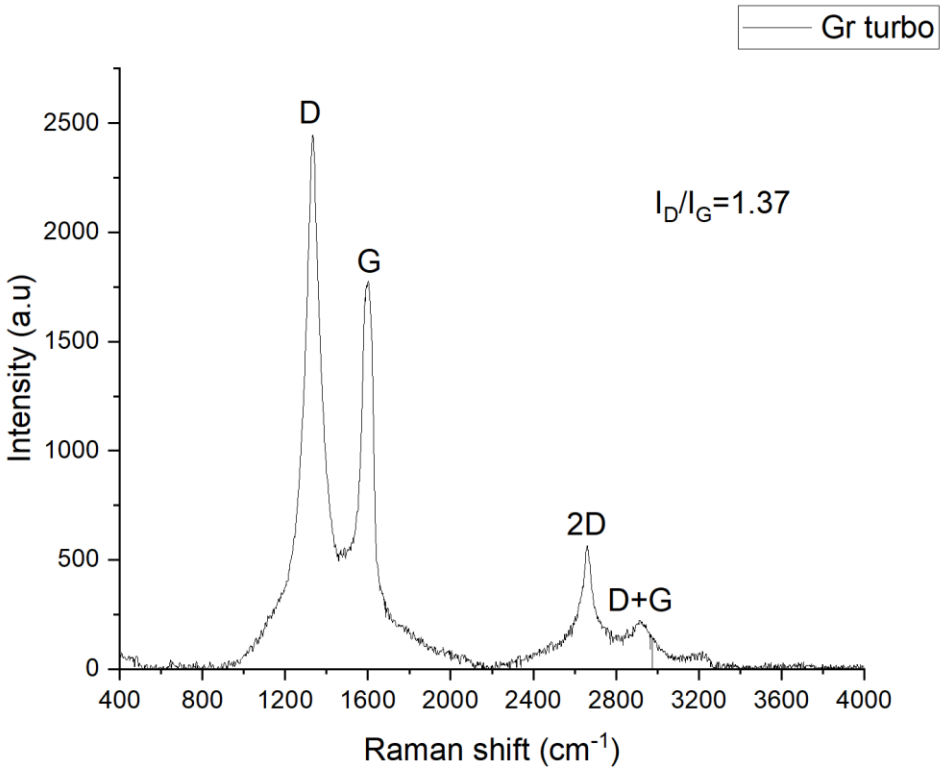

Figure 32. Raman spectrum of turbostratic graphite.

The XPS analysis shows the presence of mainly carbon, oxygen, and chlorine. The fact that magnesium is not detected denotes that the leaching process was effective in removing the magnesium oxide from the reinforcement. However, due to this process, there is a percentage of oxygen similar to the one found in the case of exfoliated graphite. In the XPS spectrum shown in Fig. 33 there are characteristic peaks of carbon and oxygen with electrons coming from the 1s orbital along with some auger peaks. In addition, there are peaks characteristic of chlorine with

electrons coming from the 2s and 2p orbitals. Table 5 shows the chemical composition of the turbostratic graphite.

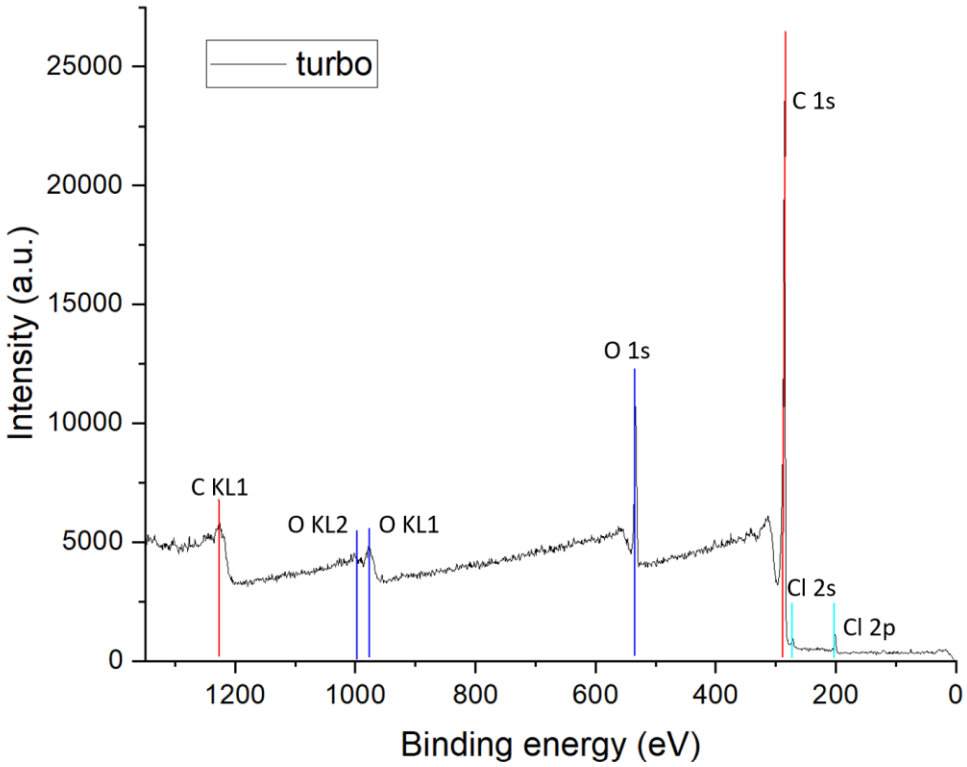

Figure 33. XPS spectrum of turbostratic graphite.

Table 5. Chemical composition of turbostratic graphite.

Element	Atomic %
C	86.43
O	12.34
Cl	1.23

The high-resolution scan of the C 1s peak shows the same peaks seen in the case of exfoliated graphite with the addition of one more peak due to the C-Cl bond around 287 eV [77]. Firstly, the difference between the C=C and C-C percentages is lower due to the higher degree of structural disorder, which agrees with the results found in the Raman analysis. In addition, the percentage of hydroxyl and ether groups found in the analysis is almost the same in the case of exfoliated graphite. However,

in the case of carbonyl group, it is clearly decreased compared with exfoliated graphite likely because of chlorine, which might be moving the oxygen apart to generate a bond with carbon. Fig. 34 shows the scan of the C 1s peak and Table 6 shows the bond percentage of turbostratic graphite.

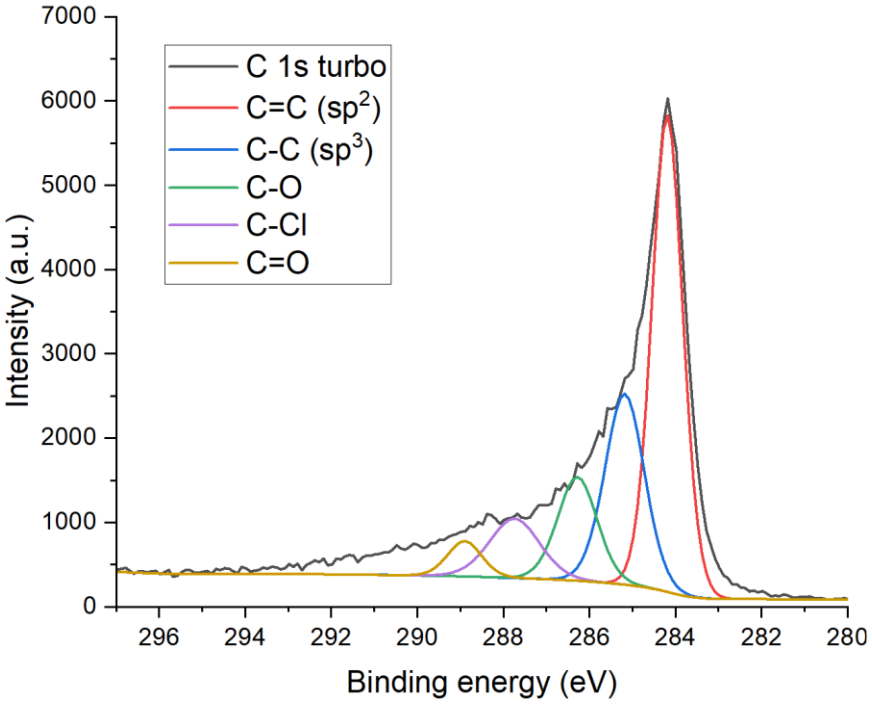

Figure 34. High-resolution scan of the C 1s peak of turbostratic graphite.

Table 6. Bond percentage of turbostratic graphite.

C 1s	Bond %
C=C (sp^2)	47.77
C-C (sp^3)	24.58
C-O	13.37
C-Cl	9.76
C=O	3.92

5.2 Mechanical characterization

5.2.1 Press & Fold process

Three composite materials were prepared by this process using 20 P&F cycles, each of the composites with a load of 0.02 wt.% with different reinforcement, the times used for heating and pressing were 1 and 3 minutes, respectively. It should be mentioned that the first composite was fabricated with heating and press times of 2 and 5 minutes respectively. However, the material started to get very brittle at 28 cycles, presumably, because of the increase of the crystallinity. This was the reason for the change in the heating and pressing time, to allow more cycles without getting the material too brittle. The tensile samples were prepared in the hot press with a mold with the dimensions of the type of sample selected.

After testing the 3 composites and the neat PLA, none of the samples showed a clear increase in Young's modulus and tensile strength. Otherwise, there was a decrease in all the materials. This was something somehow expected since the literature establishes that when too low amounts of reinforcement are incorporated into the matrix, this can generate that these particles, instead of acting as reinforcement, act as heterogeneities, generating a decrease in the mechanical properties of the composites because the transfer of stress from the polymer to the particles is not carried out efficiently. Istrate and coworkers fabricated composite materials using PET as the matrix and exfoliated graphene layers as reinforcement in contents of reinforcement between 0.001 and 0.1 wt.%. They realized that when the loads of reinforcement were lower than 0.04%, the presence of the graphene layers prohibited the reorientation of polymer chains, leading to the premature break of the polymer chains [78]. However, all these composites had something else in common, it was still possible to detect some little agglomerations with the naked eye. Therefore, the distribution was not as good as it should be to generate an increase in mechanical properties. It is because of this that the next two composites were fabricated first, with a higher amount of exfoliated graphite (0.1 wt.%), and second, for one of the composites the times for heating and press were reduced to 1 minute for both, allowing a higher number of cycles, getting to 30 cycles. After testing the materials, none of them showed an increase, they showed even lower mechanical properties than the first three composites. The amount of reinforcement might have been still not high enough to generate an increase. The next two composites were fabricated with 1 wt.% of reinforcement, one reinforced with exfoliated graphite and the second with expanded graphite, to verify if this decrease in the mechanical properties had to deal with reinforcement in specific. Again, 30 cycles were used.

After the tensile test, both composites, like the others, showed decreased mechanical properties, with the one reinforced with expanded graphite having the lowest values.

All composites until this point were fabricated at 180 °C, supposing that the polymer's melting point was between 170 and 176 °C. A DSC test was carried out to determine

the polymer's melting point. In this test the sample of PLA was firstly heated to 200°C, then cooled down to 20°C, and finally, heated again to 200°C. In the DSC curve, there is an endothermic related to the melting of the PLA. As a result of this analysis, it was discovered that the melting point of the polymer was 153°C. Therefore, since the Press & Fold method requires the temperature to be just above the melting point, it might be possible that the composites were not reinforced because the temperature was too high. Fig. 35 shows the DSC curve of neat PLA.

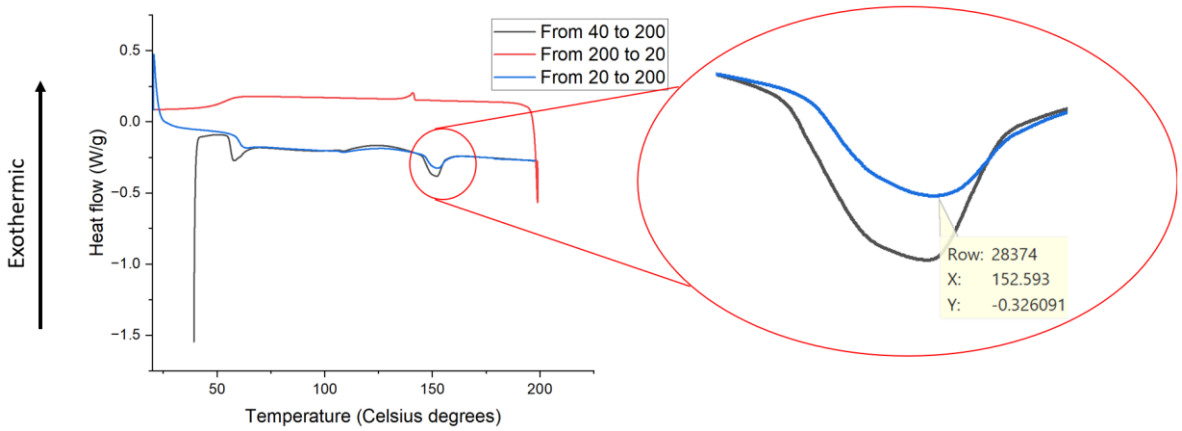

Figure 35. DSC curve of neat PLA.

Two more composites were prepared at lower temperature (160°C). Both composites were reinforced with 1 wt.% of exfoliated graphite, but one of the composites was fabricated with a heating and press time of 30 seconds, each one allowing 50 P&F cycles, while the other kept the heating and press time of one minute, allowing 30 cycles. The composite fabricated with 50 cycles showed an increase in Young's modulus and tensile strength of about 3 and 7.5 %, respectively. On the other hand, the composite fabricated with 30 cycles showed a decrease of 5% in Young's modulus and an increase of 3% in tensile strength. Despite the increase achieved in the composite fabricated with 50 cycles, this increment is very low for the load of reinforcement used. Cataldi and coworkers fabricated PLA composite materials reinforced with graphene nanoplatelets by a solvent casting process and a mixture of both solvent casting followed by a hot press step. They realized that the elastic modulus of the neat PLA was decreased after the hot press step, and it was attributed to the change in crystallinity. Moreover, they highlighted that the increase in the elastic modulus is not that high due to the semi-crystallinity and inherent stiffness of PLA polymer that tend to impede polymer chain mobility, limiting the reinforcement reorientation within the matrix [39]. Fig. 36 shows the

stress-strain curves of the composites fabricated by the Press & Fold process. Moreover, Table 7 shows the mechanical properties of neat PLA and composites fabricated with Press & Fold process. The table's nomenclature is used to specify each composite's parameters. For example, a composite with heating and pressing times of 3 and 1 minutes, respectively, is marked as t31. In addition, the temperature used in the process is also shown for each composite.

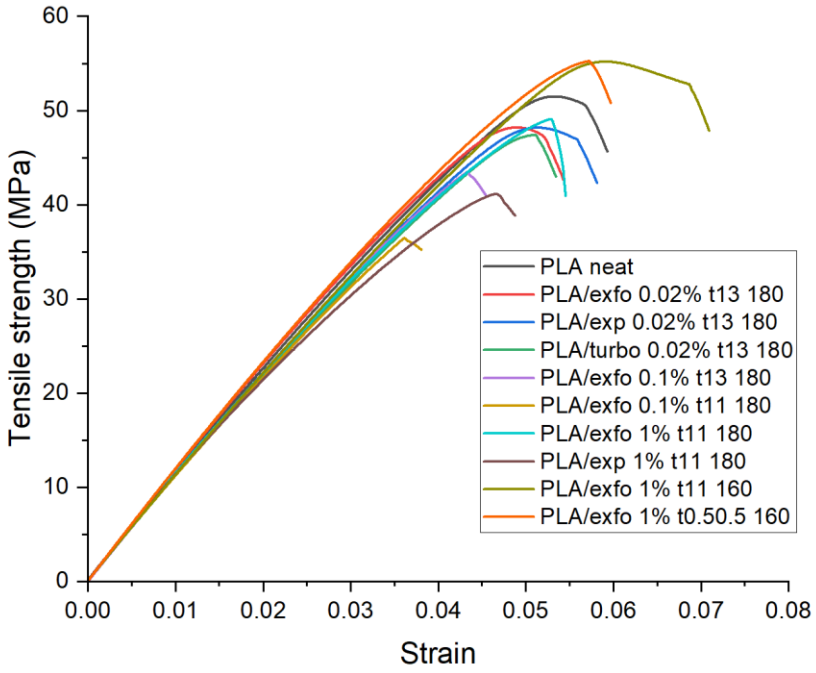

Figure 36. Stress-strain curves of the composites fabricated by the Press & Fold process.

Table 7. Mechanical properties and comparative chart of composites fabricated by P&F method.

Material	Young's modulus (GPa)	Tensile strength (MPa)	Young's modulus increase/decrease (%)	Tensile strength increase/decrease (%)
PLA	1.07 ± 0.03	51.57 ± 1.27	0.00	0.00
PLA/exfo 0.02% t13 180	1.06 ± 0.02	49.49 ± 1.11	-0.84	-4.03
PLA/exp 0.02% t13 180	1.1 ± 0.03	48.35 ± 1.96	2.68	-6.25
PLA/turbo 0.02% t13 180	1.04 ± 0.04	47.77 ± 1.47	-3.05	-7.36
PLA/exfo 0.1% t13 180	1.06 ± 0.03	45.25 ± 3.14	-0.90	-12.26
PLA/exfo 0.1% t11 180	1.03 ± 0.07	41.32 ± 4.6	-4.04	-19.88
PLA/exfo 1% t11 180	1.05 ± 0.03	49.79 ± 0.92	-2.11	-3.45
PLA/exp 1% t11 180	1.06 ± 0.04	42.42 ± 2.63	-1.06	-17.75
PLA/exfo 1% t11 160	1.02 ± 0.02	53.19 ± 0.61	-5.01	3.13
PLA/exfo 1% t0.50.5 160	1.1 ± 0.02	55.45 ± 1.48	3.07	7.52

5.2.2 Solvent casting

The composites fabricated by this method were reinforced with loads of 1, 2, and 3 wt.% using each reinforcement. The materials reinforced with exfoliated graphite, at 1 wt.%, showed a clear increase in both Young's modulus and tensile strength. At 2 wt.% of reinforcement, the increase in the Young's modulus was double that of the composite reinforced with a load of 1 wt.%, and there was also a clear increase in the tensile strength, although not as high as the Young's modulus.

At 3 wt.% of reinforcement, there was a little increase in Young's modulus and a small decrease in the tensile strength. Likely, this happened because of the agglomeration of the reinforcement which did not affect Young's modulus, but it showed a clear impact in tensile strength, although it is still considerably higher than the values of neat PLA. Fig. 37 shows the stress-strain curves of the neat PLA and its composites reinforced with exfoliated graphite, and Table 8 shows the mechanical properties of neat PLA and its composites reinforced with exfoliated graphite.

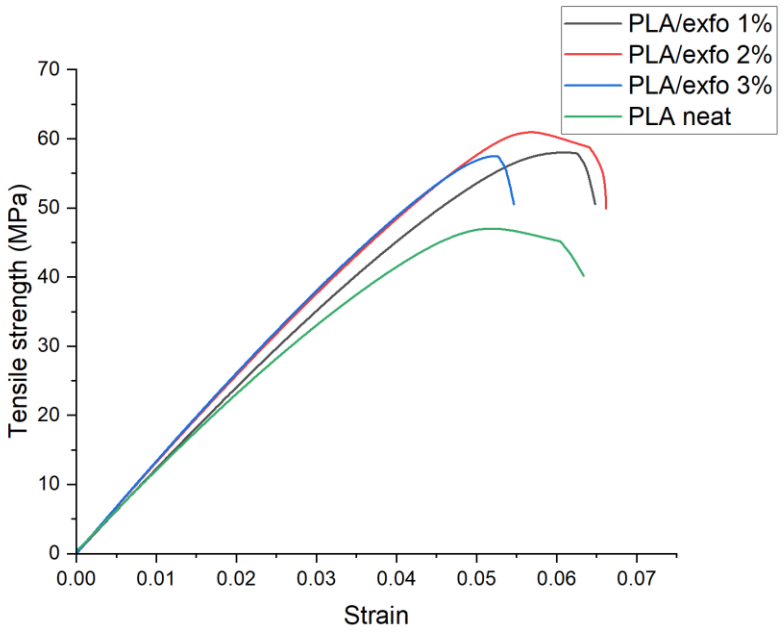

Figure 37. Stress-strain curves of neat PLA and its composites reinforced with exfoliated graphite.

Table 8. Mechanical properties of neat PLA and its composites reinforced with exfoliated graphite.

Material	Young's modulus (GPa)	Tensile strength (MPa)
PLA neat	1.00 ± 0.02	47.66 ± 1.07
PLA/exfo 1%	1.14 ± 0.02	58.30 ± 1.68
PLA/exfo 2%	1.22 ± 0.04	61.03 ± 1.86
PLA/exfo 3%	1.24 ± 0.01	57.96 ± 1.53

In the case of the materials reinforced with expanded graphite, there was an increase in Young's modulus of about 22% and a small increase in the tensile strength at 1 wt.% of reinforcement. At 2 wt.%, Young's modulus remained almost the same while tensile strength lowered considerably its value. At 3 wt.% of reinforcement, Young's modulus increased, almost doubling the improvement obtained at 2 wt.%, while the tensile strength value was even lower. There is a clear trend in both properties concerning the reinforcement amount. The higher the reinforcement amount is, the higher Young's modulus is. On the other hand, the case of tensile strength was just the opposite. This can be explained due to the agglomeration formed in the material; expanded graphite is lighter than exfoliated graphite. Therefore, in volume there is a lot more expanded graphite than the exfoliated one, which generates agglomerations at a lower reinforcement load. It can be noticed that Young's modulus is not as sensible to the agglomerations as the tensile strength is, which is the reason for the high increase in Young's modulus and high decrease in tensile strength. Papageorgiou and coworkers fabricated fluoroelastomer-graphene nanocomposites with a two-roll mill. They realized that the tensile strength is much more sensitive to the formation of large aggregates that can act as failure points during the elongation of the samples and can reduce the ultimate tensile strength [79]. Fig. 38 shows the stress-strain curves of neat PLA and its composites reinforced with expanded graphite along Table 9, which shows the mechanical properties of the neat PLA and its composites reinforced with expanded graphite.

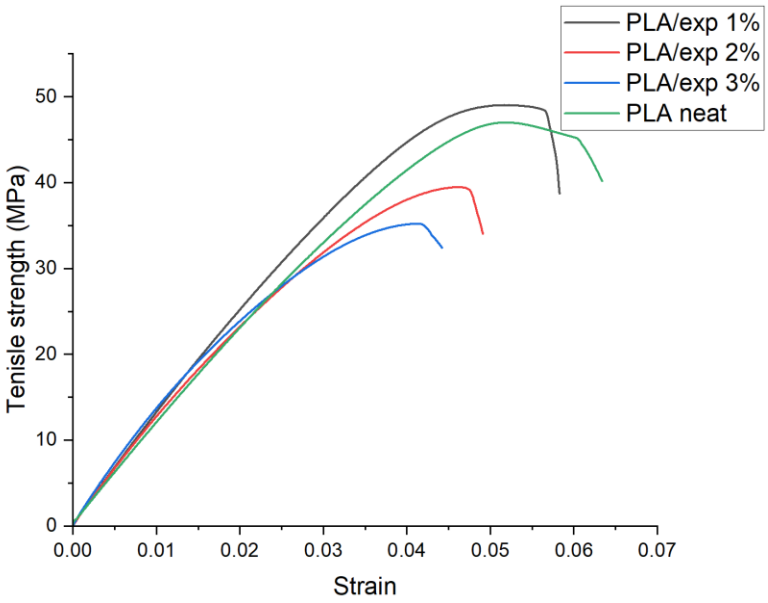

Figure 38. Stress-strain curves of neat PLA and its composites reinforced with expanded graphite.

Table 9. Mechanical properties of neat PLA and its composites reinforced with expanded graphite.

Material	Young's modulus (GPa)	Tensile strength (MPa)
PLA neat	1.00 ± 0.02	47.66 ± 1.07
PLA/exp 1%	1.23 ± 0.03	49.08 ± 1.79
PLA/exp 2%	1.24 ± 0.03	39.83 ± 1.98
PLA/exp 3%	1.43 ± 0.04	35.38 ± 1.67

In the case of the materials reinforced with turbostratic graphite, there was a notable increase in Young's modulus and tensile strength of about 16 and 25%, respectively at 1 wt.% of reinforcement. At 2 wt.% of reinforcement there was a small decrease in both mechanical properties. This can be due to the fact the particles can interact via direct contact or bridging by polymer chains and build a filler inside the matrix, which gives arise to the elastic response, giving the material less stiffness and reducing Young's modulus and tensile strength. Chieng and coworkers developed composite materials using PLA as the matrix and graphene nanoplatelets as the reinforcement in amounts between 0.1 and 1 wt.%. They observed that above loads of 0.3 wt.% the tensile strength was reduced because of the percolated network formed, which makes the reorientation harder due to excluded volume interactions between the nanoplatelets generating a decrease in tensile strength and modulus [18]. However, the mechanical properties were notably higher than the mechanical

properties of neat PLA. At 3 wt.% of reinforcement, it showed an increase of 25% in tensile strength and almost 35% in Young's modulus. Apart from the composite reinforced with a load of 2 wt.% of turbostratic graphite, the increase in the reinforcement amount leads to higher mechanical properties. Fig. 39 shows the stress-strain curves of the neat PLA and its composites reinforced with turbostratic graphite, and Table 10 shows the mechanical properties of the neat PLA and its composites reinforced with turbostratic graphite.

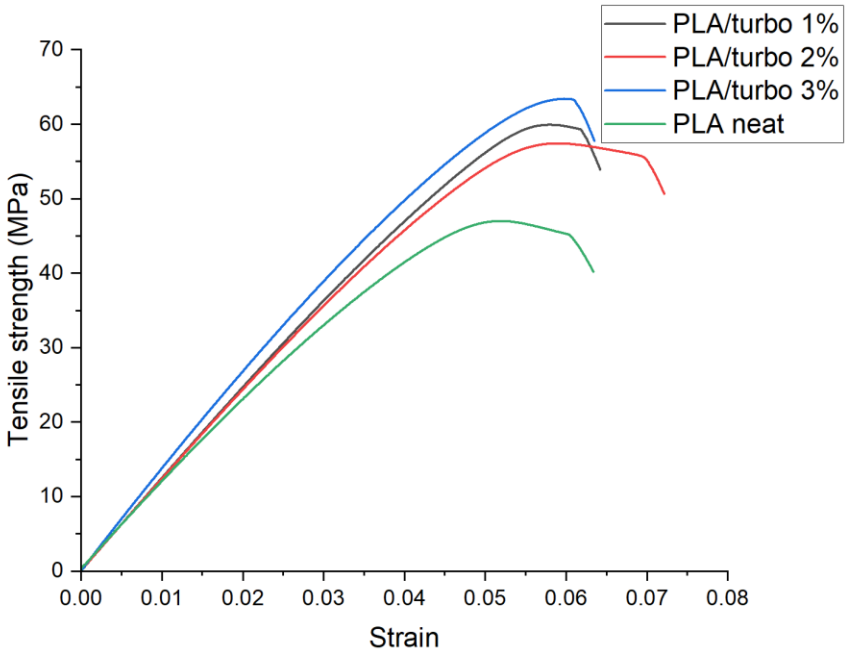

Figure 39. Stress-strain curves of neat PLA and its composites reinforced with turbostratic graphite.

Table 10. Mechanical properties of neat PLA and its composites reinforced with turbostratic graphite.

Material	Young's modulus (GPa)	Tensile strength (MPa)
PLA neat	1.00 ± 0.02	47.66 ± 1.07
PLA/turbo 1%	1.17 ± 0.01	60.02 ± 0.75
PLA/turbo 2%	1.16 ± 0.02	57.45 ± 1.64
PLA/turbo 3%	1.27 ± 0.01	63.48 ± 0.70

In the case of the materials reinforced with original graphite, there was also an increase in both mechanical properties. However, as the amount of reinforcement

increases, Young's modulus and tensile strength show different trends a constant increase and a constant and slight decrease can be seen, respectively. Both trends can be due to the agglomeration of the reinforcement, some authors states that small reinforcement particles are dispersed more easily than in case of larger particles. Kalaitzidou and coworkers used polypropylene and graphene nanoplatelets to produce composite materials with different filler sizes. They observed that the larger particles generated agglomerations at all the reinforcement loads. In the other hand, a better distribution was observed in the case of smaller particles. The agglomerations observed in the case of larger particles are then associated with the decrease in the reinforcing effect [80]. In addition, Gao and coworkers fabricated PLA composite materials reinforced with graphene nanoplatelets only varying the filler size; they observed the same trend in their work, which led to higher mechanical properties in the composite reinforced with a smaller filler size [24]. This can also explain the behaviour of the composites reinforced with expanded graphite; the large size of this filler leads to more agglomerations, which contribute to the decrease in tensile strength as the load of reinforcement increases. Fig. 40 shows the stress-strain curves of the neat PLA and its composites reinforced with original graphite, and Table 11 which shows the mechanical properties of the neat PLA and its composites reinforced with original graphite.

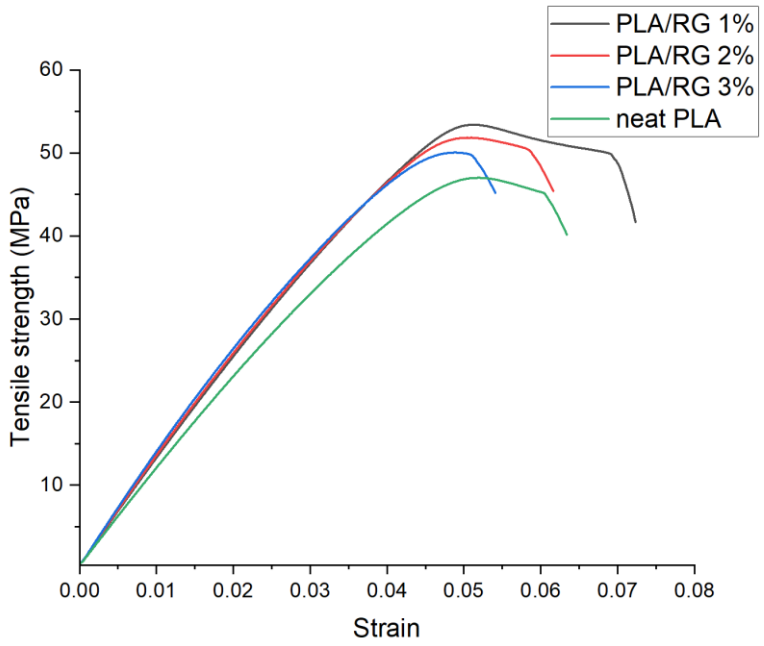

Figure 40. Stress-strain curves of neat PLA and its composites reinforced with original graphite.

Table 11. Mechanical properties of neat PLA and its composites reinforced with original graphite.

Material	Young's modulus (GPa)	Tensile strength (MPa)
PLA neat	1.00 ± 0.02	47.66 ± 1.07
PLA/RG 1%	1.16 ± 0.02	53.43 ± 0.45
PLA/RG 2%	1.20 ± 0.01	51.86 ± 0.66
PLA/RG 3%	1.26 ± 0.02	50.13 ± 2.11

Comparing the mechanical properties of all the composites, the one with the highest tensile strength was the one reinforced with 3 wt.% of turbostratic graphite, the one with the highest Young's modulus was the one reinforced with 3 wt.% of expanded graphite, the one that gets the hypothesis at lower reinforcement loads is the one reinforced with 1 wt.% of turbostratic graphite, and the one with the best combination of properties is the one reinforced with 3 wt.% of turbostratic graphite. Fig. 41 shows comparative graphics of the mechanical properties of the composites, and Table 12 which shows the increase and decrease of the different composites concerning the reinforcement loads; the same can be seen graphically in Fig. 42.

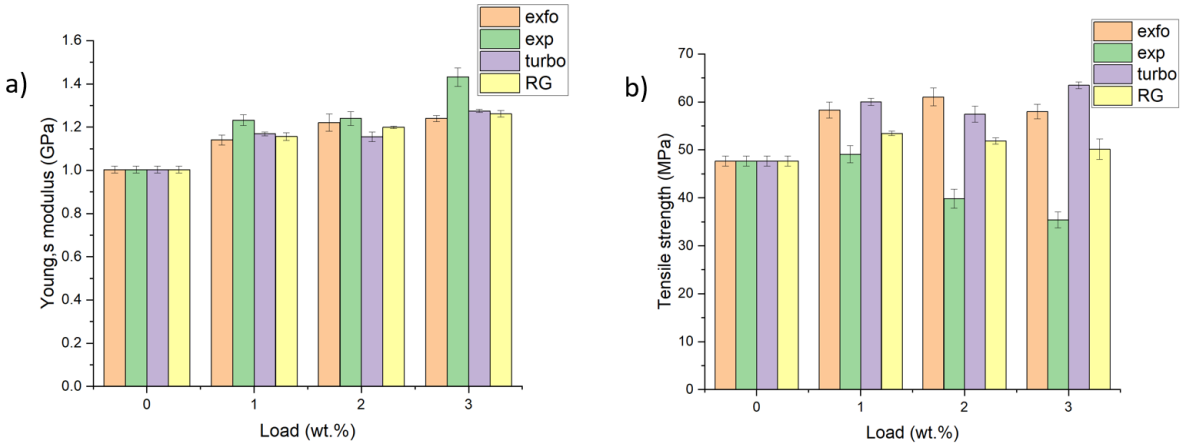

Figure 41. Comparative graphics of the mechanical properties of the composite materials: a) Young's modulus, and b) Tensile strength.

Table 12. Increase and decrease the composite materials for reinforcement loads.

Reinforcement	Property	Reinforcement amount (wt.%)	Increase/decrease (%)
Exfoliated graphite	Young's modulus	1	13.66
		2	21.66
		3	23.61
	Tensile strength	1	22.32
		2	28.06
		3	21.62
Expanded graphite	Young's modulus	1	22.85
		2	23.56
		3	42.68
	Tensile strength	1	2.99
		2	-16.43
		3	-25.76
Turbostratic graphite	Young's modulus	1	16.48
		2	15.19
		3	27.02
	Tensile strength	1	25.94
		2	20.55
		3	33.19
Regular graphite	Young's modulus	1	15.23
		2	19.50
		3	25.76
	Tensile strength	1	12.10
		2	8.81
		3	5.19

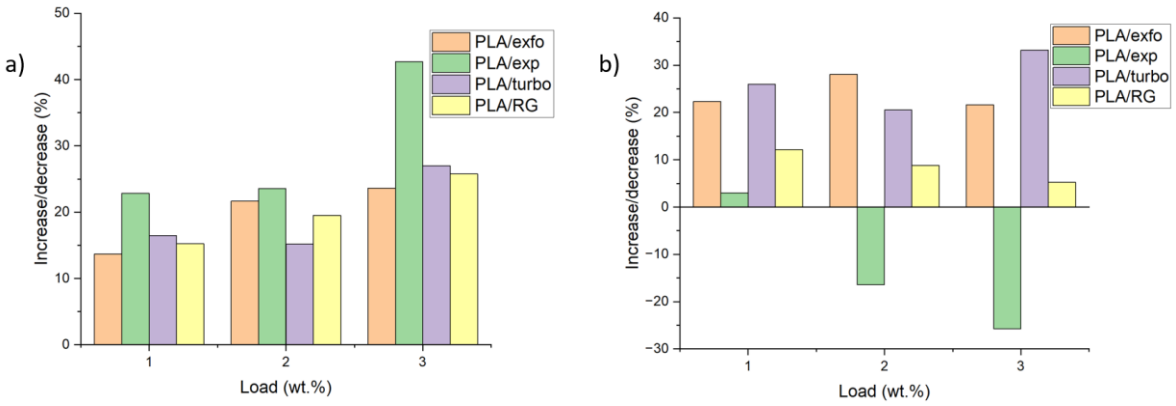

Figure 42. Comparative graphics of the mechanical behavior of the composites for reinforcement load: a) Young's modulus, and b) tensile strength.

The difference between the mechanical properties of the composites is related to the morphology and properties of each reinforcement. The worm morphology of

expanded graphite, with its low density and larger size, as a result of the expansion process, tends to generate agglomerations inside the PLA matrix, decreasing the tensile strength. The exfoliated graphite particles tend to be small as a result of the exfoliation process making it easier to generate agglomerations at higher reinforcement loads. Turbostratic graphite is characterized by its disordered structure in which the graphene layers are neither in the same orientation nor distance. This can lead to a weaker interaction between layers, which can result in all these layers getting separated during the tap sonication in the solvent casting process, increasing the surface area and mechanical properties even at higher loads.

5.3 Thermal characterization

5.3.1 Press & Fold

As mentioned before, the higher the number of cycles used to fabricate the composite, the higher the material's brittleness. This is likely because of the increase in crystallinity as a result of the constant melting and pressing during the process. DSC tests were carried out on the first composite fabricated, which showed a high brittleness, and on the neat polymer without any modification to determine the change in crystallinity due to the fabrication process. In the case of the neat PLA, it showed a melting enthalpy of 4.42 J/g; knowing the value of the melting enthalpy at 100% of crystallinity [81, 82], a simple three-rule can be used to calculate the crystallinity of PLA, giving as a result in 4.77%. This value is normal for PLA whose crystallinity value tends to be below 10% of crystallinity [83].

On the other hand, the composite showed a melting enthalpy of 33.05 J/g, resulting in 35.49% crystallinity. This rise in crystallinity is the reason for the fragilization of the material and degradation of mechanical properties of the composite overprocessed and, therefore, of all composites fabricated by the Press & Fold process. As the cycles in this process are carried out, the polymeric chains are fragmented, making them shorter, generating higher mobility of the polymeric chains, allowing them to get an ordered arrangement, and contributing to the rise in the crystallinity degree. Pages and coworkers discovered a similar behavior when melting and cooling in injection and extrusion processes were carried out with a composite material made of PLA reinforced with montmorillonite. In addition, Morcillo Esquerdo, in his research work, studied the extrusion cycles' influence on the properties of PLA; he discovered that even at low numbers of reprocessing extrusion cycles, the

mechanical properties of PLA are significantly affected by reducing the hardness, impact, and tensile strength [81, 84, 85].

It also can be noted that there are 2 melting peaks, which suggests that the material is composed of 2 different phases due to the P&F Process. It is well known that PLA can crystallize in α, β, δ, and γ crystalline forms, being the ordered and the most thermodynamically stable α form, and the less ordered δ form, previously known as α', the ones that can be obtained under normal conditions such as cold and melt crystallization. This α' crystalline form has the same conformation, but a loose package manner and lower density than the more ordered α crystal form. Therefore, this second melting peak, which appears at a lower temperature, is a melt-recrystallization process; the melting of α and the α' to α crystalline phase transition take place in this peak at the same time while the other melting peak is related to the melting of crystals formed during the α' to α crystalline phase transition and the α already formed during cold crystallinity. Tabi and coworkers annealed PLA at temperatures between 80 and 140 °C; they observed the formation of a second melting peak in the PLA when it was annealed between 110 and 130 °C, and since when the PLA was annealed at temperatures below 110 °C an exothermic peak was observed related to an incomplete crystallization, they concluded that the first melting peak corresponds to the melting-recrystallization process [86]. Limsukon and coworkers studied the degradation of PLA at different contents of L-Lactide and with two different crystallization processes (cold crystallization and melt-stretching), in a DSC analysis, they also realized of these two melting peaks behavior and described the first one as in which melting, and recrystallization take place [87]. Di Lorenzo and coworkers state that the melting is related to α', and α can grow quickly from the self-seeds that the melting of α' leaves [88]. Likewise, Backes and coworkers fabricated a composite based on PLA, and reinforced with bioglass, and reported that the cold crystallization can generate both phases α' and α [89]. Therefore, the melting of α' happens at the first melting point temperature to quickly recrystallize in α to be subsequently melted at the second melting peak temperature [90]. In Fig. 43 are shown the DSC curves of neat PLA and the overprocessed composite. In addition, Table 13 shows the crystallinity degree of both neat PLA and the overprocessed composite.

Table 13. Crystallinity degree neat PLA and overprocessed composite.

Material	Crystallinity (%)
Neat PLA	4.77
PLA/exfo 0.02% OP	35.49

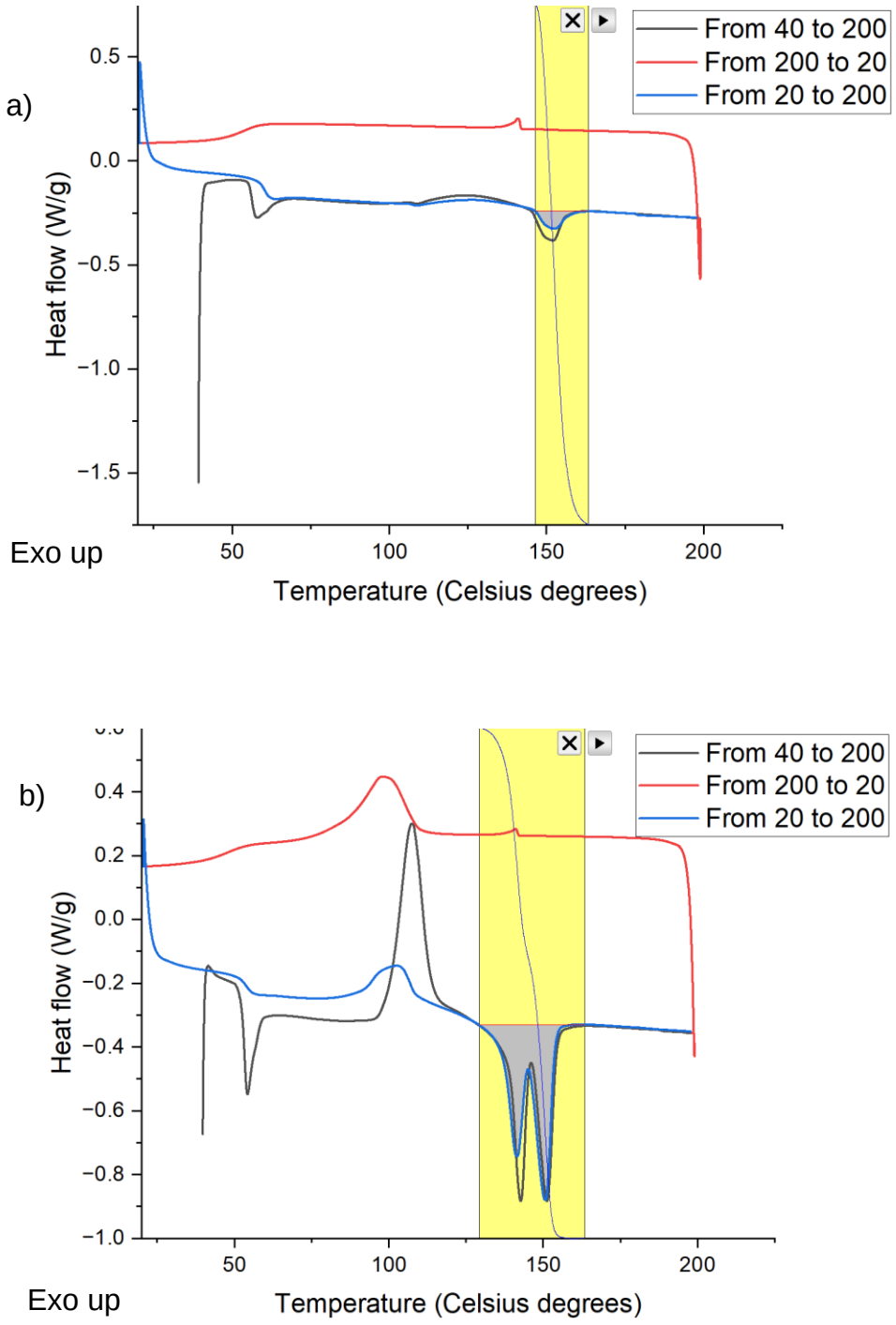

Figure 43. DSC curves: a) neat PLA and b) overprocessed composite.

TGA analysis was carried out on the neat PLA and the overprocessed composite to see any difference in the thermal stability. The composite's degradation starts at

lower temperatures than the neat PLA because of the increase in the crystallinity; the short polymeric chains allow the degradation to start sooner at around 291°C while the one for the neat PLA starts at 326°C. On the other hand, the final degradation temperature of the composite was 374°C, 6 more than the neat PLA; this can be due to the presence of the reinforcement particles since they provide a physical barrier to the movement of the decomposition products avoiding their escape [18, 19, 20, 26, 91]. Carrasco and coworkers studied the kinetics of the thermal decomposition of processed PLA. They realized that the polymer melting during the injection and extrusion processes was responsible for certain depolymerization decreasing the mean molecular weight (M_n). Therefore, the small molecules formed during material processing can volatilize easily, leading to lower thermal stability affecting mainly the initial degradation temperature [92]. In Fig. 44, both curves for neat PLA and the overprocessed composite are shown.

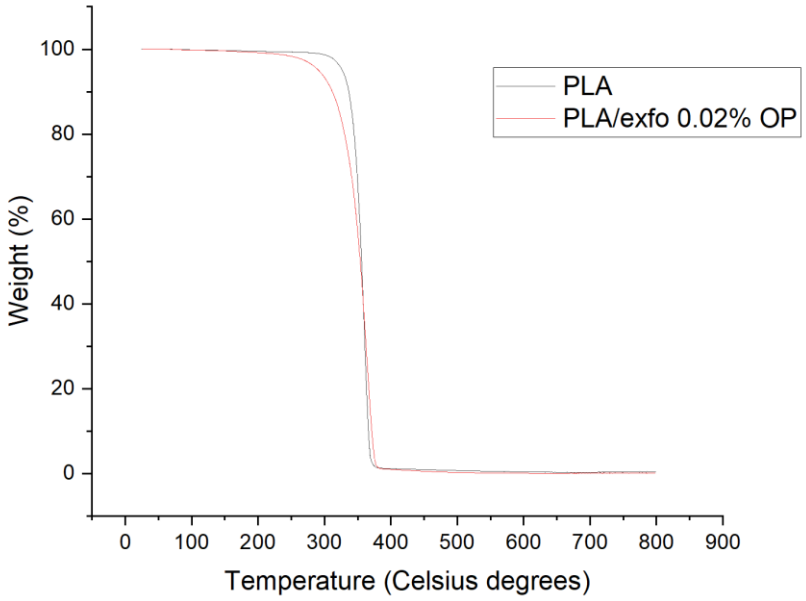

Figure 44. TGA curves for neat PLA and overprocessed composite.

Table 14 below shows the thermal properties of the neat PLA and some selected composites prepared by the P&F process. A difference can be seen mainly in the crystallinity degree between the composites and the neat PLA. As mentioned before, the constant melting and solidification of the polymer generates a high increase in crystallinity, which makes it hard to determine how much the reinforcement apports to the rise in crystallinity.

The melting point of the neat PLA is higher than the melting point of the composites, as well as the glass transition temperature. Chain scission generates shorter chains of the polymer, which leads to the decrease of the polymer's melting point due to the resulting lower molecular weight species and increase molecular weight distribution. This molecular weight reduction enhanced polymer chains' molecular mobility and reduced the glass transition temperature [93, 94]. In addition, the cold crystallization temperature is also higher for the neat PLA than for the composites, which can be for 2 reasons: due to the shorter polymer chains, which makes it easier to get some order between the chains at lower temperatures, leading to the decrease in the cold crystallization temperature, or due to the nucleation effect exerted by the reinforcement particles, which provides the same effect in the cold crystallization [17, 23, 24].

Moreover, the initial, intermediate, and final degradation temperatures (T_5, T_{50}, and T_{95}, respectively) of the neat PLA and its composites are shown. The composites show a higher initial and final degradation temperature than the neat PLA, with the composite processed at 160°C and 30 seconds of heating and pressing the one with a higher increase in both initial and final degradation temperature with increases of 10 and 18°C, respectively. Likely, the higher increase in this composite is due to the better dispersion of the reinforcement compared with the other composites, the same dispersion that also achieved a higher increase in mechanical properties compared with the other composites fabricated by this method, and the fact that the crystallinity is not as high as the other composites reducing degradation of the material. It can be concluded that the thermal properties of the composites are not only affected by the reinforcement distribution, but also by the degree of degradation suffered by the polymer as a result of the fabrication process. In the case of the intermediate degradation temperature, the lowest was the one for the composite fabricated at 180°C. On the other hand, the composite processed at 160°C showed an increase of 13°C. Fig. 45 shows the DSC and TGA curves of these materials.

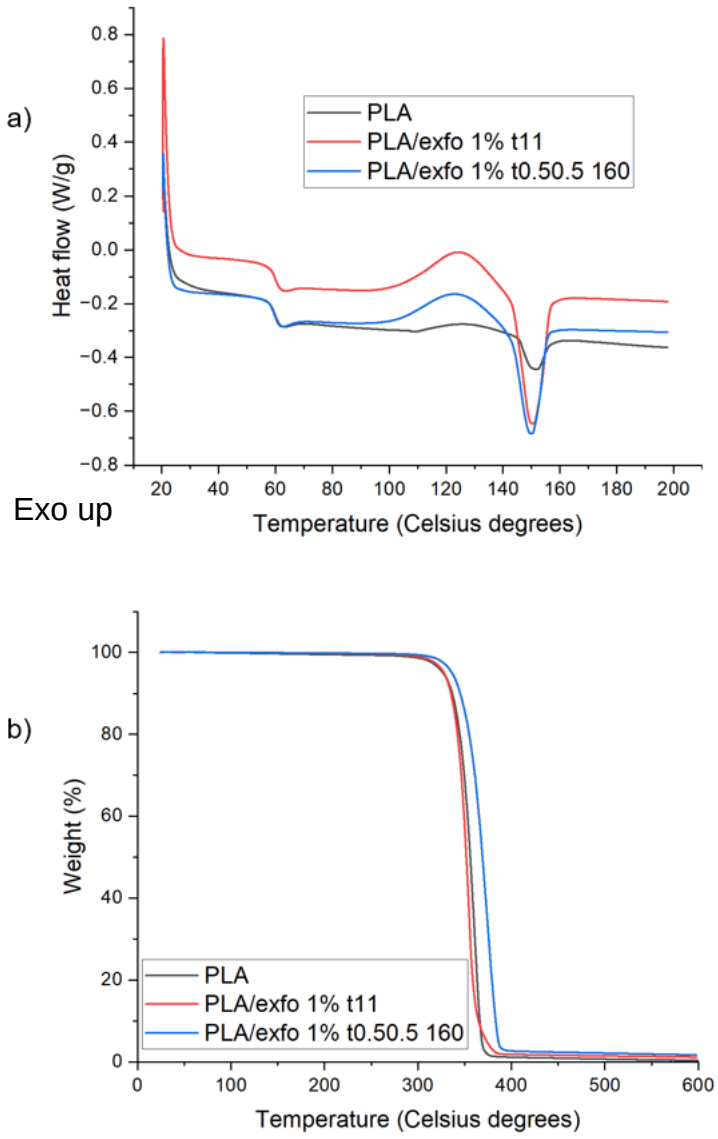

Figure 45. DSC and TGA curves of the neat PLA and the composites fabricated by the Press & Fold process.

Table 14. Thermal properties of the composites prepared by the Press & Fold process.

Material	Melting temperature (°C)	Glass transition temperature (°C)	Cold crystalization temperature (°C)	Crystallinity degree (%)	T_5 (°C)	T_{50} (°C)	T_{95} (°C)
PLA	153	60.5	128.2	4.77	326	356	368
PLA/exfo 1% t11 180	150.5	60.1	124.7	24.7	328	352	374
PLA/exfo 1% t0.50.5 160	150	59.5	123	19.5	336	369	386

5.3.2 Solvent casting

Table 15 shows the thermal properties of the composites prepared by the solvent-casting process. The crystallinity tends to decrease with the incorporation of reinforcement no matter which one is used, which not only shows a non-nucleation effect with the reinforcement but also demonstrates that the high increase in the crystallinity of the composites fabricated by the Press & Fold process is due to the constant melting and solidification of the polymer. The decrease in the crystallinity can be due to the hindering of the movement of the polymeric chains by the reinforcement particles not allowing them to get a more ordered state. In addition, the composites reinforced with exfoliated graphite are the ones with the lowest crystallinity; this can be due to the size of these particles; since they are smaller, it is possible that they hinder more the movement of the polymeric chains then the other kinds of reinforcement.

The fact that the cold crystallization temperature of the composites is higher at each load of reinforcement and with any kind of reinforcement also demonstrates that the reinforcements not only do not promotes de nucleation crystalline phase in the material, but also hinders the mobility of the polymeric chains, increasing the cold crystallization temperature. In addition, all the composites show a higher melting temperature. This is the opposite to what happened with the composites fabricated by the Press & Fold process. Moreover, except for the composites reinforced with original and expanded graphite, all the composites show an increase in the glass transition temperature. Composites that do not show an increase can be due to some agglomerations generated which decreases the tensile strength and the glass transition temperature [95, 96].

In the case of thermal stability, composites reinforced with exfoliated and turbostratic graphite show a trend to increase the initial, intermediate, and final degradation temperature; an opposite trend can be seen in the case of expanded and original graphite. This can be due to a non-homogeneous dispersion of the reinforcement, since a homogeneous dispersion acts as efficient heat sink that extracts the heat from the matrix (due to the good thermal conductivity of the particles) and does not allow the accumulation of heat in the polymer. Therefore, forming agglomerations can promote a decrease in material's thermal stability. In addition, a good dispersion of the reinforcement particles is more efficient blocking the mass transfer of the volatile pyrolyzed products [18, 19, 20, 26, 90, 91, 97, 98]. Composites reinforced with exfoliated graphite showed higher thermal stability than the rest of the composites; this can be explained by the exfoliation degree present in the reinforcement particles; as the exfoliation increases, the surface area is higher, which leads to a better bond between the matrix and the reinforcement. Therefore,

the heat transfer between both components in the composite is better [99]. Fig. 46 shows the DSC and TGA curves of some of these materials.

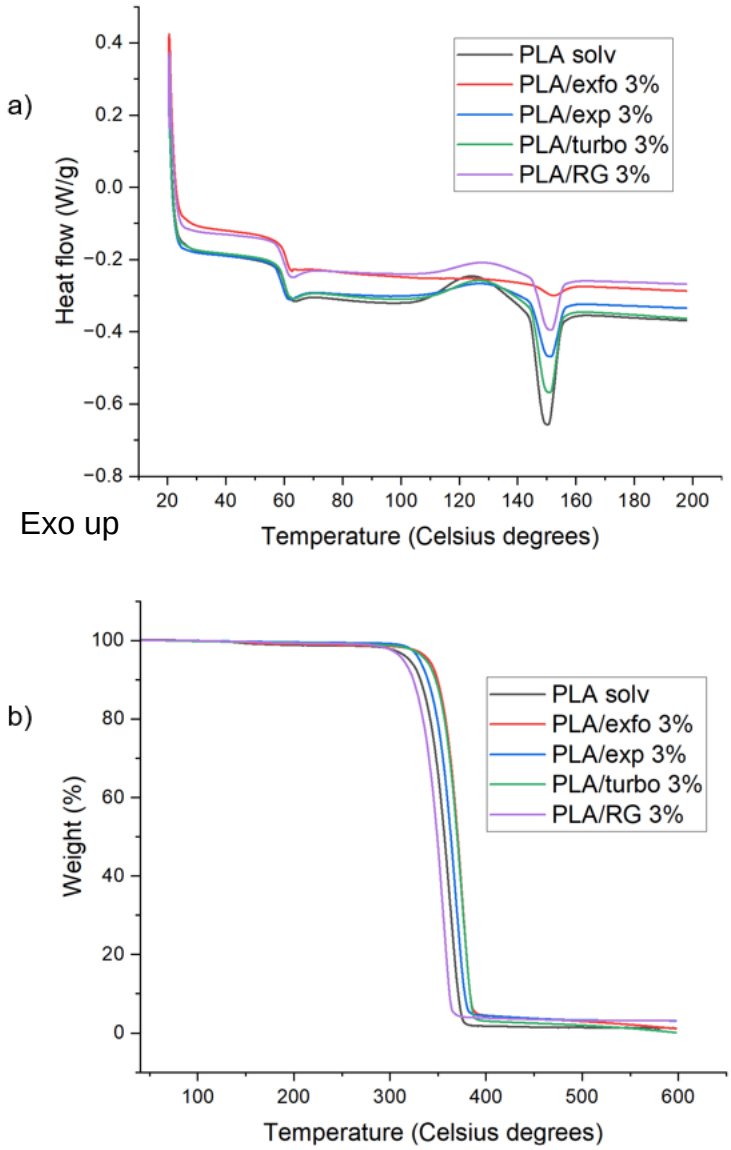

Figure 46. DSC and TGA curves of the neat PLA and some of the composites fabricated by the solvent casting method.

Table 15. Thermal properties of the composites prepared by the solvent casting method.

Material	Melting temperature (°C)	Glass transition temperature (°C)	Cold crystalization temperature (°C)	Crystallinity degree (%)	T_5 (°C)	T_{50} (°C)	T_{95} (°C)
PLA	150	59.9	124.84	13.43	320	356	374
PLA/exfo 1%	152.5	60	127.85	1.3	337	370.5	389
PLA/exfo 2%	152.5	60.75	133	0.25	340	369.5	385.5
PLA/exfo 3%	152.4	60.6	127.44	0.95	340	370.5	390
PLA/exp 1%	151.11	59.43	128.26	8.27	338	368.5	386.5
PLA/exp 2%	151.32	59	128.31	8.38	336	366	384.5
PLA/exp 3%	151.26	58.73	128	6.44	331	363	384.5
PLA/turbo 1%	150.7	60.27	127	12.24	322	354	372
PLA/turbo 2%	151.34	60	128.16	9.05	327	364	380
PLA/turbo 3%	151.23	60.23	128.28	9.12	337	370	386
PLA/RG 1%	151.45	59.9	128.52	4.48	334	366	382.5
PLA/RG 2%	151.33	59.68	128.98	4.73	330.5	366.7	384.5
PLA/RG 3%	151.41	59.54	128.86	5.64	314	349	376

5.4 Electrical characterization

The composites' and polymer's electrical resistivity and conductivity were measured using the four-probe method. Except for the composite reinforced with expanded and original graphite, the electrical resistivity and conductivity tend to decrease and increase, respectively, with the increase in the reinforcement amount. However, there is no change in the order of magnitude in any of the measurements. Therefore, the amounts used are not high enough to promote the formation of the percolation threshold inside the materials. Similar results were obtained by Guo and coworkers who developed composites of PLA reinforced with nano-graphite. They observed that the electrical resistivity did not show a significant decrease until the amount of 15 wt.% of reinforcement [94]. Gao and coworkers fabricated PLA matrix composites reinforced with graphene nanoplatelets with two different sizes, they observed that in both cases, with amounts up to 3 wt.%, the electrical resistivity shows a significant decrease [24]. Moreover, Wang and coworkers developed composites made of PLA and graphite particles and observed significant changes in electrical conductivity up to 5 wt.% of reinforcement. In addition, the same was observed in composites of PLA reinforced with graphene and carbon nanotubes in a work made by Ivanov and his coworkers [20]. The values of the electrical resistivity and conductivity can be seen in Table 16 and Fig. 47 shows the comparative graphics of the electrical properties of the composite materials.

Table 16. Electrical properties of the neat PLA and its composites.

Material	Resistivity (Ω.m)	Conductivity (S/m)
PLA	5.16E+07 ± 7.7E+06	1.99E-08 ± 3.1E-09
PLA/exfo 1%	2.86E+07 ± 4.4E+06	3.58E-08 ± 5.9E-09
PLA/exfo 2%	2.56E+07 ± 7.7E+06	4.79E-08 ± 2.4E-08
PLA/exfo 3%	4.18E+07 ± 2E+07	3.06E-08 ± 1.5E-08
PLA/exp 1%	2.52E+07 ± 3.2E+06	4.02E-08 ± 4.7E-09
PLA/exp 2%	2.84E+07 ± 9.2E+06	3.52E-08 ± 1.1E-09
PLA/exp 3%	4.47E+07 ± 1.2E+07	2.4E-08 ± 6.4E-09
PLA/turbo 1%	2.59E+07 ± 3.4E+06	3.92E-08 ± 4.8E-09
PLA/turbo 2%	2.13E+07 ± 8.2E+06	5.61E-08 ± 2.4E-08
PLA/turbo 3%	5.1E+07 ± 2.7E+07	2.53E-08 ± 1.1E-08
PLA/RG 1%	3.11E+07 ± 6.5E+06	3.36E-08 ± 6.9E-09
PLA/RG 2%	6.87E+07 ± 2.1E+07	1.58E-08 ± 4.2E-09
PLA/RG 3%	4.23E+07 ± 2.6E+07	3.22E-08 ± 1.4E-08

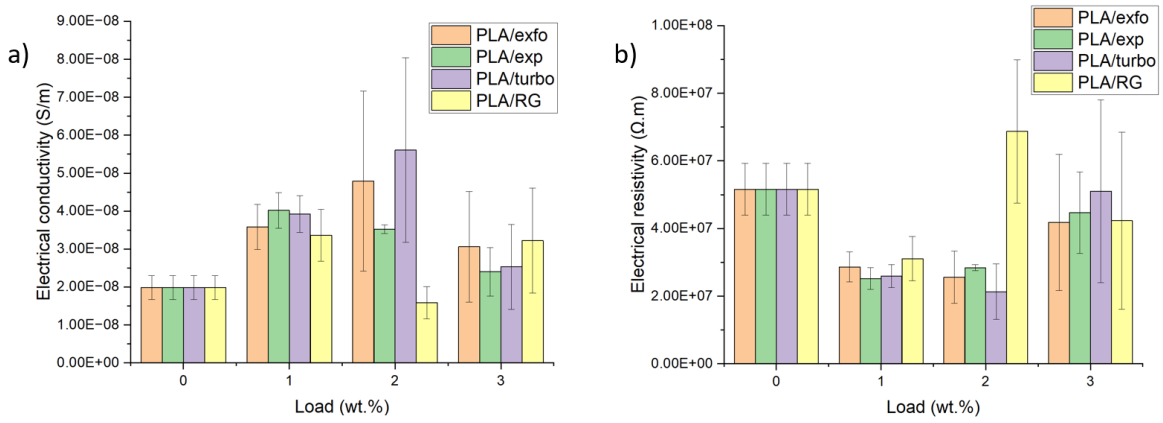

Figure 47. Comparative graphics of the electrical properties of the composite materials: a) electrical resistivity, and b) electrical conductivity.

5.5 Morphological characterization

5.5.1 Press & Fold

In Fig. 48 are shown images of the neat PLA surface fracture which is relatively flat, meaning that the typical brittle fracture was obtained. There are several strips of polymer as a result of the severe deformation of the polymer. In addition, some steps can be seen which are characteristic of the brittle fracture [95, 96, 100].

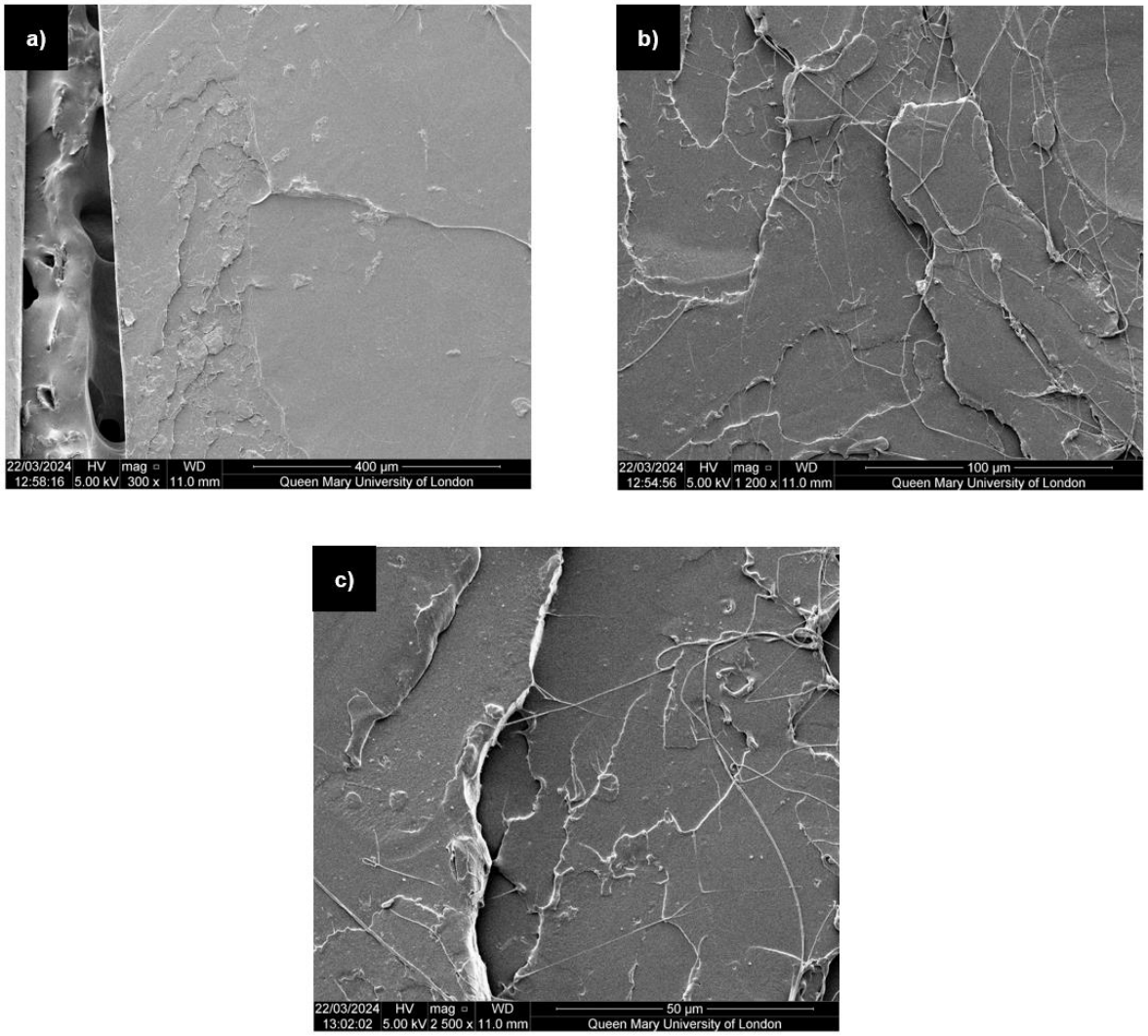

Figure 48. SEM-SE images of the fracture surface of the neat PLA.

In Fig. 49 are shown images of the surface fracture of the composite reinforced with 1 wt.% of exfoliated graphite with 1 minute of heating and pressing at 180 °C; it also seems relatively flat and shows some steps and strips. In images b) and c), some cavities on the surface can be seen, some hollow and some with agglomerated particles inside. When the fracture occurs, these particles, instead of breaking, are pulled out of the matrix, denoting a weak bond between the matrix and the

reinforcement. Ramanathan and coworkers fabricated composites using PMMA as the matrix and reinforced it with exfoliated graphite by a solution-based method. They observed that the cavities on the material's surface were due to a weak interface caused by a bad compatibility achieved between the polymer and the filler [101]. In addition, Bajpai and coworkers fabricated PLA composite materials reinforced with different natural fibers by hot compressing. They realized that the composites reinforced with cordenka had cavities on the surface with a size similar to the fibers and concluded that the fibers were pulled-out of the matrix [102]. Moreover, the same was observed in the work developed by Answer and Naguib, whose work was about the preparation of composites based on PLA reinforced with carbon nanofibers by a twin screw and co-rotating compounder [103]. The cavities that contain particles inside can be due to agglomerates of the particles formed in the material; as the fracture occurs, some of the particles inside the same hole are pulled-out, while others stay in the hole. The formation of agglomerates in the materials decreases the interfacial surface in which the bond between the matrix and filler takes place, decreasing the material's mechanical properties. On the other hand, in image d), a pair of particles on the surface which shows a good bond between the matrix and the reinforcement since there is not a space between the polymer and the particles, and the appearance of the surface in that part is flat. Moreover, in image e) can be seen some cracks formed just a side of the interface between the reinforcement and the polymer, which also denotes a good bond between both components. However, in the same image, a particle where the matrix has started to get separated from it due to the tensile test. It is possible that as the P&F cycles are carried out, the fragilization of the polymer can affect the interface, which would explain the formation of polymer strips bonded to the particle.

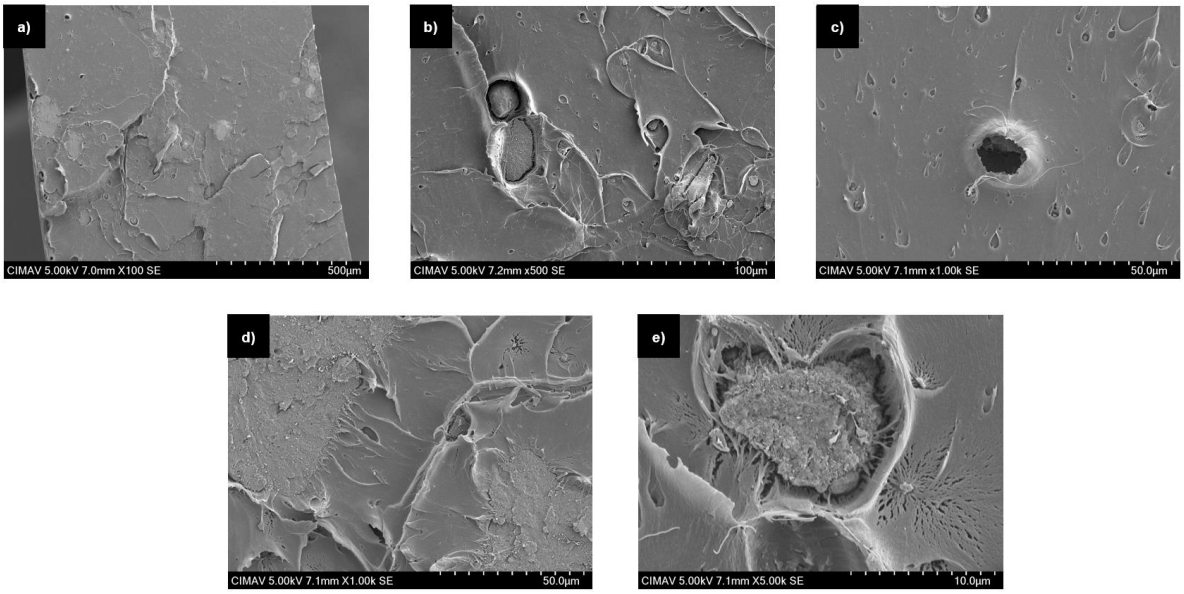

Figure 49. SEM-SE images of the composite PLA/exfo 1% t11 180°C fracture surface.

In Fig. 50 are shown images of the fracture surface of the composite reinforced with 1 wt.% of exfoliated graphite with 30 seconds of heating and pressing at 160°C. In image a), the fracture surface looks relatively flat, similar to the other composite shown in Fig 49. In image b), particles of agglomerates of exfoliated graphite can be seen showing that the dispersion of the reinforcement is not homogeneous. In addition, some cavities can be seen, and some spaces between the polymer and the particles are evident. A fracture of a reinforcing particle in image c) is shown, it is important to remark that this fracture occurred in a part that is clearly still bonded to the matrix, demonstrating a strong interface formed. On the other hand, there is a space between the matrix and the rest of the surface of the particle. It was mentioned above that the fragilization of the matrix could generate this separation when the tensile test was carried out. The same may happen in the case of this material. The fragilization can reduce the deformation that the PLA can suffer, so when the stress is applied, instead of the matrix being deformed and the interface being stable, the matrix does not suffer such deformation and the bond in the interface is undone. Image d) is an agglomerate of particles, confirming a non-homogeneous distribution of the filler; this contributes to the decrease of the mechanical properties due to decrease of the surface area available to form the interface. Nevertheless, the appearance of the particles is different from the particles shown in Fig. 19, showing that these particles were wetted by the polymer. Finally, image e) shows a particle with an apparent good bond in the interface, but is possible to realize of a little space between the matrix and the particle in a small part of the particle surface. It can be

said that the low mechanical properties of the composites fabricated by the Press & Fold process are due to a combination of the fragilization of the polymeric matrix, and the heterogeneous distribution of the reinforcement.

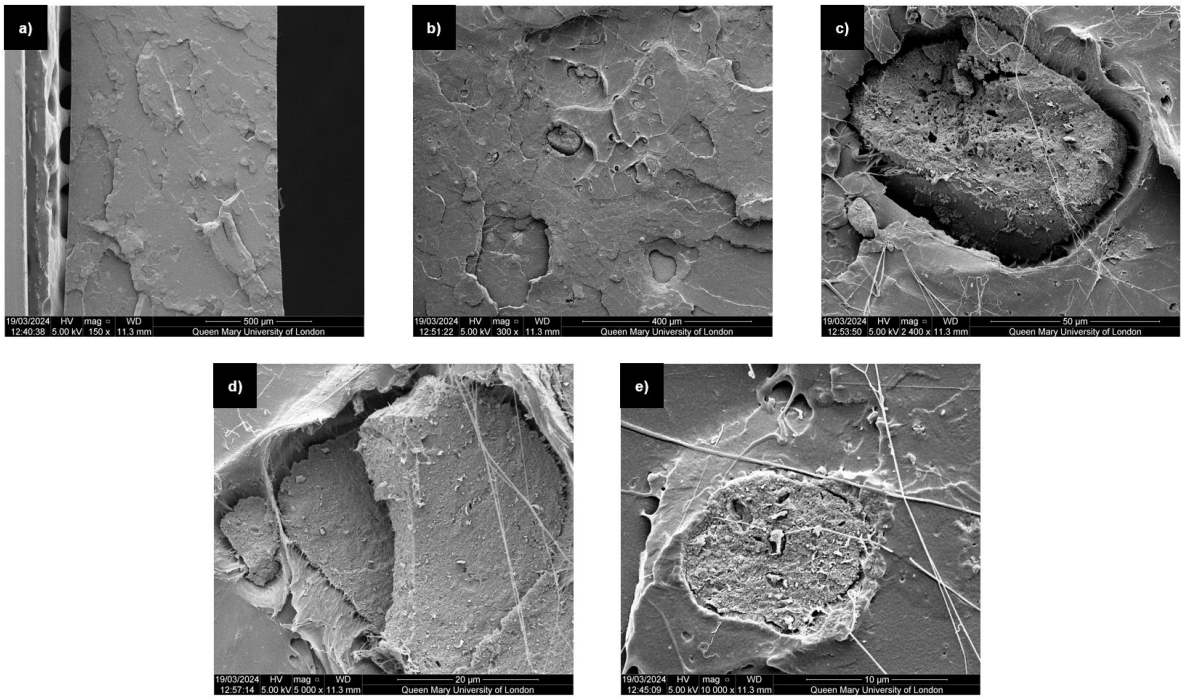

Figure 50. SEM-SE of the composite PLA/exfo 1% t0.50.5 160 °C fracture surface.

5.5.2 Solvent casting method

In Fig. 51 are shown images of the neat PLA dissolved in chloroform. Like the not-dissolved neat PLA, it shows a relatively flat surface with some polymer strips and steps. In addition, on the surface of this PLA can be noticed some embossing on the surface. This can be due to this polymer's higher degree of crystallinity due to the dissolution process. Moreover, there are more strips of polymer in this case. Since the mechanical properties of the dissolved polymer are lower than the non-dissolved PLA, the polymer suffers a higher degree of deformation.

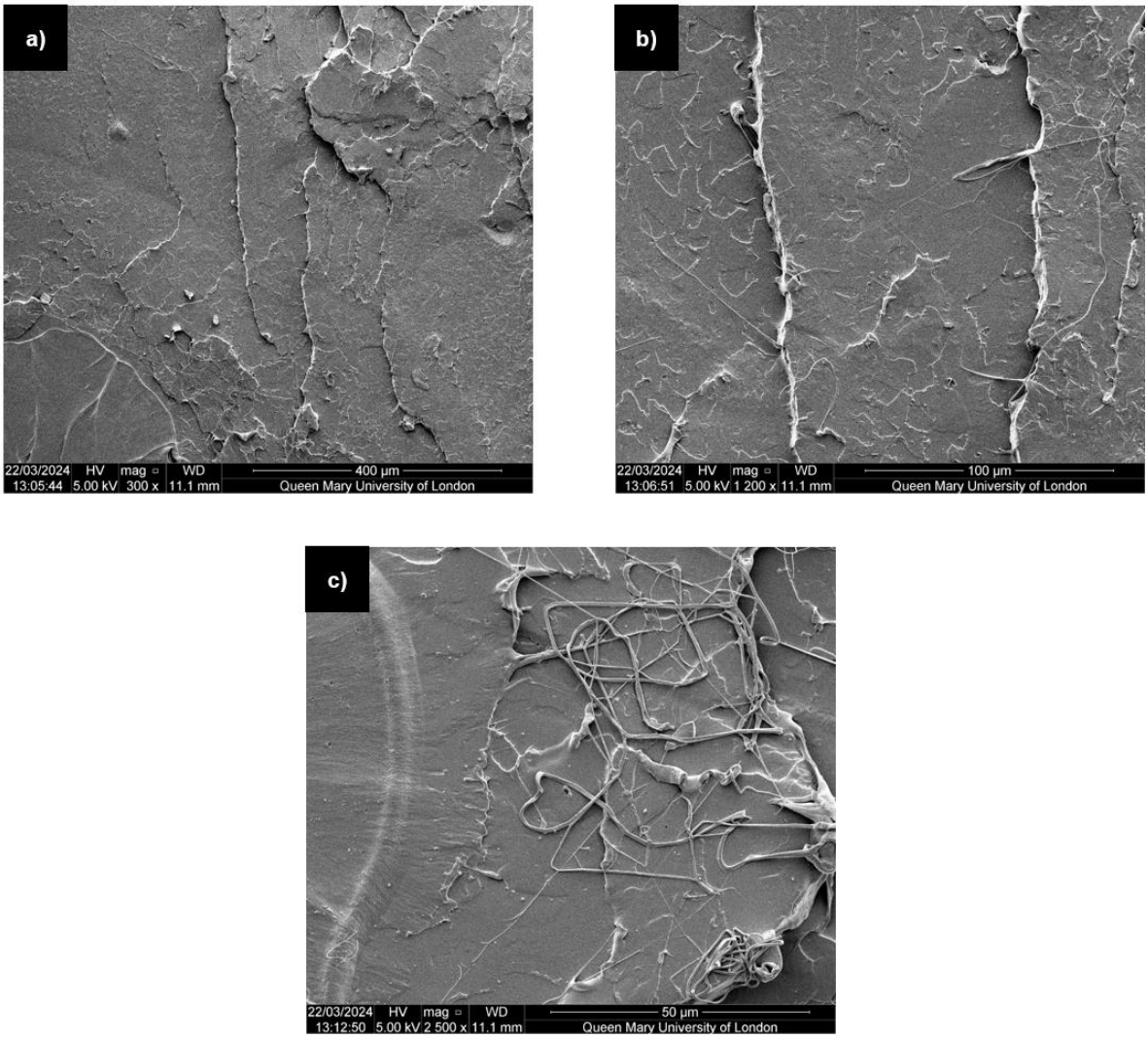

Figure 51. SEM-SE images of the fracture surface of the PLA dissolved in chloroform.

Fig. 52 shows images of the fracture surface of the composite reinforced with 1 wt.% of exfoliated graphite. In image a) can be seen again the surface looks relatively flat, with no apparent sight of cavities, agglomerates or spaces between the matrix and reinforcement. In image b) the characteristic strips of polymer and the step of a brittle fracture are present. Moreover, particles of agglomerates can be seen on the surface. However, there is no sign of cavities. In images c), d), and e) there is an agglomerate particle that shows not only a good bond with the matrix, but also is possible to detect cracks around the particle, which denotates, a strong bond in the interface since the matrix and reinforcement are still together and the cracks start from the matrix. In contrast with the images of the composite produced by the Press & Fold process, there were not found particles of filler where the matrix was separated from the particles, which confirms that the fragilization of the matrix

generates this effect in the interface, decreasing the strength of the bond between both components.

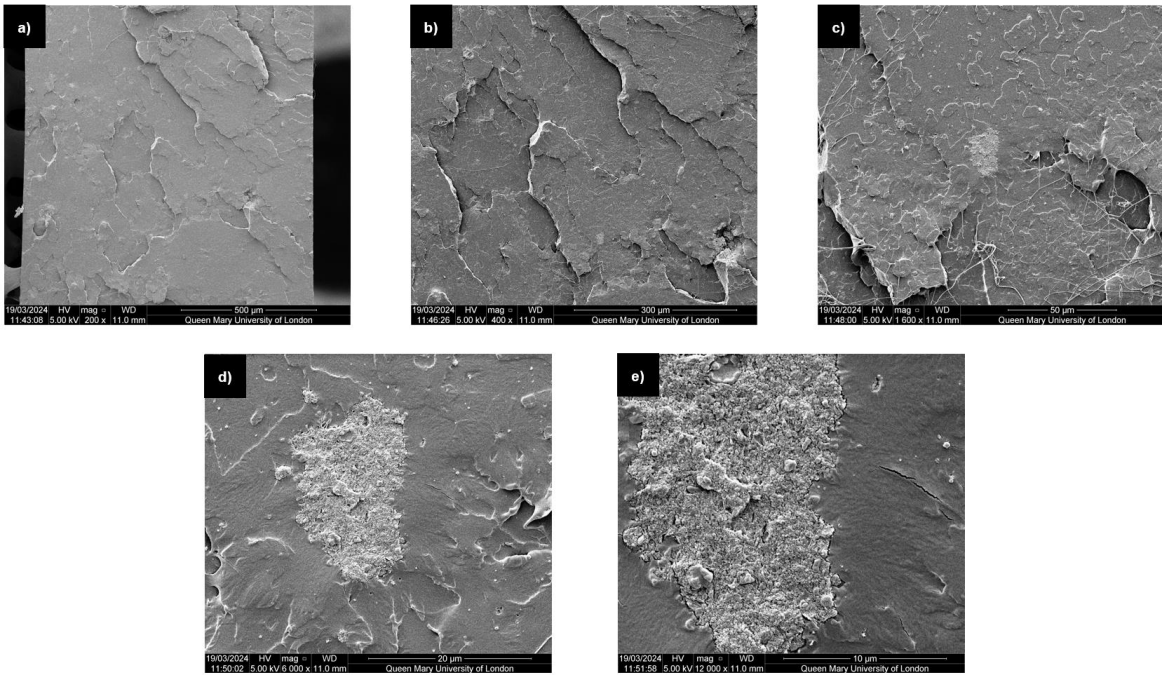

Figure 52. SEM-SE images of the composite PLA/exfo 1% fracture surface.

Fig. 53 shows images of the fracture surface of the composite reinforced with 1 wt.% of original graphite. In image a), the surface looks very different from the one shown in Fig. 52; this one has higher roughness than the last one, it is more deformed, and has many cavities on the surface. In image b, some steps and strips of polymer with some cavities, some empty and others containing reinforcement particles can also be seen. Images c) and d) show a zoom in of the cavities. This talks about heterogeneous distribution of reinforcement and a not strong interface formed in this system. Finally, in image e), some particles that present a bad bond with the matrix are shown since there is a space between both. Some authors state that fillers with larger particle sizes tend to be harder to disperse homogeneously than particles with a shorter size. Mngomezulu and coworkers fabricated composite materials based on PLA reinforced with exfoliated graphite by a melt-mixing process. They realized that larger particles generate agglomerates at lower reinforcement loads. They also pointed out that the cavities found on the surface were signals of poor compatibility between the particles and the matrix generating a weak interface [96]. The same was observed by Gao and coworkers in a project related to the fabrication and characterization of composites of PLA as the matrix and graphene nanoplatelets of

different sizes as the reinforcement [24]. The roughness present in the agglomerates of exfoliated graphite particles as a result of the exfoliation process seems to promote a better bond with the matrix than the original graphite particles which show a very flat surface. So, the exfoliated graphite provides a higher surface area to generate the bond and distribute the stress better.

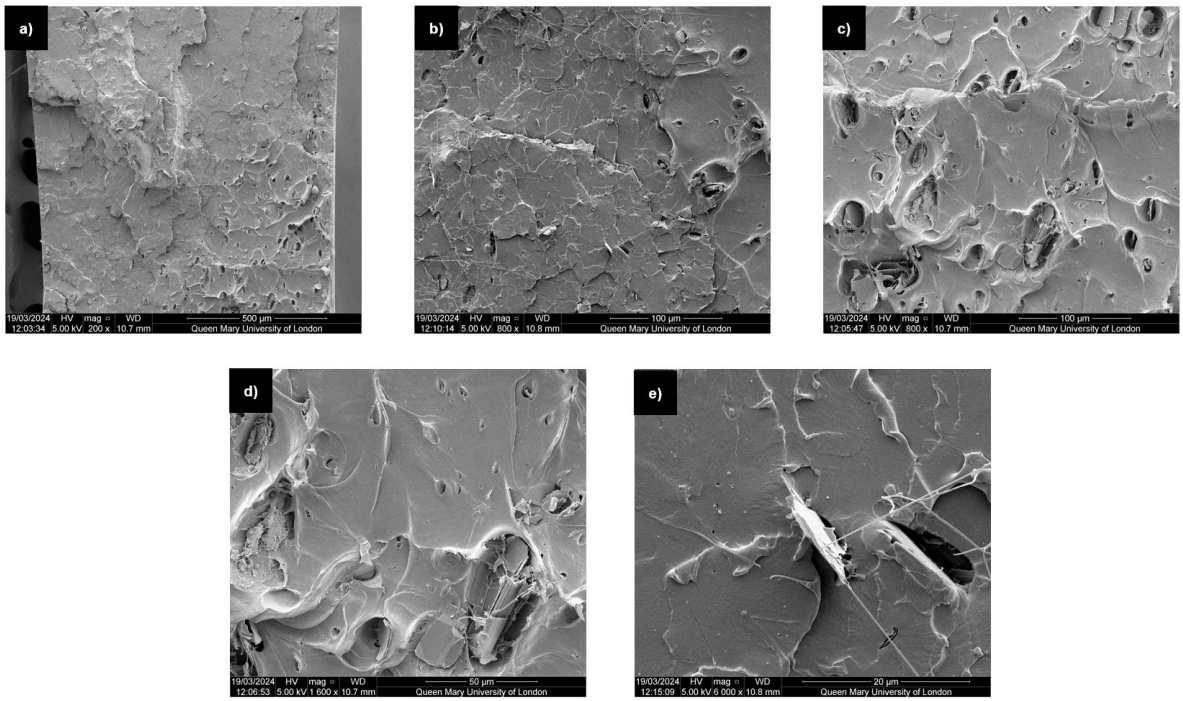

Figure 53. SEM-SE images of the composite PLA/RG 1% fracture surface.

Fig. 54 shows images of the fracture surface of the composite reinforced with 1 wt.% of turbostratic graphite. In image a), the surface is relatively flat and, in general, along with image b), shows some particles of agglomerates of the reinforcement and the typical brittle fracture seen along the morphological characterization, with strips and steps. It is possible to see in the images c) and d) the fracture of turbostratic graphite and some of the fragments as a result of this fracture, respectively. This, including what the image e) shows, denotes a good bond in the matrix/reinforcement interface.

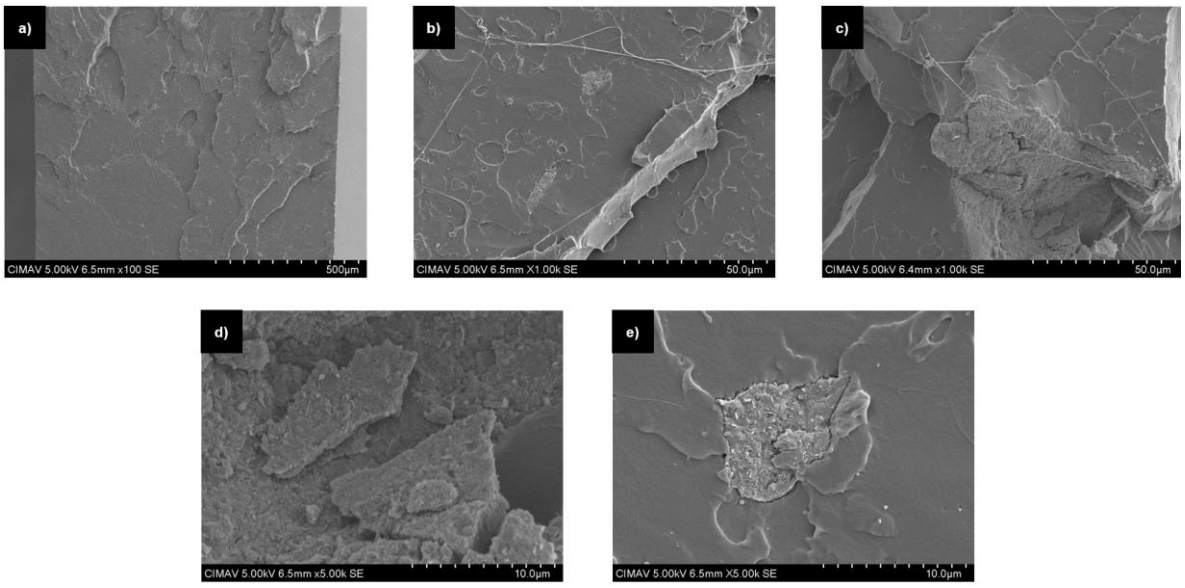

Figure 54. SEM-SE images of the composite PLA/turbo 1% fracture surface.

Fig. 55 shows images of the fracture surface of the composite reinforced with 1 wt.% of expanded graphite. Image a) shows a rough surface, the roughest between the materials analyzed until this point. Images b) and c) show steps, strips, and agglomerates of the expanded graphite on the fracture surface. Since expanded graphite particles are several times larger than the rest of the reinforcements, as mentioned before, the dispersion of larger particles is harder. Therefore, more agglomerates are formed, which also explains the low tensile strength of the sample and the relatively high elastic modulus. Images d), e), and f) a particle of reinforcement show spaces between the particle and the matrix which denotes a deficient matrix/filler interface. In addition, it is impossible to observe polymer between the layers of expanded graphite. The polymer cannot penetrate inside the layers, which also reduces the mechanical and thermal properties of the material since the surface that is available to form the interface is decreased, and consequently, generating a concentration of stress and a deficient heat transfer. Debelak and Lafdi fabricated composites based on EPON Resin 862 reinforced with expanded graphite. They noticed that the polymer could not penetrate between the layer of the particles, which led to the formation of agglomerates and a reduction of the interface area [104].

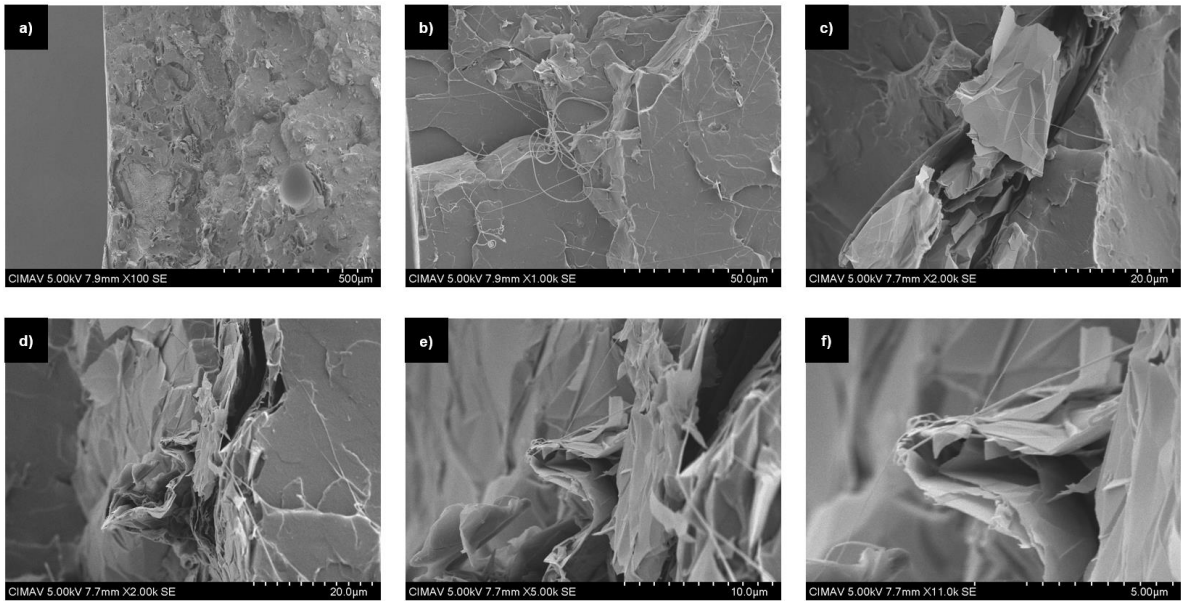

Figure 55. SEM-SE images of the composite PLA/exp 1% fracture surface.

In Fig. 56 are shown images of the fracture surface of the composites reinforced with 2 and 3 wt.% of exfoliated graphite. Images a) and b) show the fracture surface of the material reinforced with 2 wt.%. Image c) shows the crack propagation starting from the matrix, which is stopped by an agglomerate of exfoliated graphite. This particle then withstands the stress until its own fracture takes place, generating the failure of the bulk material [100, 102, 105]. This image confirms the good bond generated in the interface of this coupled system. Images d) and e) show the fracture surface of the composite reinforced with 3 wt.%. This time, the surface looks rougher than the other composites reinforced with this filler, and for the first time, cavities are seen on the surface in this material's system prepared by the solvent casting process A closer look at the surface reveals that the cavities are deep, and some contain particles of exfoliated graphite agglomerates. This would explain the drop in the tensile strength of the composite at this load.

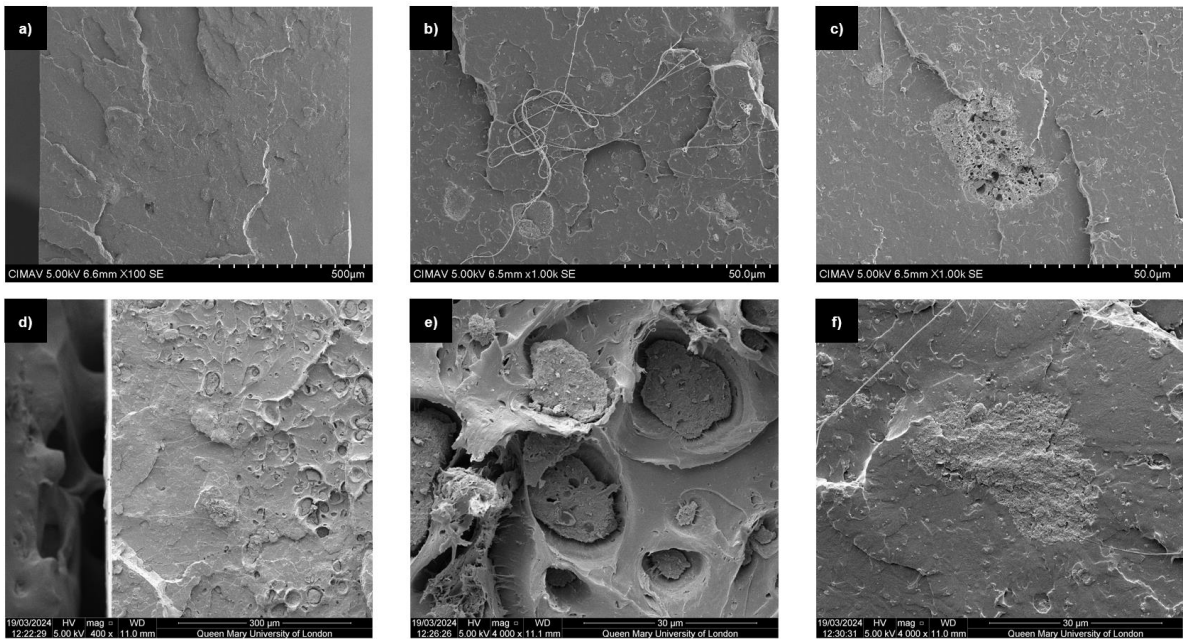

Figure 56. SEM-SE images of the composites PLA/exfo 2 (a), b), and c)) and 3% (d), e), and f)) fracture surface.

In Fig. 57 are shown images of the fracture surface of the composites reinforced with 2 and 3 wt.% of original graphite. Images a), b), and d) and e) show the surface of 2 and 3 wt.% reinforced materials, respectively. The roughness and presence of cavities tend to increase with the increase of the filler load, which explains the constant drop in the tensile strength of these composites as the reinforcement amount arises. Therefore, the interface does not have a good bond in the case of these material's system. Unlike exfoliated graphite agglomerate particles, the particles of original graphite show a flatter surface, which likely does not provide good conditions to generate a strong interface with the matrix since the bond generated is made only by intermolecular forces and a chemical reaction does not take place [106]. Moreover, as mentioned in the reinforcement characterization, the exfoliated graphite contains functional groups that can generate hydrogen bridge bonding, which is a stronger bond [105]. Therefore, this also contributes to forming a good interface in the system where the filler is exfoliated graphite compared with the composites reinforced with original graphite.

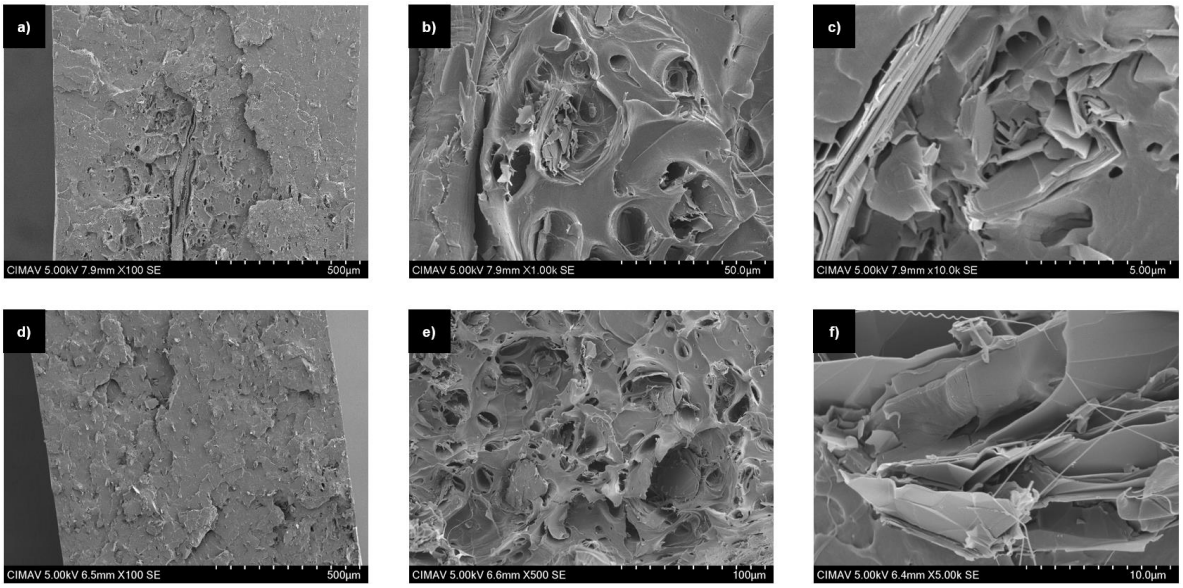

Figure 57. SEM-SE images of the composites PLA/RG 2 (a), b), and c)) and 3% (d), e), and f)) fracture surface.

Fig. 58 shows images of the fracture surface of the composites reinforced with 2 and 3 wt.% of turbostratic graphite. In the case of the composite reinforced with 2 wt.%, there are several agglomerations like those, which would explain the drop in mechanical properties at that filler load. In the case of the one reinforced with 3 wt.%, there are just a few of these agglomerates, which would explain the increase of the mechanical properties at this load, being the one with the highest tensile strength. Is important to mention that the particles in image b), despite the agglomeration, look like they were covered with something, which denotes a good wettability between matrix and reinforcement. This can be confirmed with images c) and f), in which 2 particles of agglomerates of turbostratic graphite are shown; neither shows a space between the filler and the matrix. In addition, it is possible to appreciate the deformation of the matrix bonded to the particle in image c). Since this filler also showed the presence of functional groups, it is possible that some hydrogen bridge bonds are generated, which also apports in forming a good interface. However, the same functional groups that generate a better interface can likely generate agglomerates of reinforcement in the case of exfoliated and turbostratic graphite. Bera and coworkers generated amine functional groups in graphene oxide to use as reinforcement in a PLA matrix; they noticed that after 0.2 wt. % the reinforcement started to agglomerate and generate a second phase inside the composite, decreasing tensile strength [105].

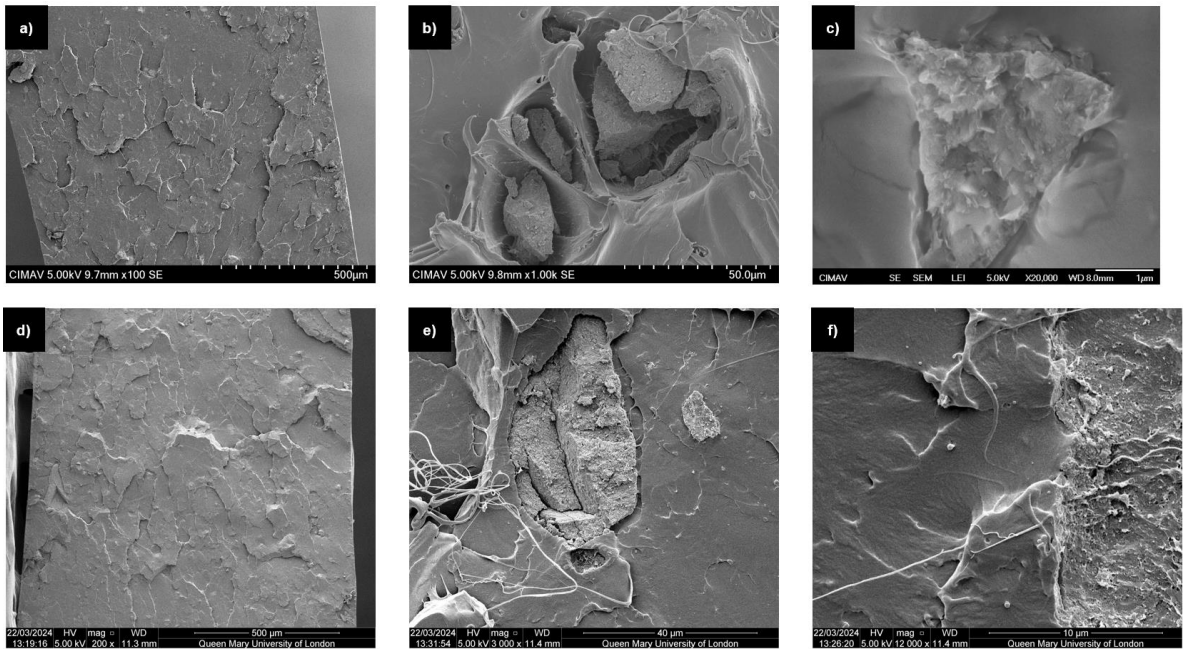

Figure 58. SEM-SE images of the composites PLA/turbo 2 (a), b), and c)) and 3% (d), e) and f)) fracture surface.

Fig. 59 shows images of the fracture surface of the composites reinforced with 2 and 3 wt.% of expanded graphite. All this roughness is related to the forming of big agglomerates in the material. There are also cavities, and layers of expanded graphite that protrude from the surface, which also contributes to the high roughness found. Images b) and d) show some particles of expanded graphite on the surface and big cavities as a result of the filler being pulled out the surface, respectively. Both images show a weak interface in this material's system. In addition, image c) also shows some space between the reinforcement particles and the polymer. Moreover, in both images c) and f), there is clearly no polymer between the layers of the expanded graphite, which also contributes to the weakening of the interface matrix/filler. Besides, functional groups in this reinforcement are lower than turbostratic and exfoliated graphite, which could restrict the bond in the interface to mainly intermolecular forces.

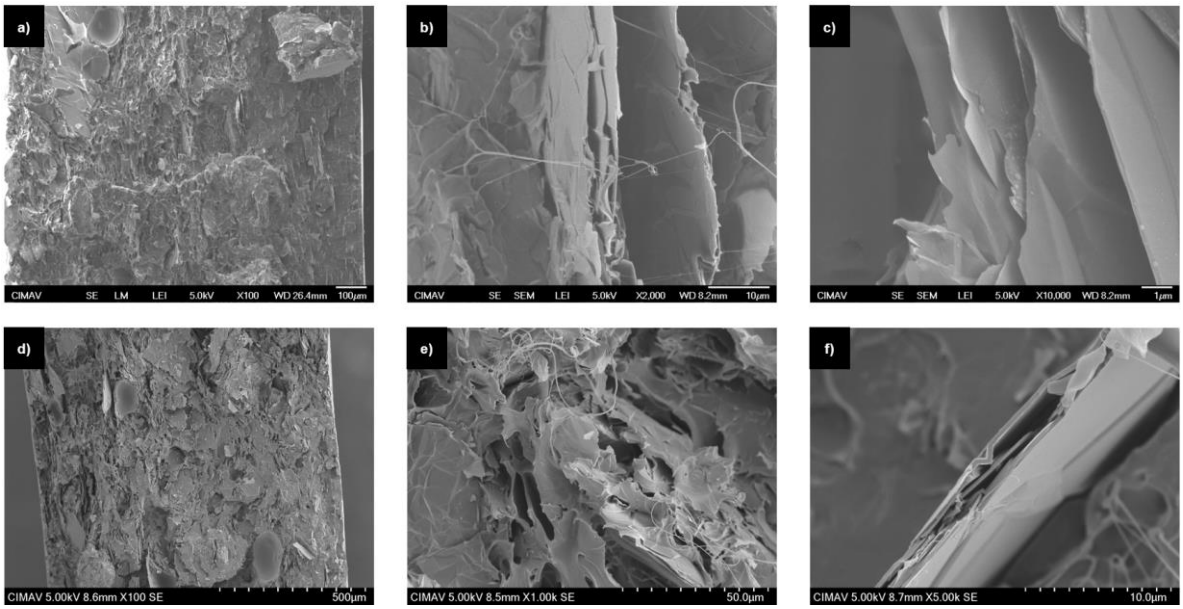

Figure 59. SEM-SE images of the composites PLA/exp 2% (a), b). c)) and 3% (d), e), and f)) fracture surface.

Conclusions

- Raman spectroscopy detected the structural differences between the fillers despite the similarities and differences in morphology. Turbostratic graphite was the only filler that showed a symmetric shape of the 2D band along with an overtone, and the highest I_D/I_G ratio due to its disordered structure.
- XPS technique showed some chemical differences of the reinforcements. Functional groups like hydroxyl, ether, and carbonyl were found. Therefore, the bonds in the interface include hydrogen bridges, intermolecular forces, and mechanical bonding due to the roughness (in the case of exfoliated and turbostratic graphite). The mechanisms by which the interface takes place are infiltration absorption, electrostatic interaction, and mechanical link. In addition, the functional groups in the filler could also promote the agglomeration of the reinforcement.
- PLA suffers degradation as the cycles in the P&F process are carried out, which limits the filler distribution. This affects negatively not only the mechanical but also thermal properties. In addition, morphological characterization showed gaps between the reinforcement and the matrix, which can be owing to the matrix fragilization.

- In contrast, the solvent casting composites achieved a higher increase in mechanical and thermal properties at the same filler load and the prepared composite does not show these gaps.
- The morphological characterization showed that none of the fabrication processes achieved a homogeneous fillers dispersion. Therefore, the evident difference between the composites prepared by one process and the other, could be related to polymer fragilization.
- Expanded and original graphite tend to generate cavities and agglomerates which induces a weak interface. The larger filler size makes it harder to get a homogeneous dispersion, which adversely affects the mechanical and thermal properties.
- The electrical characterization showed differences in electrical conductivity as the reinforcement load increased. The used amounts were not enough to form the percolation threshold and generate a transition from an insulator to a conductive material.
- The P&F process showed in previous works its potential to generate a homogeneous filler dispersion. But in the case of thermally sensitive polymers (like PLA), these are not the ideal materials to work with.
- Considering the mechanical, electrical and thermic properties of the prepared composites, the most prominent applications may be in the electronic and electrical industries as insulator materials and in the 3D printing sector.

Future research lines

Some research coming from this project can be fabrication and characterization of polymer matrix composites by the P&F process using other kinds of biopolymer, petroleum-based alternative polymers, and different kinds of reinforcements (short fibers, 2D flakes, spherical particles, natural fibers, graphene, graphene oxide, etc.) and different loads (ultra-low, low, high, etc.). Likewise, fabrication and characterization of polymer composite materials with exfoliated, turbostratic and expanded graphite with other biopolymers, petroleum-based alternative polymers, and using some other grafting methods to generate more functional groups in both the polymer and the fillers. In addition, use of these fillers in other kind of composites like metal and ceramic matrix composites, and hybrid composites. In addition, preparing composites with a solvent that is not dangerous for the human body can allow the composite use for medical applications.

References

[1] Wang, R. M, S. R. Zheng and Y. P. Zheng. (2011). **Polymer matrix composites and technology.** Woodhead Publishing Limited. https://www.sciencedirect.com/book/9780857092212/polymer-matrix-composites-and-technology

[2] Callister, W. D. (2001). **Fundamentals of Materials Science and Engineering.** 4th Edition. John Wiley & Sons, Inc. United states. 920 pp.

[3] Da Costa, C. E, F. Velasco López and J. M. Torralba Castello. (2000). **Materiales compuestos de matriz metálica. I parte. Tipos, propiedades y aplicaciones.** Revista metalurgia. Vol 36: 179-192.

[4] D. R. Askeland. (1998). **Ciencia e ingeniería de los materiales.** 3rd Edition. International Thomson Editors. United States. 649 pp.

[5] Fernandez. P, V. Martínez, M. Valencia and J. Cruz. (2006). **Aplicación de los materiales compuestos de matriz metalica en el sector eléctrico y electrónico.** Dyna. Vol 149: 131-140.

[6] Chawla, K. K. (2013). **Composite materials.** Springer. 10.1007/978-0-387-74365-3.

[7] Garzón, A. O, D. A. Landínez, J. Roa and J. Ramos. (2017). **Materiales compuestos de matriz polimérica usados para el blindaje de interferencia electromagnética.** Ciencia E Ingeniería Neogranadina. Vol: 27. 5-26.

[8] Åström, B. T. (2012). **Manufacturing of polymer-matrix composites (PMCs).** Elsevier. https://shop.elsevier.com/books/manufacturing-techniques-for-polymer-matrix-composites-pmcs/advani/978-0-85709-067-6

[9] Reddy, H. N., and N. Ganta. (2019). **Overview of Manufacturing PMC's.** International Journal of Recent Research in Civil and Mechanical Engineering. Vol: 6. 4-7.

[10] Santagiuliana, G, O. T. Picot, M. Crespo, H. Porwal, H. Zhang, Y. Li, L. Rubini, S. Colonna, A. Fina, E. Barbieri, A. B. Spoelstra, G. Mirabello, J. P. Patterson, L. Botto, N. M. Pugno, T. Peijs and E. Bilotti. (2018). **Breaking the Nanoparticle Loading Dispersion Dichotomy in Polymer Nanocomposites with the Art of Croissant-Making.** ASC Nano. Vol: 12. 9040-9050.

[11] Ahmed, S, V. M. Chauhan, A. M. Ghaemmaghami and J. W. Aylott. (2019). **New generation of bioreactors that advance extracellular matrix modelling and tissue engineering.** Biotechnol Lett. Vol: 41. 1-25. https://doi.org/10.1007/s10529-018-2611-7.

[12] Lade, M. S, S. A. Payghan, Z. J. Tamboli and J. I. Disouza. (2013). **Polymer Based Wafer Technology: A Review.** International Journal of Pharmaceutical % Biological Archives. Vol: 4. 1060-1074. https://www.researchgate.net/publication/309134813.

[13] Prasad, A, M. R. Sankar, and V. Katiyar. (2017). **Materials Today: Proceedings.** Vol: 4. 898-907. https://doi.org/10.1016/j.matpr.2017.01.101.

[14] Taib, N. A. A, M. R. Rahman, D. Huda, K. K. Kuok, S. Hamdan, M. K. B. Bakri, M. R. M. Bin and A. Khan. (2022). **A review on poly lactic acid (PLA) as a biodegradable polymer.** Polymer Bulletin. Vol:80.1179–1213. https://doi.org/10.1007/s00289-022-04160-y.

[15] DeStefano, V, S. Khan and A. Tabada. (2020). **Applications of PLA in modern medicine.** Engineered Regeneration. Vol:1. 76–87. https://doi.org/10.1016/j.engreg.2020.08.002.

[16] Balla, E, V. Daniilidis, G. Karlioti, T. Kalamas, M. Stefanidou, N. D. Bikiaris, A. Vlachopoulos, I. Koumentakou and D. N. Bikiaris. (2021). Poly(lactic Acid): **A Versatile Biobased Polymer for the Future with Multifunctional Properties—From Monomer Synthesis, Polymerization Techniques and Molecular Weight Increase to PLA Applications.** Polymers. Vol:13. 1822. https://doi.org/10.3390/polym13111822.

[17] Zerankeshi,M. M, S. S. Sayedain, M. Tavangarifard and R. Alizadeh. (2022). **Developing a novel technique for the fabrication of PLA-graphite composite filaments using FDM 3D printing process.** Ceramics International. Vol: 48. 31850–31858. https://doi.org/10.1016/j.ceramint.2022.07.117

[18] B. W. Chieng, N. A. Ibrahim, M. Z. Wan, M. Z. Hussein and Y. Y. Loo. (2014). **Effect of graphene nanoplatelets as nanofiller in plasticized poly(lactic acid) nanocomposites.** J Therm Anal Calorim. Vol:118. 1551–1559. 10.1007/s10973-014-4084-9.

[19] Zhou, Y, L. Lei, B. Yang, J. Li and J. Ren. (2018). **Preparation and characterization of polylactic acid (PLA) carbon nanotube nanocomposites.** Polymer Testing. Vol: 68. 34–38. https://doi.org/10.1016/j.polymertesting.2018.03.044.

[20] Kim, I. H. and Y. J. Jeong. (2010). **Polylactide/Exfoliated Graphite Nanocomposites with Enhanced Thermal Stability, Mechanical Modulus, and Electrical Conductivity.** Journal of Polymer Science: Part B: Polymer Physics. Vol: 48. 850-858. 10.1002/polb.21956.

[21] Ivanov, E, R. Kotsilkova, H. Xia, Y. Chen, R. K. Donato, K. Donato, A. P. Godoy, R. Di Mario, C. Silvestre and V. Angelov. (2019). **PLA/Graphene/MWCNT Composites with Improved Electrical and Thermal Properties Suitable for FDM 3D Printing Applications.** Applied Science. Vol: 9. 1209. doi:10.3390/app9061209.

[22] Batakliev, T, V. Gerogiev, E. Ivanov, R. Kotsilkova, R. Di Mario, C. Silvestre and S. Cimmino. (2018). **Nanoindentation analysis of 3D printed poly(lactic acid)-based composites reinforced with graphene and multiwall carbon nanotubes.** Journal of Applied Polymer Science. 10.1002/APP.47260.

[23] Przekop, R. E, M. Kujawa, W. Pawlak, M. Dobrosielska, B. Sztorch, and W. Wieleba. (2020). **Graphite Modified Polylactide (PLA) for 3D**

Printed (FDM/FFF) Sliding Elements. Polymers. Vol: 12, 1250. doi:10.3390/polym12061250.

[24] Gao, Y, O. T. Picot, E. Bilotti and T. Peijs. (2016). **Influence of filler size on the properties of poly(lactic acid) (PLA)/graphene nanoplatelet (GNP) nanocomposites.** European Polymer Journal. Vol: 86. 117-131. http://dx.doi.org/10.1016/j.eurpolymj.2016.10.045.

[25] Wang, G, G. Zhoa, S. Wang, L. Zhang, and C. B. Park. (2018). **Injection-molded microcellular PLA/graphite nanocomposites with dramatically enhanced mechanical and electrical properties for ultra-efficient EMI shielding applications.** Royal Society of Chemistry. Vol: 6. 6847. 10.1039/c8tc01326h.

[26] Li, X, Y. Xiao, A. Bergeret, M. Longerey, and J. Che. (2013). **Preparation of Polylactide/Graphene Composites From Liquid-Phase Exfoliated Graphite Sheets.** Polymer Composites. Vol: 32. 1362-1368. DOI 10.1002/pc.

[27] Piñón-Vázquez A. K, S. M. Vega-Díaz, D. Meneses- Rodríguez, L. A. Alcaraz-Caracheo, and F. Tristán. (2023). **Self-standing tridimensional structures from crumpling techniques made with composite films of polylactic acid and exfoliated graphite.** Materials and Design. Vol: 232. 112102. https://doi.org/10.1016/j.matdes.2023.112102.

[28] Sullivan, E. M, Y. J. Oh, R. A. Gerhardt, B. Wang, and K. Kalaitzidou. (2014). **Understanding the effect of polymer crystallinity on the electrical conductivity of exfoliated graphite nanoplatelet/polylactic acid composite films.** Journal of Polymer Research. Vol: 21. 1-9. 10.1007/s10965-014-0563-8.

[29] Miranda, A. (2018). **Conducta al desgaste de un compósito base cobre reforzado con carburo de titanio y adiciones de grafito**. [Master's thesis]. Universidad Michoacana de San Nicolás de Hidalgo.

[30] Dirección general de desarrollo minero. (2018). **Perfil de mercado de grafito.** Secretaría de Economía.

[31] Kim, H. and C. W. Macosko. (2008). **Morphology and Properties of Polyester/Exfoliated GraphiteNanocomposites.** Macromolecules. Vol: 41. 3317-3327. 10.1021/ma702385h.

[32] Mendoza, J. M, F. C. Robles, C. D. Gómez, J. G. Miranda, C. G. Garay, I. Estrada y R. Martínez. (2020). **Exfoliated graphite preparation based on an eco-friendly mechanochemical route.** Journal of Environmental Chemical Engineering. Vol: 8. 104370. doi.org/10.1016/j.jece.2020.104370

[33] C. D. Gomez, E. Rocha and R. Martinez. (2022). **Effect of Process Parameters on the Graphite Expansion Produced by a Green Modification of the Hummers Method.** Molecules. Vol: 27. 7399. https://doi.org/10.3390/molecules27217399.

[34] D. D. L. Chung. (2016). **A review of exfoliated graphite.** Journal of Master Science. Vol: 51. 554-568. DOI 10.1007/s10853-015-9284-6.

[35] Afanasov, I. M, V. A. Morozov, A. V. Kempan, S. G. Ionov, A. N. Seleznev, G. Vaan Tendeloo, and V. V. Avdeev. (2009). **Preparation, electrical and thermal properties of new exfoliated graphite-based composites.** Carbon. Vol: 47. 263-270. doi:10.1016/j.carbon.2008.10.004.

[36] Tarango, G, J. M. Mendoza, A. Santos, I. Estrada, C. G. Garay, P. Piza, Kang, F, Y. P. Zheng, H. N. Wang, Y. Nishi, and M. Inagaki. (2002). **Effect of preparation conditions on the characteristics of exfoliated graphite.** Carbon. Vol: 40. 1575-1581. S0008-6223(02)00023-4.

[37] Cuadros, E, M. Pinon, H. A. Martinez, D. Lardizabal, I. Estrada, J. M. Herrera and C. Carreno. (2022). **Turbostratic Carbon/Graphene Prepared via the Dry Ice in Flames Method and Its Purification Using Different Routes: A Comparative Study.** Materials. Vol: 15. 2501. https://doi.org/10.3390/ma15072501.

[38] Yang, W, E. Fortunati. F. Dominici, J. M. Kenny, and D. Puglia. (2015). **Effect of processing conditions and lignin content on thermal, mechanical, and degradative behavior of lignin nanoparticles/polylactic (acid) bionanocomposites prepared by melt extrusion and solvent casting.** European Polymer Journal. Vol: 71. 126-139. http://dx.doi.org/10.1016/j.eurpolymj.2015.07.051.

[39] Cataldi, P, I. S. Bayer. G. Nanni, A. Athanassiou, F. Banaccorso, V. Pellegrini, A. E. Del Río-Castillo, F. Ricciardella, S. Artyukhin, M. A. Tronche, Y. Gogotsi, and R. Cingolani. (2016). **Effect of graphene nano-platelet morphology on the elastic modulus of soft and hard biopolymers.** Carbon. Vol: 109. 331-339. http://dx.doi.org/10.1016/j.carbon.2016.08.026.

[40] Stuart, B. H. (2004). **INFRARED SPECTROSCOPY: FUNDAMENTALS AND APPLICATIONS.** John Wiley & Sons. 224pp. DOI:10.1002/0470011149.

[41] Gasca, R. (1995). **Microscopía electrónica una visión del microcosmos.**

[42] Pérez-Pueyo, R. (2005). **Procesado y Optimización de Espectros Raman mediante Técnicas de Lógica Difusa: Aplicación a la identificación de Materiales Pictóricos.** [PhD's thesis]. Universitat Politècnica de Catalunya.

[43] ASTM D638: Standard Test Method for Tensile Properties of Plastics", ASTM, West Conshohocken, 2014.

[44] Miccoli, I, F. Elder, H. Pfnur, and C. Tegenkamp. (2015). **The 100th anniversary of the four-point probe technique: the role of probe geometries in isotropic and anisotropic systems.** Journal of Physics: Condensed Matter. Vol: 27. 223201. http://dx.doi.org/10.1088/0953-8984/27/22/223201.

[45] Lujan-Ortega, A. (2020). **MATERIAL DIDACTICO PARA EL LABORATORIO ANALISIS TERMICO.**

[46] J. Vac. Sci. Technol. **A 38**, 063204 (2020); https://doi.org/10.1116/6.0000412.

[47] Cheing, B. W, N. A. Ibrahim, W. M. Z. M. Yunus, and M. Z. Hussein. (2014). **Poly(lactic acid)/Poly(ethylene glycol) Polymer Nanocomposites: Effects of Graphene Nanoplatelets.** Polymers. Vol: 6, 96-104. https://doi.org/10.3390/polym6010093.

[48] Mofokeng, J. P, A. S. Luyt, T. Tabi, and J. Kovacs. (2011). **Comparison of injection moulded, natural fibre-reinforced composites with PP and PLA as matrices.** Journal of Thermoplastic Composites Materials. Vol: 25, 927-948. https://doi.org/10.1177/0892705711423291.

[49] Choksi, N, and H. Desai. (2017). **Synthesis of Biodegradable Polylactic Acid Polymer By Using Lactic Acid Monomer.** Research India Publication. Vol: 13. 377-384. https://www.ripublication.com/ijac17/ijacv13v2_19.pdf.

[50] Wei, P, S. Cui, and S. Bai. (2017). **In situ exfoliation of graphite in solid phase for fabrication of graphene/polyamide-6 composites.** Composite Science and Technology. Vol: 153. 151-159. https://doi.org/10.1016/j.compscitech.2017.10.009.

[51] Ferrari, A. C. (2007). **Raman spectroscopy of graphene and graphite: Disorder, electron–phonon coupling, doping and nonadiabatic effects.** Solid state communication. Vol: 143. 47-57. http://dx.doi.org/10.1016/j.ssc.2007.03.052.

[52] Ma, H, Z. Shen, M. Yi, S. Ben, S. Liang. L. Liu, Y. Zhang, X. Zhang, and S. Ma. (2017). **Direct exfoliation of graphite in water with addition of ammonia solution.** Journal of Colloid and Interface Science. Vol: 503. 68-75. https://doi.org/10.1016/j.jcis.2017.04.070.

[53] Zhao, Q, X. Cheng, J. Wu, and X. Yu. (2014). **Sulfur-free exfoliated graphite with large exfoliated volume: Preparation, characterization and its adsorption performance.** Journal of Industrial and Engineering Chemistry. Vol: 20. 4028-4032. http://dx.doi.org/10.1016/j.jiec.2014.01.002.

[54] A. S. Tikhomirov, N. E. Sorokina, O. N. Shornikova, V. A. Morozov, G. Van Tendeloo, and V. V. Andeev. (2011). **The chemical vapor infiltration of exfoliated graphite to produce carbon/carbon composites.** Carbon. Vol: 49. 147-153. http://dx.doi.org/10.1016/j.carbon.2010.08.054.

[55] Wang, C. S, G. T. Wu, and W. Z. Li. (1998). **Lithium insertion in ball-milled graphite.** Journal of Power Sources. Vol: 76. 1-10. PII: S0378- 7753 98 00114-1.

[56] Zolyomi, V, J. Koltai, and J. Kurti. (2011). **Resonance Raman spectroscopy of graphite and graphene.** Physics Status Solid. Vol: 11. 2435-2444. 10.1002/pssb.201100295.

[57] Del Río, F, M. G. Boado, A. Rama, and F. Guitián. (2017). **A comparative study on different aqueous-phase graphite exfoliation methods for few-layer graphene production and its application in alumina matrix composites.** Journal of the European Ceramic Society. Vol: 37. 3681-3693. https://doi.org/10.1016/j.jeurceramsoc.2017.04.029.

[58] Sharma, S, D. Susan, N. C. Kothiyal, and R. Kaur. (2018). **Graphene oxide prepared from mechanically milled graphite: Effect on strength of novel fly-ash based cementitious matrix.** Construction and Building Materials. Vol: 177. 10-22. https://doi.org/10.1016/j.conbuildmat.2018.05.051.

[59] You, S., S. M. Luzan, T. Szabo, and A. V. Talyzin. (2013). **Effect of synthesis method on solvation and exfoliation of graphite oxide.** Carbon. Vol: 52. 171-180. http://dx.doi.org/10.1016/j.carbon.2012.09.018.

[60] Jiang, L., J. Zhang, X. Xu, J. Zhang, H. Liu, Z. Guo, Y. Kang, Y. Li, and J. Xu. (2015). **Characterization and application of expanded graphite modified with phosphoric acid and glucose for the removal of Ni(II) from aqueous solution.** Applied Surface Science. Vol: 357. 2355-2363. http://dx.doi.org/10.1016/j.apsusc.2015.09.241.

[61] Krawczyk, P. (2011). **Effect of ozone treatment on properties of expanded graphite.** Chemical Engineering Journal. Vol: 172. 1096-1102. doi:10.1016/j.cej.2011.06.005.

[62] Lei, Y., B. D. Ossonon, J. Chen, J. Perreault, and A. C. Tavares. (2021). **Electrochemical characterization of graphene-type materials obtained by electrochemical exfoliation of graphite.** Journal of Electroanalytical Chemistry. Vol: 887. 115084. https://doi.org/10.1016/j.jelechem.2021.115084.

[63] Hou, B., H. J. Sun, T. J. Peng, X. Y. Zhang, and Y. Z. Ren. (2020). **Rapid preparation of expanded graphite at low temperature.** New Carbon Materials. Vol: 35. 262-268. DOI: 10.1016/S1872-5805(20)60488-7.

[64] Shin K. Y., J. H. Hong, S. Lee, and J. Jang. (2012). **High electrothermal performance of expanded graphite nanoplatelet-based patch heater.** Journal of Materials Chemistry. Vol: 22. 23404. DOI: 10.1039/c2jm34196d.

[65] Niu, L., M. Li, X. Tao, Z. Xie, X. Zhuang, X. Zhou, A. P. A. Raju, R. J. Young, and Z. Zheng. (2013). **Salt-assisted direct exfoliation of graphite into high-quality, large-size, few-layer graphene sheets.** Nanoscale. Vol: 5. 7202. DOI: 10.1039/c3nr02173d.

[66] Kumar, K. V., A. Islam, P. S. Kiran, N. Pandit, R. Kumar, S. Indupuri, and A. K. Keshri. (2024). **Exfoliation of graphite to turbostratic graphene.** 2D Materials. Vol: 11. 015022. https://doi.org/10.1088/2053-1583/ad1675.

[67] Fan, X., W. Peng, Y. Li, X. Li, S. Wang, G. Zhang, and F. Zhang. (2008). **Deoxygenation of Exfoliated Graphite Oxide under Alkaline**

Conditions: A Green Route to Graphene Preparation. Advanced Materials. Vol: 20. 4490-4493. DOI: 10.1002/adma.200801306.

[68] Morgan, D. J. (2021). **Comments onthe XPS Analysis of Carbon Materials.** Journal of Carbon Research. Vol: 51. https://doi.org/10.3390/c7030051.

[69] Coros, M., F. Pogacean, M. C. Rosu, C. Socasi, G. Borodi, L. Magerusan, A. R. Biris, and S. Pruneanu. (2016). **Simple and cost-effective synthesis of graphene by electrochemical exfoliation of graphite rods.** Royal Society of Chemistry. Vol: 6. 2651. DOI: 10.1039/c5ra19277c.

[70] Lan, R., W. Su, and J. Li. (2019). **Preparation and Catalytic Performance of Expanded Graphite for Oxidation of Organic Pollutant.** Catalysts. Vol: 9. 280. doi:10.3390/catal9030280.

[71] Athanasiou, M., N. Samartzis, L. Sygellou, V. Dracopoulos, T. Ioannides, and S. N. Yannopoulos. (2021). **High-quality laser-assisted biomass-based turbostratic graphene for high-performance supercapacitors.** Carbon. Vol: 172. 750-761. https://doi.org/10.1016/j.carbon.2020.10.042.

[72] Krawczyk, P., and B. Gurzeda. (2016). **Electrochemical properties of exfoliated graphite affected by its two-step modification.** Journal of Soid State Electrochemistry. Vol: 20. 361-369. DOI 10.1007/s10008-015-3051-0.

[73] Chiang, C. L., and S. W. Hsu. (2008). **Synthesis, characterization and thermal properties of novel epoxy/expandable graphite composites.** Society of Chemical Industry. Vol: 59. 119-126. DOI 10.1002/pi.2699.

[74] Kumar, N, R. Pandian, P. K. Das, T. R. Ravindran, S. Dash, and A. K. Tyagi. (2013). **High-temperature phase transformation and low friction behaviour in highly disordered turbostratic graphite.** Journal of Physics D: Applied Physics. Vol: 46. 395305. http://dx.doi.org/10.1088/0022-3727/46/39/395305.

[75] Radhika, R, N. Kumar, R. Pandian, T. R. Ravindran. S. Dash, and A. K. Tyagi. (2014). **Structural transformation and friction behavior in turbostratic graphite sliding against Si3N4, SiC and Al2O3 balls.** Surface & Coatings Technology. Vol: 253. 300-306. http://dx.doi.org/10.1016/j.surfcoat.2014.06.001.

[76] Binder, C, T. Bendo, G. Hammes, G. O. Neves, R. Binder, J. D. B. de Mello, and A. N. Klein. (2017). **Structure and properties of in situ-generated two-dimensional turbostratic graphite nodules.** Carbon. Vol: 124. 685-692. https://doi.org/10.1016/j.carbon.2017.09.036.

[77] Zhang, X., T. Schiros, D. Nordlund, Y. C. Shin, J. Kong, M. Dresselhaus, and T. Palacios. (2015). **X-Ray Spectroscopic Investigation of Chlorinated Graphene: Surface Structure and Electronic Effects.** Advanced Functional Materials. Vol: 25. 4163-4169. DOI: 10.1002/adfm.201500541.

[78] Istrate, O. M, K. R. Paton, U. Khan, A. O'Nell, A. P. Bell, and J. N. Coleman. (2014). **Reinforcement in melt-processed polymer–graphene composites at extremely low graphene loading level.** Carbon. Vol: 78. 243-249. http://dx.doi.org/10.1016/j.carbon.2014.06.077.

[79] Papageorgiou, D., I. A. Kinloch, M. Liu, P. Cataldi, and R. J. Young. (2021). **High-performance fluoroelastomer-graphene nanocomposites for advanced.** Composite Science and Technology. Vol: 202, 108592. https://doi.org/10.1016/j.compscitech.2020.108592.

[80] Kalaitzidou, K, H. Fukushima, and L. T. Drzal. (2007). **Mechanical properties and morphological characterization of exfoliated graphite–polypropylene nanocomposites.** Composite Part A: Applied Science and Manufacturing. Vol: 38. 1675-1682. https://doi.org/10.1016/j.compositesa.2007.02.003.

[81] Pages, P, F. Carrasco, J. Gomez-Perez, O. O. Santana, and M. L. Maspoch. (2010). **Procesado del ácido poliláctico (PLA) y de nanocompuestos PLA/montmorillonita en planta piloto: Estudio de sus cambios estructurales y de su estabilidad térmica.** Afinidad LXVI. Vol: 546. 107-113. https://raco.cat/index.php/afinidad/article/view/269088.

[82] Hoyos-Torres, S. (2012). **SÍNTESIS Y CARACTERIZACIÓN DE ÁCIDO POLI L-LÁCTICO DE BAJO PESO MOLECULAR PARA APLICACIONES BIOMÉDICAS.** [Belchor's thesis]. Universidad del Valle.

[83] Zhang, J, D. X. Yan, J. Z. Xu, H. D. Huang. J. Lei, and Z. M. Li. (2012). **Highly crystallized poly (lactic acid) under high pressure.** AIP Advances. Vol: 2. 042159. http://dx.doi.org/10.1063/1.4769351.

[84] Morcillo-Esquerdo, M. (2019). **Estudio de la influencia de los ciclos de reprocesado de ácido poliláctico, PLA en las propiedades finales.** [Master's thesis]. Universitat Politécnica de Valencia.

[85] Farah, S, D. G. Anderson, and R. Langer. (2016). **Physical and mechanical properties of PLA, and their functions in widespread applications — A comprehensive review.** Advanced Drug Delivery Reviews. Vol: 107. 367-392. http://dx.doi.org/10.1016/j.addr.2016.06.012.

[86] Tabi, T, S. Hajba, and J. G. (2016). **Effect of crystalline forms (a0 and a) of poly(lactic acid) on its mechanical, thermo-mechanical, heat deflection temperature and creep properties.** European Polymer Journal. Vol: 82. 232-243. http://dx.doi.org/10.1016/j.eurpolymj.2016.07.024.

[87] Di Lorenzo, M. L, and R. Androsch. (2019). **Influence of*α′-/α*-crystal polymorphism onproperties of poly(L-lactic acid).** Polymer International. Vol: 68. 320- 334. https://doi.org/10.1002/pi.5707.

[88] Limsukon, W, R. Auras, and T. Smith. (2021). **Effects of the Three-Phase Crystallization Behavior on the Hydrolysis of Amorphous and Semicrystalline Poly(lactic acid)s.** Applied Polymer Materials. Vol: 3. 5920-5931. https://doi.org/10.1021/acsapm.1c01080.

[89] Bakes, E. H, L. N, Pires, L. C. Costa, F. R. Passador, and L. A. Pessan. (2019). **Analysis of the Degradation During Melt Processing of PLA/Biosilicate® Composites.** Journal of Composite Science. Vol: 3. 52. http://dx.doi.org/10.3390/jcs3020052.

[90] Echeverría, C, I. Limón, A. Muñoz-Bonilla, M. Fernandez-Garcia, and D. López. (2021). **Development of Highly Crystalline Polylactic Acid with β-Crystalline Phase from the Induced Alignment of Electrospun Fibers.** Polymers. Vol: 13. 2860. https://doi.org/10.3390/polym13172860.

[91] Wang, Y, Y. Cheng, J. Chen, D. Wu, Y. Qiu, X. Yao, Y. Zhou, and C. Chen. (2015). **Percolation networks and transient rheology of polylactide composites containing graphite nanosheets with various thicknesses.** Polymer. Vol: 67. 216-226. http://dx.doi.org/10.1016/j.polymer.2015.04.076.

[92] Beyler, C. L., & Hirschler, M. M. (2002). **Thermal decomposition of polymers. SFPE handbook of fire protection engineering**, Vol: 2, 111-131.

[93] Straus, S., & Wall, L. A. (1959). **Influence of Impurities on the Pyrolysis of Polyamides.** Journal of Research of the National Bureau of Standards. Section A, Physics and Chemistry. Vol: 63. 269. https://nvlpubs.nist.gov/nistpubs/jres/63A/jresv63An3p269_A1b.pdf.

[94] Carrasco, F., P. Pages, J. Gamez-Perez, O. O. Santana, and M. L. Maspoch. (2010). **Kinetics of the thermal decomposition of processed poly(lactic acid).** Polymer Degradation and Stability. Vol: 95. 2508-2514. http://dx.doi.org/10.1016/j.polymdegradstab.2010.07.039.

[95] Guo, R, Z. Ren, H. Bi, M. Xu, and L. Cai. (2019). **Electrical and Thermal Conductivity of Polylactic Acid (PLA)-Based Biocomposites by Incorporation of Nano-Graphite Fabricated with Fused Deposition Modeling.** Polymers. Vol: 11. 549. http://dx.doi.org/10.3390/polym11030549.

[96] Mngomezulu, M. E, A. S. Luyt, and M. J. Jhon. (2019). **Morphology, thermal and dynamic mechanical properties of poly(lactic acid)/expandable graphite (PLA/EG) flame retardant composites.** Journal of Thermoplastic Composite Materials. Vol: 32. 89-107. http://journals.sagepub.com/home/jtc.

[97] Li, B, and W. H. Zhong. (2011). **Review on polymer/graphite nanoplatelet nanocomposites.** Journal of Material Science. Vol: 46. 5595-5614. DOI 10.1007/s10853-011-5572-y.

[98] Pielichowski, K., Leszczyńska, A., & Njuguna, J. (2009). **Mechanisms of Thermal Stability Enhancement in Polymer Nanocomposites.** Optimization of Polymer Nanocomposite Properties, Vol: 9, 4.

[99] Potts, J. R, D. R. Dreyer, C. W. Bielawski, and R. S. Rouff. (2011). **Graphene-based polymer nanocomposites.** Polymer. Vol: 52. 5-25. https://doi.org/10.1016/j.polymer.2010.11.042.

[100] Azlin, M. N. M., S. M. Sapuan, M. Y. M. Zuhri, and E. S. Zainudian. (2022). **Mechanical, Morphological and Thermal Properties of Woven**

Polyester Fiber Reinforced Polylactic Acid (PLA) Composites. Fibers and Polymers. Vol: 23. 234-242. DOI 10.1007/s12221-021-0139-2.

[101] Ramanathan, T., A. A. Abdala, S. Stankovich, D. A. Dikin, M. Herrera-Alonso, R. D. Piner, D. H. Adamson, H. C. Schniepp, X. Chen, R. S. Ruoff, S. T. Nguyen. I. A. Aksay, R. K. Prud'Homme, and L. C. Bridson. (2008). **Functionalized graphene sheets for polymer nanocomposites.** Nature Nanotechnology. Vol: 3. 327-331. http://www.nature.com/doifinder/10.1038/nnano.2008.96.

[102] Bajpai, P. K., I. Singh, and J. Madaan. (2012). **Comparative studies of mechanical and morphological properties of polylactic acid and polypropylene based natural fiber composites.** Journal of Reinforced Plastics and Composites. Vol: 31. 1712-1724. DOI: 10.1177/0731684412447992.

[103] Anwer, M. A. S. and H. E. Naguib. (2016). **Study on the morphological, dynamic mechanical and thermal properties of PLA carbon nanofibre composites.** Composite Part B. Vol: 91. 631-639. http://dx.doi.org/10.1016/j.compositesb.2016.01.039.

[104] Debelak, B. and K. Lafdi. (2007). **Use of exfoliated graphite filler to enhance polymer physical properties.** Carbon. Vol: 45. 1727-1734. doi:10.1016/j.carbon.2007.05.010.

[105] Bera, M., P. Gupta, and P. K. Maji. (2019). **Efficacy of ultra-low loading of amine functionalized graphene oxide into glycidol-terminated polyurethane for high-performance composite material.** Reactive and Functional Polymers. Vol: 139. 60-74. https://doi.org/10.1016/j.reactfunctpolym.2019.03.008.

[106] Idowu, A., B. Boesl, and A. Agarwal. (2018). **3D graphene foam-reinforced polymer composites-A review.** Carbon. Vol: 135. 52-71. https://doi.org/10.1016/j.carbon.2018.04.024.